

# THE EARTH'S DYNAMIC MAGNETOTAIL

A. NISHIDA

*Institute of Space and Astronautical Science, Sagami-hara 229-8510, Japan*

(Received 11 August, 1999)

**Abstract.** Geomagnetic field lines that are stretched on the nightside of the Earth due to reconnection with the interplanetary magnetic field constitute the Earth's magnetotail. The magnetotail is a dynamic entity where energy imparted from the solar wind is stored and then released to generate disturbance phenomena such as substorms. This paper gives an updated overview on the physics of the magnetotail by drawing heavily from recent research conducted with the GEOTAIL satellite. It summarizes firstly the basic properties of the magnetotail such as shape, size and magnetic flux content, internal motion and plasma regimes. Then it describes characteristics of tail plasmas of the solar-wind and the ionosphere origins. Thirdly it addresses acceleration and heating of plasmas in the magnetotail, where reconnection between the stretched field lines is the main driver but the site of the acceleration is not limited to the immediate vicinity of the neutral line. In the collisionless regime of the plasma sheet kinetic behaviors of ions and electrons control the acceleration process. The paper closes by enumerating the problems posed for future studies.

## 1. Introduction

Geomagnetic field lines stretched by the solar wind form the geomagnetic tail, or the magnetotail, on the nightside of the Earth. The magnetotail has a diameter of several tens of  $R_E$  and contains various plasma regimes. The magnetotail is a dynamic entity. Its time variations occur primarily in direct response to the variable conditions of the solar wind and the interplanetary magnetic field (IMF). Additional variations involve conversion of magnetic field energy that has been imparted to the magnetotail from the solar wind. Accelerated particles and field-aligned currents that result from this energy conversion lead to a variety of activities in the inner magnetosphere including the high-latitude ionosphere. The magnetotail is a key element of the magnetosphere that links the inner magnetosphere with the solar wind.

The first comprehensive survey of the magnetotail was conducted some 35 years ago with the IMP 1 satellite. It defined the basic structure of the extended magnetotail as well as the plasma sheet imbedded therein, and suggested that magnetic reconnection occurs at the neutral sheet that separates the oppositely directed field lines in the upper and lower halves of the tail (Ness, 1969). Since that time numerous satellite observations have been made in the tail and have advanced our understanding of its physics. One of the most recent missions, GEOTAIL launched in July 1992, was specifically designed to studying the magnetotail from the near



tail (from the distance of  $10 R_E$ ) to the distant tail (down to  $220 R_E$ ), and by virtue of the optimized orbit and instrumentation it has added substantially to our knowledge on the magnetotail. The present paper is an updated introduction to the magnetotail physics that draws much from the new findings made by this mission.

Section 2 is on formation of the magnetotail and the basic characteristics of the tail such as shape and convection. Section 3 is on nature and source of the plasma population that fills the magnetotail. Section 4 is the core part of this paper and deals with acceleration and heating process in the magnetotail. It emphasizes the kinetic aspect of this process where significant advances have recently been made, and it also addresses the relation between magnetospheric substorm and reconnection in the tail. Section 5 enumerates important issues which are still unresolved and remain for future studies.

## 2. Formation of the Magnetotail

This section describes the mechanism of the tail formation and introduces basic properties of the tail. Since reconnection between IMF and geomagnetic field lines is the dominant mechanism of the tail formation, shape of the tail as well as internal dynamics in the tail is governed by the IMF. Several distinct plasma regimes are formed inside the tail reflecting the global dynamics.

### 2.1. TAIL FORMATION DUE TO MAGNETIC RECONNECTION

It has now been well established that reconnection of the geomagnetic field with the IMF is the dominant mode of the interaction between the solar wind and the magnetosphere. The interaction may also occur through diffusive entry of the solar wind plasma into the magnetosphere but its effect as measured by the electric potential difference generated in the magnetosphere is only a few kV (Mozer et al., 1994) which is less than 10% of the potential generated by reconnection.

The reconnected field lines are stretched anti-sunward with the solar wind (Dungey, 1965). This process is illustrated in Figure 1 by using results of numerical simulations of the solar wind-magnetosphere interaction. Three panels of this figure correspond to three cases of the IMF orientation; (a) due southward, (b) due duskward, and (c) halfway between duskward and northward. In this simulation the solar wind density and velocity are assumed to be  $5 \text{ cm}^{-3}$  and  $300 \text{ km s}^{-1}$ , and the IMF strength to be 5 nT. Magnetic field lines are projected to the midnight meridian, and their topologies are expressed by using different colors: green is used for the closed field lines that have both feet in the ionosphere, blue for open field lines that have one foot in the ionosphere and the other in the solar wind, and red for the IMF field lines that have neither feet in the ionosphere. The open field lines constitute the lobes of the magnetotail.

When the IMF direction is due southward reconnection occurs on the dayside magnetopause. Figure 1(a) shows that the open field lines produced by this recon-

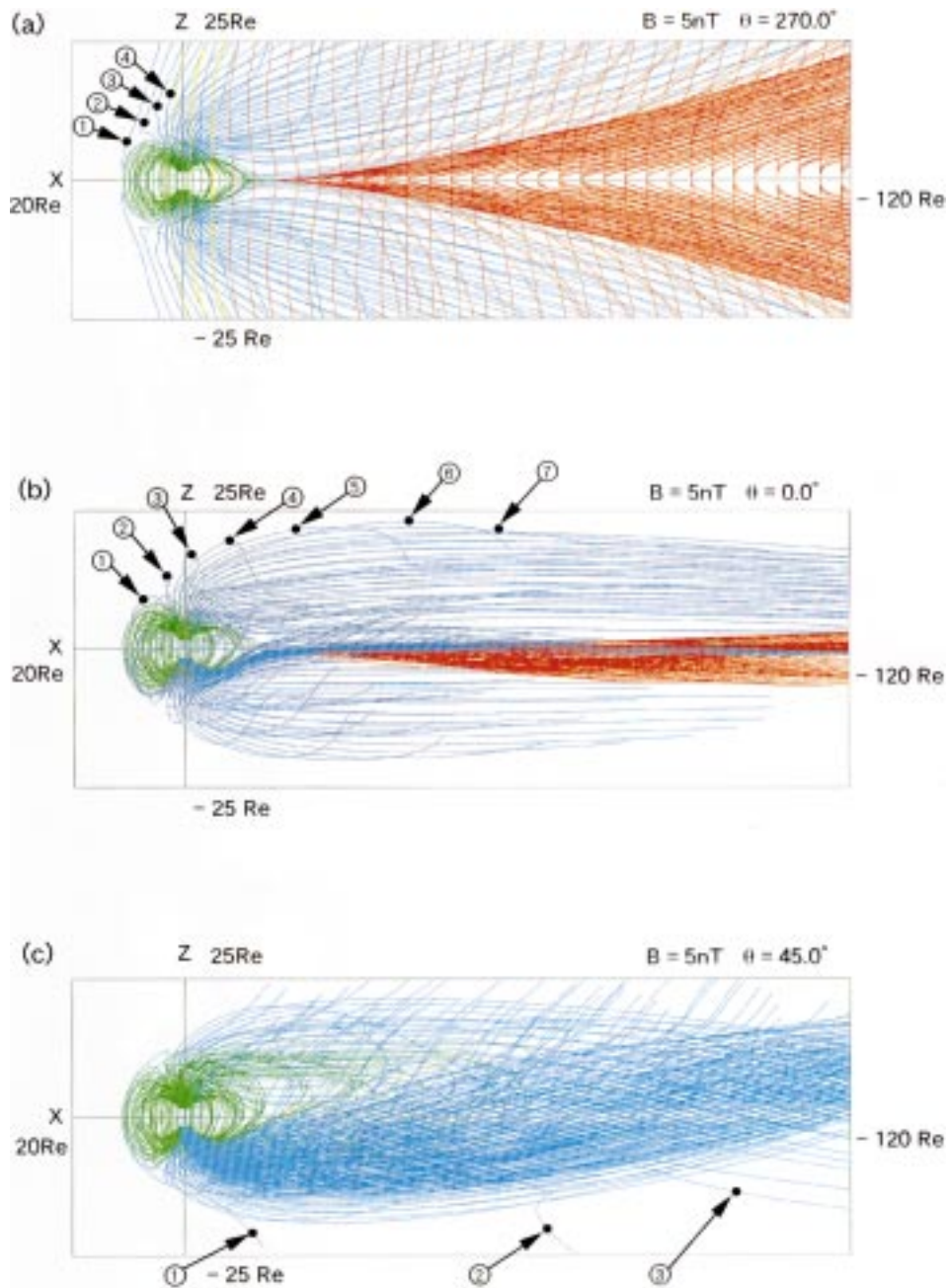


Figure 1. Magnetotail is formed by anti-sunward transport of magnetic field lines caused by magnetic reconnection. This is shown by magnetic field configurations obtained by numerical simulations. (a), (b) and (c) correspond to due southward, duskward, and north-duskward directions of the incoming IMF, respectively, and green, blue, and red colors represent closed, open, and IMF field lines, respectively (Nishida and Ogino, 1998; modified). These were obtained by the simulation scheme of Ogino et al. (1992).

nection move anti-sunward as labeled 1, 2, 3, and 4 as their solar-wind ends are carried further downstream. The tail of geomagnetic field lines is formed in this manner. In Figure 1(b) where the IMF is directed duskward, solar wind ends of the open field lines move anti-sunward and become stretched in the similar manner. The sequence of the anti-sunward motion of open field lines is labeled 1 to 7 in this Figure 1(b). The open field lines extend to the dawn or dusk sector of the magnetosheath in this case (b) while they extend to the north or south sector in the case (a) for the southward IMF. (The magnetosheath is a layer of the solar wind plasma enveloping the magnetosphere that has been decelerated at the bow shock.) The tail is formed also in Figure 1(c), where the IMF has the northward component, by anti-sunward motion and stretching of the open field lines which are reconnected with the IMF on the surface of the tail. In this case (c) the open field lines cross the equatorial plane; for example, the open field lines labeled 1, 2, and 3 that are rooted in the northern polar cap extend to the southern magnetosheath.

Two categories of the IMF field lines are illustrated in Figure 1(a). Those which are nearly vertical are the original IMF field lines in the magnetosheath and are draped around the magnetosphere. The others which are centered at the equatorial plane in the tail and wedge-shaped are produced by reconnection of the open field lines inside the magnetotail. They do not really represent the IMF but have topologically a common character in that they have neither feet in the ionosphere. In the absence of an appropriate and widely accepted terminology we shall call the latter as IMF-type field lines in the rest of this paper. The simulation shows that the IMF-type field lines in the tail are formed also when the IMF is duskward (Figure 1(b)) or dawnward, but may not be produced when the IMF is inclined further toward north (Figure 1(c)). Reconnection inside the magnetotail will be a major topic of this paper.

Although the simulation of Figure 1 reproduces many of the basic features of the magnetotail, we have to note that it places the transition from the closed field lines to the IMF-type field lines much closer to the Earth than is actually observed.

## 2.2. SHAPE OF THE MAGNETOTAIL

Since the magnetotail is formed by reconnection, its shape is controlled not only by dynamic pressure of the solar wind but also by the IMF. The pressure exerted on the tail surface is larger and hence the tail field is stronger when the flaring angle, that is the angle which the tail magnetopause makes with the sunward direction, is larger. Figure 2 shows the dependence of the flaring angle  $\alpha$  on the northward component  $B_z$  of the IMF. In this figure the angle  $\alpha$  has been normalized to take account of its dependencies on dynamic pressure  $\rho v_{sw}^2$  and downtail distance  $x$  by using empirical relations, and

$$\sin^2 \alpha^* = 0.190 \sin^2 \alpha (\rho v_{sw}^2)^{0.527} e^{-0.085x} \quad (1)$$

is plotted against  $B_z$ . Units are nanopascals for dynamic pressure and  $R_E$  for  $x$  which is the Geocentric Solar Magnetospheric  $x$  Coordinate and negative in the tail.

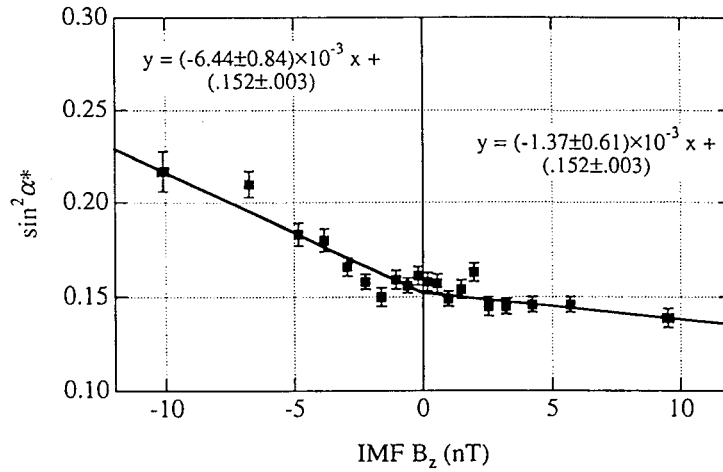


Figure 2. Dependence of the tail flaring angle on the  $B_z$  component of the IMF (Petrinec and Russell, 1996).

When the IMF is southward the flaring angle increases as  $|B_z|$  increases, while the flaring angle does not vary much when the IMF is northward (Petrinec and Russell, 1996). Thus the flaring angle is larger so that the tail field is stronger when the southward component of the IMF is larger, as would be expected from comparison of Figures 1(a) and 1(b). The above result has been obtained from comparison of the solar wind observations by IMP 8 with the ISEE 2 tail observations in the distance range of 10 to 22  $R_E$  by assuming that the lobe field is vacuum field and uniform along a line which intersects the spacecraft position and is perpendicular to the tail boundary. An empirical formula relating the tail radius to dynamic pressure and  $B_z$  has also been obtained in the same work.

Figure 3 shows the dependence of  $B_L^*$ , the field strength in the lobe normalized to the distance of 20  $R_E$ , on dynamic pressure (Figure 3(a)) and  $B_z V_{sw}$  (Figure 3(b)) that expresses transport rate of IMF magnetic flux toward the magnetosphere. It is seen that  $B_L^*$  increases with an increase both in dynamic pressure and in the transport rate of the southward flux (Nakai et al., 1991). Tendency of  $B_L^*$  to increase slightly with an increase in the transport rate of the northward magnetic flux is intriguing but the correlation coefficient there may be too low to be significant.

A recent work which is based on a large number of data points obtained from eleven spacecraft at  $-15 > x > -70 R_E$  has derived an empirical formula for the lobe magnetic field strength B (in nT):

$$B = 600.11x^{-1.25} + 8.47 \tag{2}$$

and

$$B_{30}^2 = -96.5 + 294.5(n_{sw} m v_{sw}^2)^{0.5} + 2.36 B_{IMF}^2 \sin^2(\theta/2), \tag{3}$$

where  $x$  is in  $R_E$ ,  $B_{30}$  is the lobe field strength normalized to a distance of 30  $R_E$ , and  $\theta$  varies from  $0^\circ$  for northward to  $180^\circ$  for southward IMF (Fairfield and Jones,

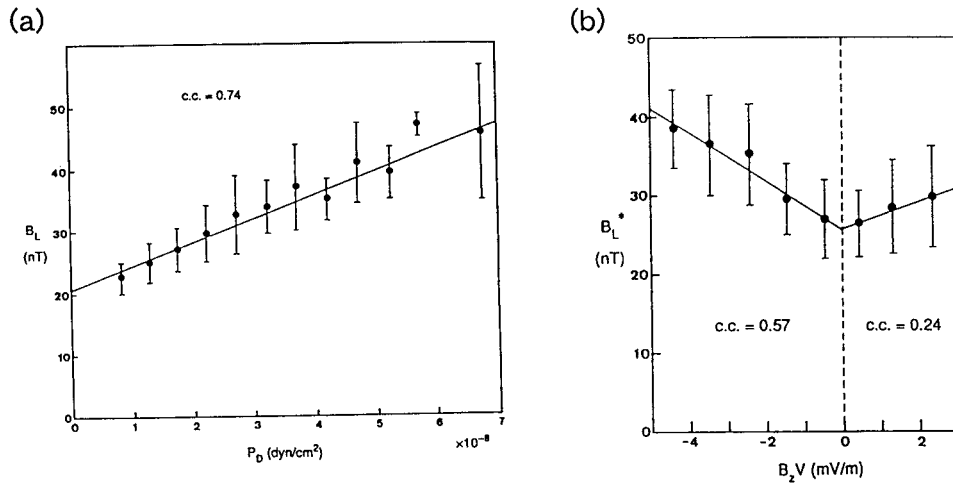


Figure 3. Dependence of  $B_L^*$ , the lobe field strength normalized to  $20 R_E$ , on (a) dynamic pressure of the solar wind and on (b) the rate  $B_z V_{sw}$  of transport of the northward IMF with the solar wind toward the magnetosphere (Nakai et al., 1991).

1996).  $B_{30}^2$  is correlated better with square root of the dynamic pressure rather than being proportional to it because the flaring angle is reduced when dynamic pressure is increased. The empirical formula for  $B$  down to  $220 R_E$  derived from ISEE 3 observations is (Slavin et al., 1985)

$$B = 125x^{-0.53} \quad (x > -120 R_E), \quad \text{and} \quad = 9.2 \quad (x < -120 R_E). \quad (4)$$

The constancy of  $B$  beyond  $120 R_E$  suggests that the flaring of the tail surface ceases on average at this distance. Figure 4 plots the strength of the lobe field measured by GEOTAIL versus the  $x'$  coordinate down to  $-210 R_E$ , where  $x'$  is measured along the direction of solar wind whose aberration angle is assumed to be  $4^\circ$  (Yamamoto et al., 1994). Most of the data points follow the trend found by earlier observations, but there is a number of unusual points which are substantially higher than this general trend. In such events the magnetotail has been compressed by high-density and fast-streaming solar wind and subsequently the tail radius is increased when additional magnetic flux is transported to the tail in response to arrival of strong southward component of the IMF (Kokubun et al., 1996). These events are mostly seen during growing stage of the ring current that means energetic particles are being injected into the trapped orbits on the closed field lines. The ring current is the characteristic feature of an interval of high geomagnetic activity called a magnetic storm.

From a statistical summary of GEOTAIL observations in the distant tail at  $x = -83$  to  $-210 R_E$  during 13 storm intervals, magnetic flux contents of the tail during quiet times and during the storm main phase have been estimated to be  $1.0 \times 10^4 \text{ nT } R_E^2$  ( $4.1 \times 10^{16} \text{ Mx}$ ) and  $1.9 \times 10^4 \text{ nT } R_E^2$  ( $8.1 \times 10^{16} \text{ Mx}$ ), respectively,

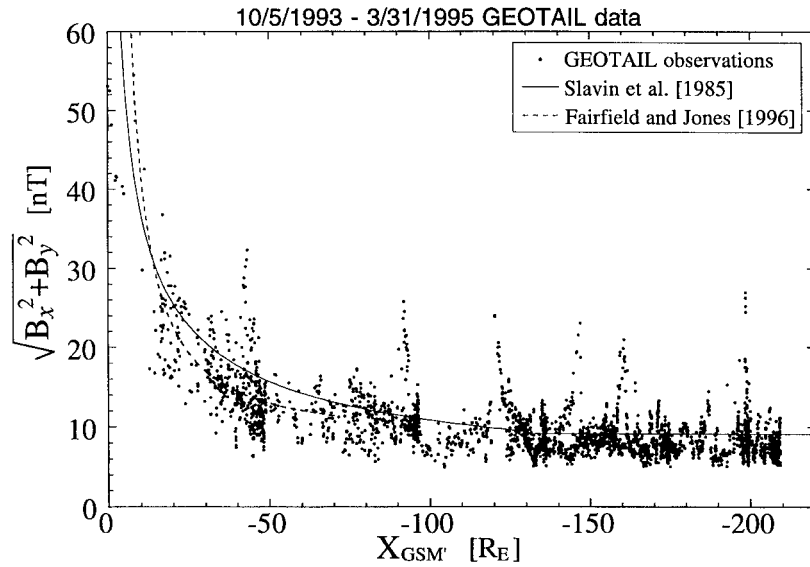


Figure 4. Plot of the lobe magnetic field strength against the distance  $X'$  along the tail axis.  $X'$  is measured along the nominal flow direction of the solar wind that is aberrated by  $4^\circ$  relative to the Earth-sun direction (Yamamoto et al., 1994; revised). Empirical relations obtained by earlier works are superposed. Sometimes the observed values are substantially higher than the general trend.

and correspondingly magnetic energy stored between  $x = -100$  and  $-200 R_E$  is  $2 \times 10^{15}$  J and  $7 \times 10^{15}$  J (Nakamura et al., 1997).

Since the open field lines are stretched not only anti-sunward but also in the dawn-dusk direction in the general case when the IMF has a  $B_y$  component, it has been suggested that the tail is twisted (Cowley, 1981). Numerical simulations of Figure 1, as well as of others (e.g., Ashour-Abdalla et al., 1998), support this conjecture, and observations have confirmed that this is indeed the case. Figure 5 shows the occurrence frequency of northern and southern lobes of the magnetotail beyond  $x = -150 R_E$  in the coordinate system where the  $x$  axis is aligned with the solar wind velocity which is observed simultaneously by another satellite. The  $y$  axis is parallel to the vector product of the  $x$  direction and the Earth's dipole. Cases with negative  $B_y$  have been reverted. Red color means that the northern tail lobe is observed more often than the southern lobe, while the opposite is meant by green color. It is clearly seen that the neutral sheet, which is delineated by a thick white line, is twisted for both northward  $B_z$  (Figure 5(a)) and southward  $B_z$  (Figure 5(b)) conditions. The angle of the twist is greater when the IMF is northward than when it is southward, and the averages are  $32^\circ$  and  $15^\circ$  for each, respectively (Maezawa et al., 1997; Maezawa and Hori, 1998). In this analysis low ion temperature ( $T_i < 3 \times 10^6$  K) and slow flow speed (less than 80% of the upstream solar wind speed) are used as the defining characteristics of the tail lobe.

## Tilt of the Distant Neutral Sheet

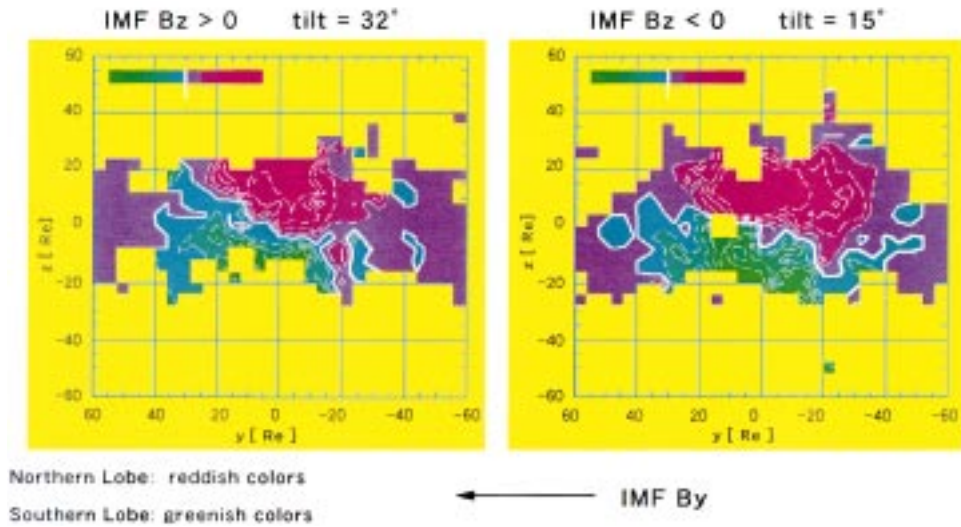


Figure 5. Contour map of the difference between the probabilities of observing northern tail lobe and southern tail lobe for each  $4 \times 4 R_E$  bin for positive IMF  $B_y$  and (a) positive  $B_z$  and (b) negative  $B_z$  (Maezawa and Hori, 1998). Cases with negative  $B_y$  have been reverted with respect to the Z axis. Reddish color (greenish color) means that the northern (southern) lobe is observed more often.

The above analysis has also yielded  $55 R_E$  as the average diameter of the tail cross section in the  $x \sim -150$  to  $-220 R_E$  range both in  $y$  and  $z$  directions (Maezawa and Hori, 1998). Earlier analyses of the ISEE 3 data have yielded a comparable value of  $24 R_E$  (Fairfield, 1992) and  $30 R_E$  as radius (Slavin et al., 1985) of the distant tail. Nakamura et al. (1997) have derived  $35 \times 23 R_E$  and  $26 \times 34 R_E$  as the radii of the distant magnetotail (at 80 to 200  $R_E$ ) during quiet and storm times, respectively. Filamentation of the magnetotail is not suggested by the magnetopause normal directions observed by ISEE 3 (Sibeck et al., 1985) and GEOTAIL (Nishida et al., 1995) satellites.

The twist angle of the tail has been determined also from the orientation of the edge of the plasma sheet boundary layer as estimated from the gradients of energetic ion intensity observed by ISEE 3. It is found that for southward IMF  $B_z$  the twist is  $-12^\circ$  for IMF  $B_y > 0$  and  $6^\circ$  for  $B_y < 0$ , and for northward IMF  $B_z$  it is  $-24^\circ$  for  $B_y > 0$  and  $13^\circ$  for  $B_y < 0$ . Here data obtained from the near tail to the distant tail (down to  $240 R_E$ ) seem to have been used in averaging (Owen et al., 1995). While twist angles obtained from averaging are a few tens of degrees or less, much greater twist has been seen in some individual cases. For example, Sibeck et al. (1985) and Macwan (1992) have reported the cases where the magnetotail is twisted by more than  $90^\circ$  so that a larger part of the northern (southern) tail is below (above) the equatorial plane.

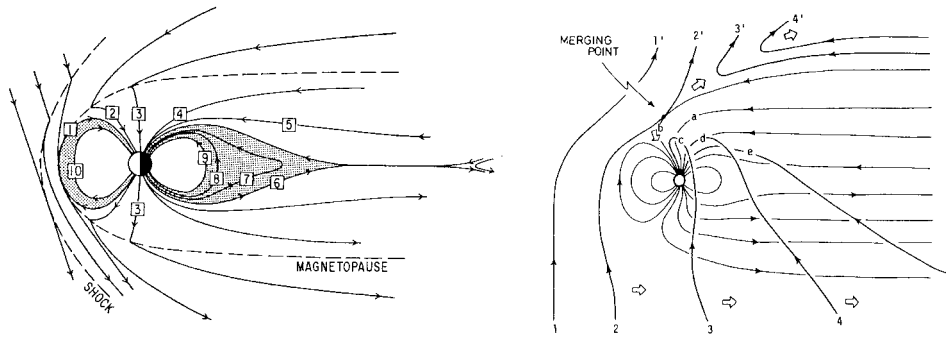


Figure 6. Two basic types of the magnetospheric convection. In (a) the convection is generated by reconnection of IMF with the closed field lines on the dayside magnetopause (Levy et al., 1964) while in (b) with the open field lines on the surface of the lobe (Maezawa, 1976). These typically correspond to southward and northward IMF conditions, respectively.

Numerical simulations have suggested that the magnetotail consists entirely of the closed field lines when the IMF is exactly northward (Fedder and Lyon, 1995). It is difficult to prove such simulation results by using in-situ magnetic field observations, because the northward component  $B_z$  cannot be taken as a signature of the closed field lines in the magnetotail when the tail is severely twisted. Extended periods of such IMF orientation should be extremely rare, anyway. From particle observations at ionospheric altitudes Newell et al. (1997) have suggested that the field lines from the polar cap completely close when  $\text{IMF } B_z > |B_y|$  for about 4 hours, but that even brief (6–7 min) southward excursions of the IMF can fill the polar cap with open field lines.

### 2.3. CONVECTION IN THE MAGNETOTAIL

While reconnection on the magnetopause adds magnetic fluxes more or less continually to the magnetotail, the size of the tail does not grow indefinitely. This is because magnetic fluxes are convected throughout the magnetosphere and the addition of the flux to the tail is balanced with the loss, on average, of an equal amount by convection out of the magnetotail. The nature of the convection is the  $\mathbf{E} \times \mathbf{B}$  drift of magnetohydrodynamics, where  $\mathbf{E}$  and  $\mathbf{B}$  represent electric and magnetic fields.

Figure 6 shows the two elementary types of the convection that are generated in the magnetosphere. The convection of Figure 6(a) prevails when the IMF polarity is southward (Levy et al., 1964). The characteristic feature of this profile is that the field lines change their topology between the closed and the open. First, magnetic reconnection occurs with the closed field lines on the frontside of the magnetopause (field line labeled 1) and produces open field lines (2) that are transported to the tail. Later the open field lines of the northern and the southern tail approach each other at certain distance (5), and become reconnected at the neutral sheet of the magnetotail (6) resulting in the loss of the open magnetic flux. This reconnection

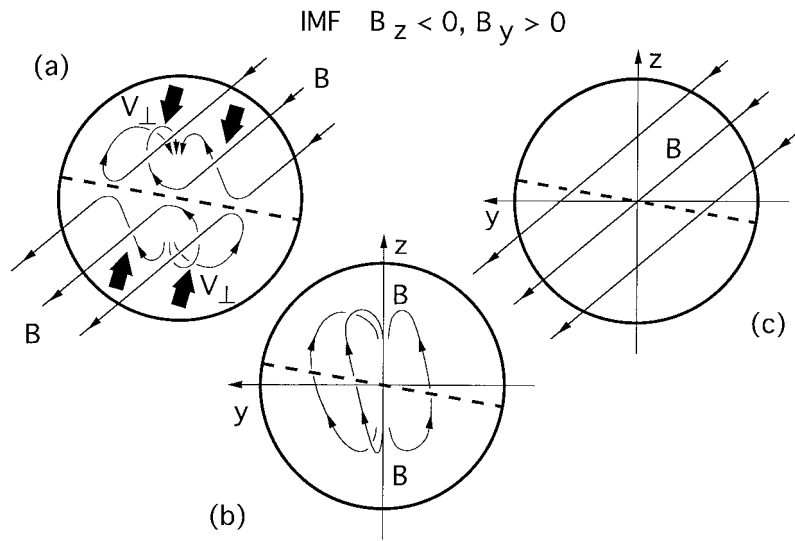


Figure 7. Magnetic field lines ( $\mathbf{B}$ ) and their convection velocity ( $\mathbf{V}_{\perp}$ ) in the magnetotail under the southward IMF are projected to the  $y - z$  plane. (a) The open field lines approach the neutral sheet from both sides, and (b) their reconnection results in closed field lines on the earthward side and (c) IMF-type field lines on the tailward side (Nishida et al., 1998).

produces a pair of field lines comprising the closed field lines on the earthward side (7) and the IMF-type field lines on the anti-earthward side of the reconnection line. Figure 7 shows the same sequence as viewed along the tail axis toward the Earth for the condition of IMF  $B_z < 0$  and  $B_y > 0$ . In Figure 7(a) open field lines of the northern and the southern tail approach the neutral sheet (dashed line) from both directions, and result in closed field lines (Figure 7(b)) and IMF-type field lines after reconnection (Figure 7(c)). Subsequently these closed field lines move to the dayside to be reconnected again with the IMF on the magnetopause, thereby closing the convection cell.

The convection of this type is generated not only when IMF  $B_z$  is southward but also when it is northward. Figure 8 illustrates the motion of the field lines in the tail when IMF  $B_z$  is weakly northward. Although it is basically the same as for the southward case, there are some apparent differences; the open field lines approach the neutral sheet by moving in dawn/dusk direction rather than in north/south direction (Figure 8(a)), and because of the severe twist of the neutral sheet the IMF-type field lines have the northward polarity although they traverse the neutral sheet from the north to the south (Figure 8(c)) (Nishida et al., 1998). It has been known that northward field lines are convected tailward in geomagnetically quiet times and this was once interpreted to represent the flow of the closed field lines away from the Earth (Heikkila, 1988), but the above seems to be a more viable interpretation of the observation.

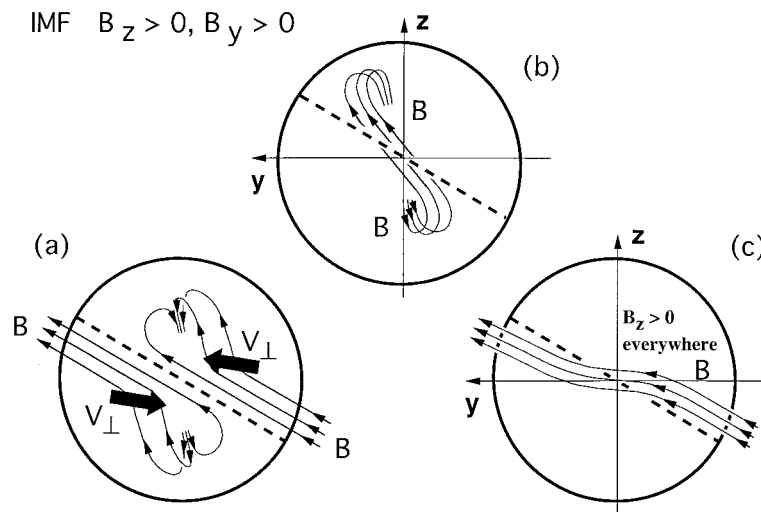


Figure 8. Similar to Figure 7 but for weakly northward IMF conditions (Nishida et al., 1998). The convection pattern is the same as for the southward IMF condition, but the IMF-type field lines (c) traverse the twisted neutral sheet southward although they are directed northward.

The magnetic neutral line where the open field lines are reconnected is located primarily in the distant tail. Analysis of the data in geomagnetically active times that correspond to the southward IMF shows that the distance to the distant neutral line is about  $140 R_E$ , although in individual cases there could be considerable scatter in this distance (Nishida et al., 1996). In geomagnetically quiet times that correspond to the northward IMF the position of the distant neutral line is more difficult to determine, because we need reliable information on the twisting angle of the neutral sheet to estimate the component of the tail magnetic field normal to the instantaneous neutral sheet. The distant neutral line defines separatrices of magnetic field lines between which the plasma sheet is embedded. Another neutral line is formed in the domain of the closed field lines in the near-Earth tail; this subject will be discussed in Section 4.1.

An independent estimate of the position of the neutral line has been performed by using observations of the polar rain electrons. These electrons are usually bidirectional on open field lines since the incoming component are observed together with the reflected component from the low-altitude mirror (Baker et al., 1986), but when the field line threading the observing site is either closed or IMF type the beam becomes unidirectional since only the tailward (earthward) component can be seen on the earthward (tailward) side of the neutral line. The neutral line position obtained in this way is at  $x = -50$  to  $-150 R_E$  (Shirai et al., 1997). Location of the neutral line has been deduced also from observations of the slow-mode shock (see Section 4.3). According to this study, the neutral line is earthward for all five slow shock observations beyond  $150 R_E$ , while it is either earthward or tailward when the shocks are observed between  $60$  and  $100 R_E$  (Saito et al., 1995).

IMF  $B_z > 0, B_y > 0$

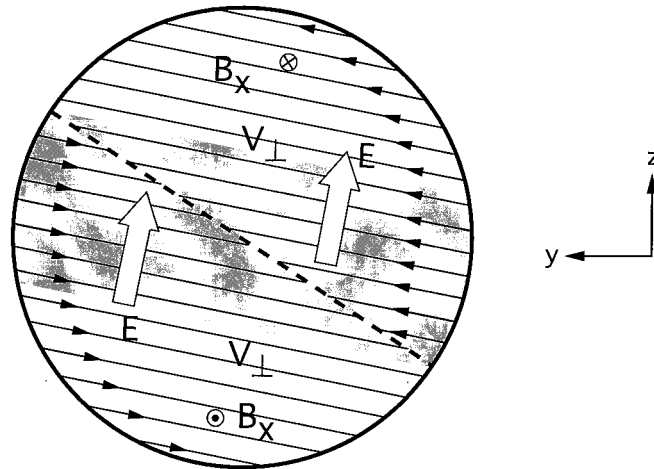


Figure 9. Streamlines of the convection velocity ( $V_{\perp}$ ) and the associated electric field ( $E$ ) in the tail section when two types of convection are both present. Some of the streamlines reach the neutral sheet while others traverse the tail from the dawn/dusk flank to the other (Nishida et al., 1998). The former streamlines belong to the convection of the type of Figure 6(a) and the latter to that of Figure 6(b).

Note that these two studies (using polar rain electrons and slow shock) have not distinguished between distant and near-Earth neutral lines.

When  $B_z$  is northward another mode of convection is generated which is illustrated in Figure 6(b). This convection is driven by reconnection of open field lines with the IMF field lines that takes place on the surface of the tail (Maezawa, 1976). This reconnection only alters the combination of the geomagnetic and the IMF field-line portions that constitute an open field line, and it does not increase the flux of the open field lines in the tail. As shown in Figure 6(b), when an open field line  $b$  reconnects with the IMF 2-2' field line on the tail surface, its far part is blown away by forming the field line 3' and is replaced by the field line 2. Subsequently this open field line moves through the tail in sequence of  $c3, d4, e5$ , and  $a$ , and return to  $b$  where it changes partner again. The convection of this type does not involve reconnection operating inside the magnetotail, and the open character of the field lines does not change by reconnection on the magnetopause.

Both types of the convection seem to be generated together under the northward IMF polarity except possibly when IMF is very nearly due northward. Convection streamlines in the cross section of the tail in such times is illustrated in Figure 9. Field lines in low latitudes (in the shaded region) flow into the neutral sheet (dashed line) and are reconnected there, but field lines in high latitudes (in the unshaded region) traverse the tail in the dawn / dusk direction and reach the other side of

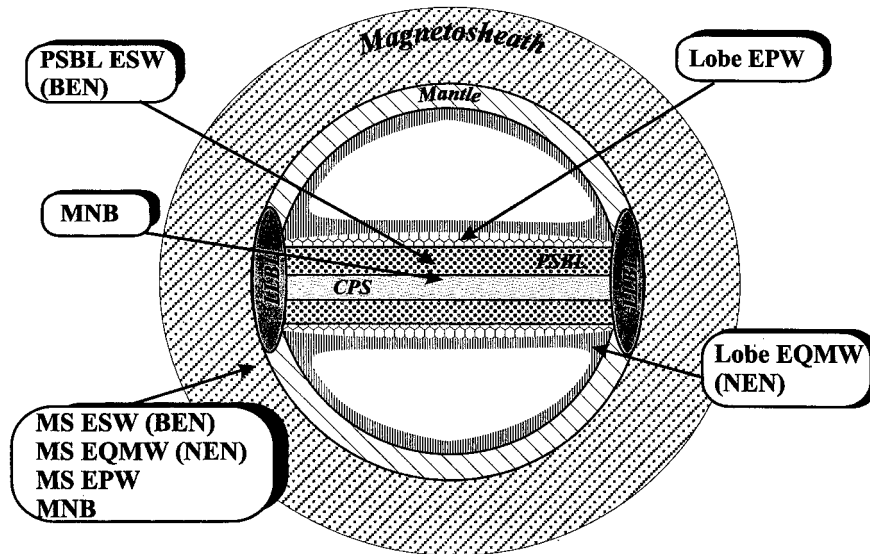


Figure 10. Plasma regimes in geospace and characteristic wave modes observed in respective regimes (Matsumoto et al., 1998). Wave modes are designated as ESW: electrostatic solitary wave, EQMW: electrostatic quasi-monochromatic wave, EPW: electron plasma wave, BEN: broad-band electrostatic noise, NEN: narrow-band electrostatic noise, and MNB: magnetic noise burst.

the tail surface (Nishida et al., 1998). Convection streamlines that reach the neutral sheet correspond to the convection type of Figure 6(a), while those that traverse the tail to that of Figure 6(b). Ionospheric projections of these convection streamlines have been called the merging cell and the lobe cell, respectively, according to the nomenclatures introduced by Reiff and Burch (1985) who first suggested that reconnection in the tail can take place even when the IMF is northward. Numerical simulation of reconnection processes on the magnetopause has clearly demonstrated that these two kinds of convection cells are generated together (Tanaka, 1999).

#### 2.4. PLASMA REGIMES IN THE MAGNETOTAIL

Two basic regimes that constitute the magnetotail are the lobes that represent the open field lines (illustrated by blue lines in Figure 1) and the plasma sheet that is imbedded between them. Magnetic field lines in the plasma sheet are the tailward extension of the closed field lines (corresponding to the tailward part of the green field lines) in the near-Earth tail and the IMF-type field lines (red field lines) in the distant tail. From relative frequency of plasma sheet and lobe observations by ISEE 3, Fairfield (1992) has obtained  $3.4 R_E$  as the average value of the half thickness of the distant plasma sheet; this estimate is likely to be strongly influenced by the cases when the plasma sheet bulged due to passages of plasmoids.

In addition to the lobe and the plasma sheet, several boundary regimes have been identified in the magnetotail, and an orthodox picture of the locations of these boundary regimes is given in Figure 10 (Matsumoto et al., 1998). At the boundary between the magnetosheath and the tail lobe there is the plasma mantle in high latitudes and the LLBL (Low-latitude boundary layer) in low latitudes. The plasma mantle is the part of the lobe into which cold plasma of the solar wind has been introduced together with the recently reconnected field lines. The LLBL is the low latitude region where the solar wind and the hot tail plasma are seen as a mixture. The PSBL (plasma sheet boundary layer) is a boundary region between the plasma sheet (CPS: central plasma sheet) and the lobe. All these regimes are symmetrically drawn here for simplicity, but this is not necessarily so. For example, the plasma mantle shows a pronounced dawn/dusk asymmetry that is dependent on the sign of the IMF  $B_y$  (Gosling et al., 1985). This is because, as illustrated in Figures 7 and 8, the open field lines together with the solar wind plasma enter the tail from dawn side in the northern tail and dusk side in the southern tail when IMF  $B_y > 0$ . The asymmetry is reversed when  $B_y < 0$ . Thickness and width of the mantle seem to increase with the downtail distance.

Empirical criteria for respective plasma regimes have been derived and used for semi-automatic region identification of GEOTAIL observations (Eastman et al., 1998; Christon et al., 1998).

Figure 10 also indicates the plasma wave modes that are characteristically observed in each regime. While this is a research area where much has been learned by the GEOTAIL mission, the subject is not covered in this article and interested readers are referred to a comprehensive review by Matsumoto et al. (1998).

### 3. Sources of the tail plasma

This section deals with sources of plasmas that populate the magnetotail. Reconnection on the magnetopause brings the solar-wind plasma into the tail and the convection transports this plasma throughout the magnetosphere. Ionospheric plasma is also supplied to the tail but, interestingly, its access is controlled by reconnection on the magnetopause. Presence of the Low Latitude Boundary Layer where the magnetosheath plasma is loaded on the heated tail plasma may suggest that there is yet another mechanism of the solar-wind plasma entry other than reconnection.

#### 3.1. ENTRY OF THE SOLAR WIND PLASMA INTO THE MAGNETOTAIL

Potential sources of plasmas that fill the magnetotail are the solar wind and the Earth's ionosphere. Both of them have their own assets; the solar wind plasma is closer to the tail plasma in energy, while the ionospheric plasma is abundant. The solar wind has generally been taken as the major source, but it has been contended that the ionosphere could provide enough plasma to the tail (Chappell et al., 1987).

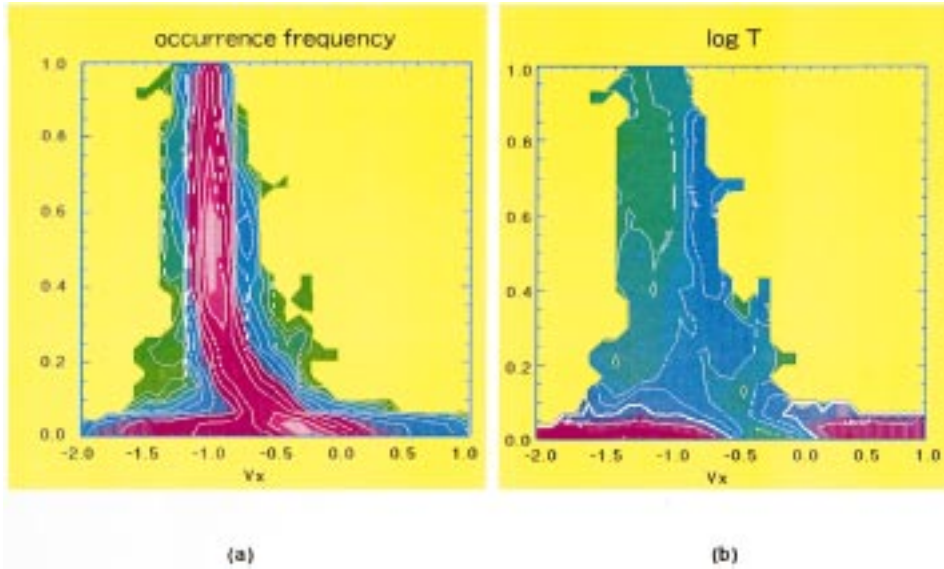


Figure 11. Dependencies of the plasma sheet parameters on the solar wind parameters; (a) ion temperature against the kinetic energy of the solar wind flow, (b) density against density, and (c) normalized density against the IMF  $\theta$  angle. Plots are color coded by IMF  $\theta$  angle in (a) and (b), and by the normalized temperature in (c) (Terasawa et al., 1997).

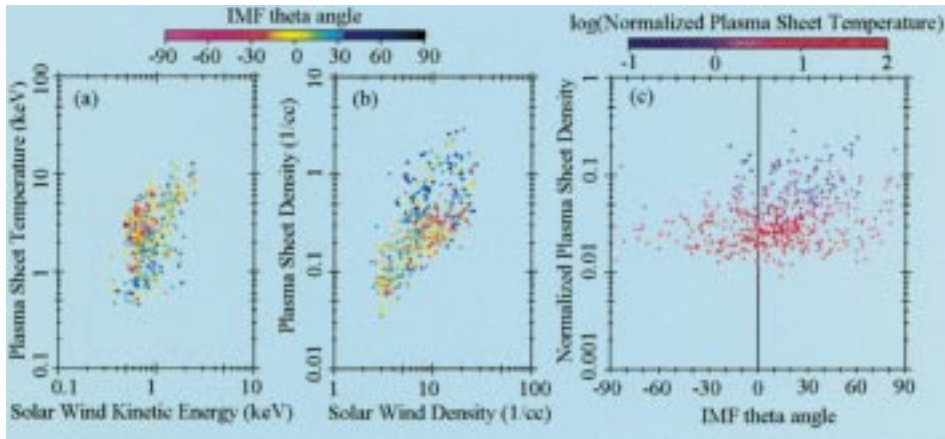


Figure 12. Contour maps of (a) occurrence frequency and (b) temperature of ions in the (density, velocity) coordinates normalized to simultaneous solar wind values observed upstream. Magnetosheath data points are included in the map. Both occurrence frequency and temperature increase from green to pink. The thick white line in (b) represents the 300 eV contour (Maezawa and Hori, 1998).

In order to see if indeed the solar wind is the major source, the properties of the tail plasma are compared with those of the solar wind. In Figure 11 the horizontal and the vertical axes are flow velocity and density of the tail plasma, respectively, which are normalized by simultaneously observed values of the upstream solar wind. GEOTAIL data obtained in the distant tail beyond  $150 R_E$  are used in this analysis. The contour map of occurrence frequency is drawn in Figure 11(a) and the ion-temperature contour is given in Figure 11(b). A clear trend is seen in Figure 11(a); this trend starts from the normalized density of 1 and velocity  $-1$  and continues smoothly to smaller values until a different state is reached at the normalized density of about 0.1. Thus density and velocity of the plasma that fills the tail connect smoothly with those of the solar wind, and this makes a very strong case for the solar-wind source of the tail plasma (Maezawa and Hori, 1998).

Sharp transition in the state of the tail plasma is seen at the normalized density of about 0.1 in Figure 11. At this transition the ion temperature changes sharply and becomes larger than about 300 eV, which is delineated by a thick white line in the figure. The flow velocity also changes and can take a wide range of values; it can be tailward or earthward, and when tailward, it can be more than twice as fast as the upstream solar wind. This transition clearly demonstrates that acceleration / heating mechanisms operate in the magnetotail, and the resulting accelerated / heated plasma fills the plasma sheet.

Density and ion temperature in the plasma sheet are governed not only by the solar wind conditions but also by the north-south  $\theta$  angle of the IMF. Figure 12 shows the dependencies of (a) the ion temperature on the upstream solar-wind kinetic energy and (b) the ion density on the upstream solar wind density, where the data points are color coded by the IMF  $\theta$  angle. Both are well correlated as expected from the dominance of the solar wind as the source of plasma. In addition to these dependencies, it is seen that the ion temperature is higher (lower) and density is lower (higher) when the IMF is southward (northward). The IMF dependence of density is better seen in Figure 12(c) where the densities normalized by the solar wind values are plotted against the  $\theta$  angle while the temperature is represented by color code. The plasma sheet tends to be (relatively speaking) tenuous and hot when the IMF is southward but dense and cold when it is northward. The GEOTAIL data in the near tail region at  $-50 < x < -15 R_E$  have been used and a careful procedure is adopted to eliminate the possible dependence of the parameters on the distance from the neutral sheet as expressed by  $B_x$ . The correlation during northward IMF periods is improved when the solar wind values are averaged for 9 hours preceding to the tail observations (Terasawa et al., 1997). Reflecting the IMF polarity dependencies of the plasma sheet characteristics, densities of  $H^+$  and  $He^{++}$  in the plasma sheet decrease with increase in the geomagnetic activity while their mean energy per nucleon increases (Lennartsson, 1992).

Electron and ion temperatures are highly correlated in the plasma sheet, and the  $T_i/T_e$  ratio takes a nearly constant value (about 7 at  $-17 < x < -9 R_E$ ) in the central plasma sheet over a wide range of temperatures (Baumjohann et al., 1989).

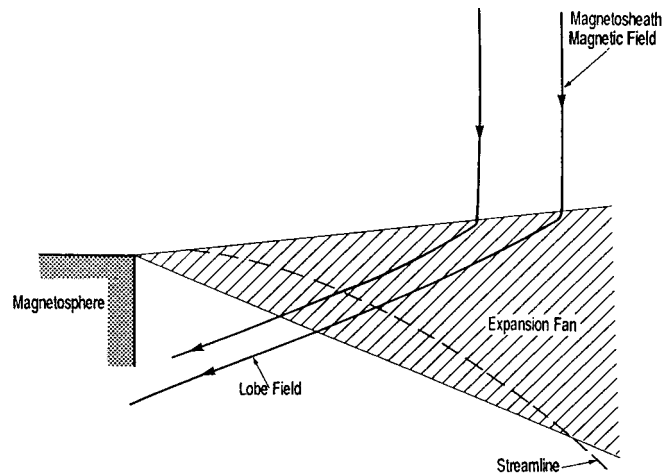


Figure 13. Field and plasma flow lines through a slow-mode expansion fan representing the plasma mantle for the case where the IMF and the tail field are coplanar (Siscoe and Sanchez, 1987).

The ratio obtained from GEOTAIL observations in the 10 to 30  $R_E$  range is 4.5 (Paterson and Frank, 1994). According to ISEE 3 observations the ratio (where the ion temperature is deduced from the pressure balance between the lobe and the plasma sheet) is 7.8 at  $|x|$  of 30–60  $R_E$ , 6.7 at 60–100  $R_E$ , 4.8 at 100–210  $R_E$ , and 5.7 at  $|x| > 210 R_E$  (Slavin et al., 1985).

Properties of the solar wind plasma that forms the plasma mantle have been examined theoretically by Siscoe and Sanchez (1987). They have taken the convection model of Figure 6(a), in which newly opened field lines are transported to the tail, as the framework and have suggested that a standing slow-mode expansion fan turns solar-wind flow in these field lines into the plasma mantle and converts the magnetosheath field into the tail lobe field. The situation can be idealized geometrically as an expansion around a sharp corner as illustrated in Figure 13. The magnetosheath plasma expands into a wind-shadow vacuum of the lobe, and a standing wave front is formed since the slow-mode wave that is produced from the vacuum propagates toward the magnetosheath as fast as the plasma streams into the tail. Figure 13 is for the case where the IMF and the tail field are coplanar, and in general a rotational discontinuity is formed on the magnetosheath side to align the fields properly at the slow-mode fan.

Figure 14 compares the prediction of the slow-mode fan model with the GEOTAIL observation when the mantle is traversed many times at  $x = -170 R_E$ . For the upstream values of the density, speed and magnetic field strength, use has been made of the measurements when the spacecraft was closest to the magnetosheath. Two runs with high and low sonic Mach numbers, which respectively correspond to the smallest and the highest  $T_e$  measured in the magnetosheath, are made. Comparisons are made for (a) the magnetic field (B)-vs-velocity, (b) B-vs-density, and (c) density-vs-velocity relations for these two runs. It is seen that the

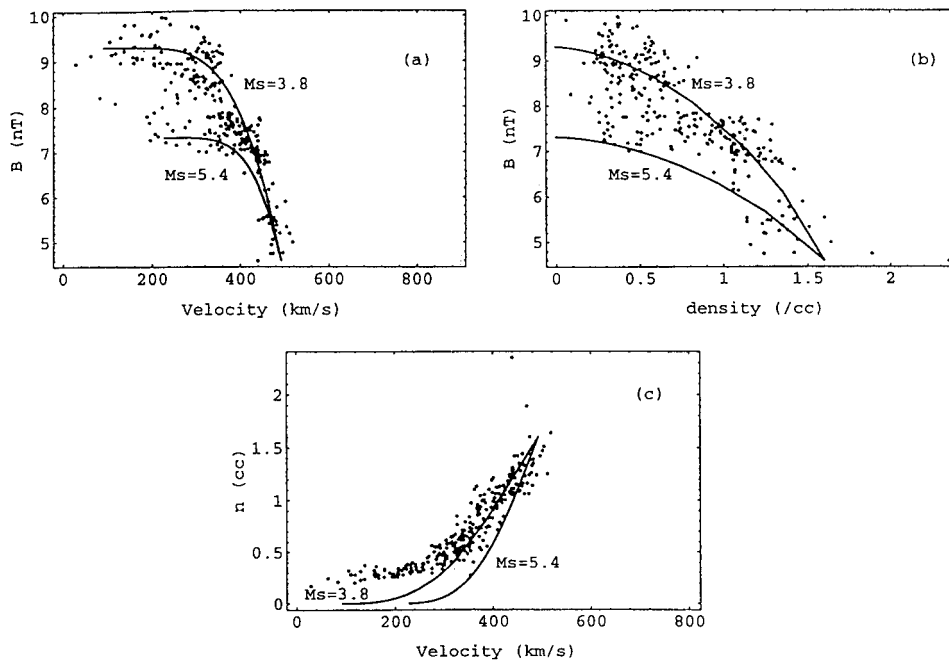


Figure 14. Comparison of the predicted magnetic field strength ( $B$ ) and density ( $n$ ) of the slow-mode expansion fan model with those observed. Two values of the sonic Mach numbers are used (Shodhan et al., 1996).

model profiles bracket the observations reasonably well (Shodhan et al., 1996). The density-velocity relation of Figure 11(a) has also been found to be consistent with the prediction of the slow-mode expansion fan model (Maezawa and Hori, 1998).

The reason why two values of  $T_e$  have been used in the above comparison is that the electrons are heated in the mantle while both ions and electrons should cool as they expand through the mantle. This means that electrons are not governed by the physics of the slow-mode expansion fan model alone and the reason remains to be understood (Shodhan et al., 1996).

Entry of the solar wind plasma into the mantle has been confirmed by continuity of the plasma characteristics across the magnetosheath-tail boundary; In the energy-time spectrograms of the ions it is often observed that a band representing a plasma population continues smoothly from the magnetosheath to the mantle. Both density and flow speed in the mantle are seen to decrease with increasing separation from the boundary region, as expected for the expansion of the magnetosheath plasma bounded by the slow-mode expansion fan (Hirahara et al., 1998; their Figures 1a and 4). However, more complex cases are also observed, and here we shall discuss such an example of the plasma observations in the magnetosheath-tail boundary region.

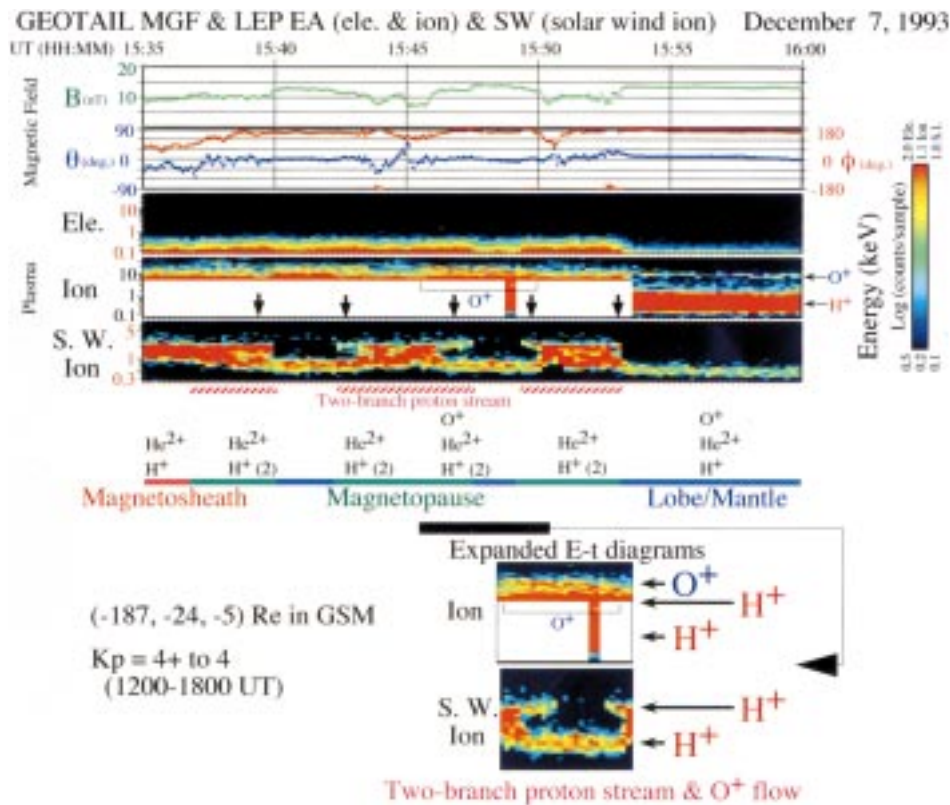


Figure 15. Magnetic field and plasma observations for an interval involving crossings of the tail magnetopause (Hirahara et al., 1997). See text.

This example is given in Figure 15. The top five panels show magnetic field strength (green), field direction (purple for  $\theta$  and red for  $\phi$ ), and energy-time ( $E-t$ ) spectrograms for electrons, tailward flowing ions in the EA mode, and ions in the SW mode. In the present situation where the flow is tailward the relevant difference between EA and SW modes is that the low- (high-) energy part is better seen in the SW (EA) mode data. The observation was made in the distant tail at  $x = -187 R_E$ .

Starting from the beginning of the interval, the SW-mode  $E-t$  spectrogram shows the tailward streaming hot protons of the magnetosheath. As the spacecraft enters the tail, this band splits into low and high energy branches, that is, two-branch proton stream is observed. The low-energy branch is at several hundred eV and the high-energy branch is at a few keV. As indicated by downward arrows above the SW-mode  $E-t$  spectrogram, such two-branch proton beams are seen each time on the tail side of the transition region. An expanded diagram is given at bottom right of the figure. Among these two bands the low-energy band persists throughout the interval of the lobe observation in this figure, and its energy decreases or increases as the spacecraft moves into or away from the lobe. This

## GEOTAIL LEP-SW &amp; EA-ion

## Velocity Distribution December 7, 1993

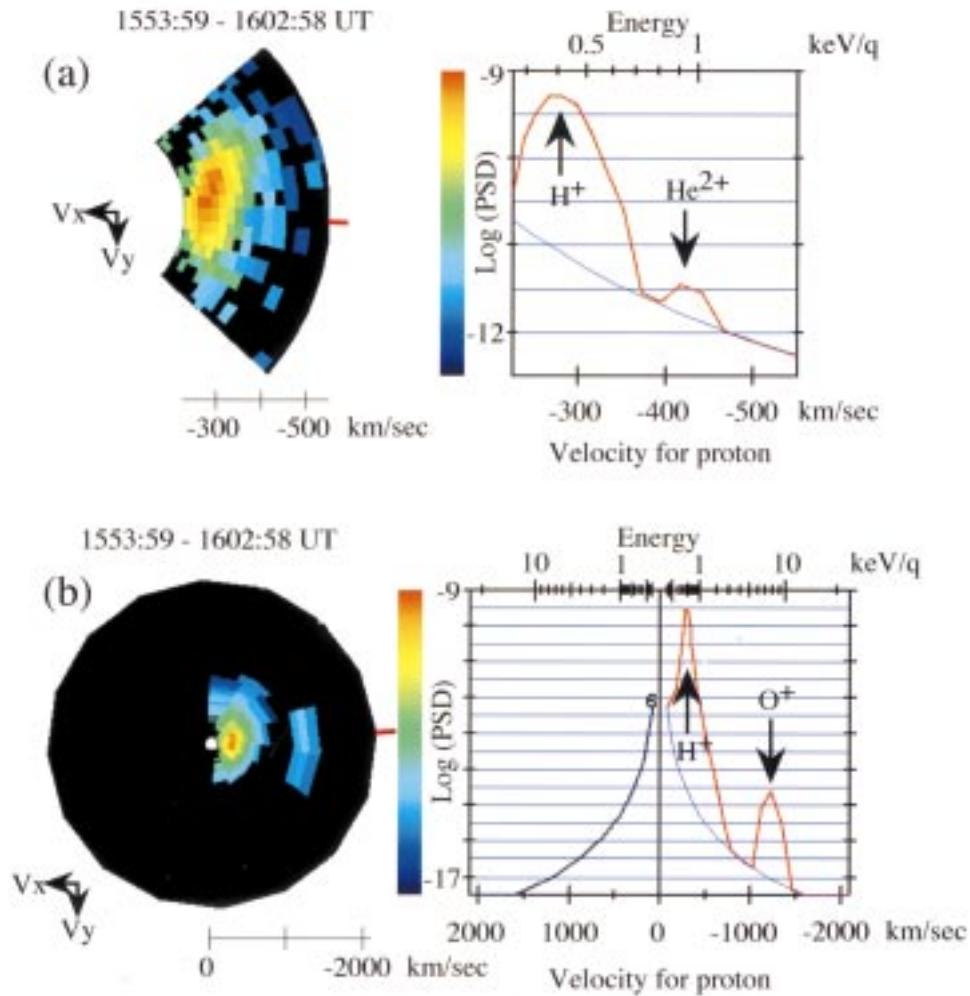


Figure 16. Velocity distribution functions observed in the mantle region by (a) the SW detector and (b) EA detector (Hirahara et al., 1997). Observations of the mantle plasma by these two detectors emphasize different energy ranges. Real speed of  $O^+$  is one quarter of the values given in the axes.

low-energy band should represent the entrant solar wind protons constituting the plasma mantle. The solar-wind origin of these protons is supported by the fact that they are accompanied by  $He^{++}$  ions; as seen in Figure 16(a) the velocity distribution function of the ions below a few keV in the plasma mantle has two peaks which can be identified as protons and  $He^{++}$  ions (Hirahara et al., 1997).

In Figure 15 the upper-energy band is observed at each transition from the magnetosheath to the mantle but not deep inside the mantle. Its energy is continuous with the high energy part of the solar-wind ions in the magnetosheath and increases toward the mantle. This suggests that the solar-wind ions are accelerated locally on the tail surface and injected into the mantle. Such accelerated magnetosheath ions have often been observed on the magnetotail side of the tail surface, and they seem to be due to magnetic reconnection that occurs on the tail surface (Hirahara et al., 1997) when the local magnetic field has large shears, that is, the magnetic fields are close to being locally antiparallel (Gosling et al., 1996). In the events of Figure 15 the drift motion of the tail plasma is observed to be directed from the mantle toward the magnetosheath in agreement with the interpretation in terms of reconnection.

The origin of the upper branch ions can be understood in two ways. The first interpretation is based on the convection of Figure 6(b) which is generated by reconnection of the IMF with the geomagnetic field lines on the surface of the magnetotail. These geomagnetic field lines are open field lines, and their reconnection with the IMF produces on the anti-sunward side of the reconnection site the reformed IMF field lines labeled 3' and 4' in the figure which are blown away. It is possible that such field lines are observed here. The second possible interpretation is based on the convection profile of Figure 6(a) but assumes in addition that reconnection occurs also on the tail surface. The sequence considered is; (1) open field lines are produced by reconnection on the dayside, (2) they are convected into the tail, (3) together with the solar wind plasma so that the plasma mantle is formed, (4) subsequently, some of these open field lines are reconnected again with the IMF on the tail surface, and (5) the accelerated solar wind plasma is injected locally into these re-reconnected field lines of the mantle (Hirahara et al., 1997). The site of the re-reconnection is not stationary as it migrates with the magnetosheath flow, and the ions which are accelerated on the sunward side of the re-reconnection site may be directed sunward or tailward in the inertial frame depending on the ratio of the Alfvén speed to the flow speed in the magnetosheath just adjacent to the magnetopause (Gosling et al., 1991).

The open field lines serve also as a channel of entry for the non-thermal component of the solar wind electrons called 'strahl' electrons. It has been confirmed that these electrons change their flow direction from anti-sunward to earthward as they enter the magnetotail from the magnetosheath tracing the open field lines (Shirai et al., 1998).

### 3.2. PLASMA OF THE IONOSPHERIC ORIGIN

In the EA mode ion E-t spectrogram of Figure 15 there is a band at an energy higher than those of the protons. As seen in the spectrum in Figure 16(b) this band peaks at the energy that is 16 times that of  $H^+$  observed at the same time, and hence they can be interpreted to represent a beam of cold oxygen ions that streams tailward with the same flow speed as the proton beam (Hirahara et al., 1997). Since  $O^+$  ions are

present in the Earth's ionosphere but are scarce in the solar wind which originates from the solar corona, their presence is a clear manifestation that the ionosphere also supplies plasma to the magnetotail (Frank et al., 1977; Candidi et al., 1982; Mukai et al., 1994).

The O<sup>+</sup> beam tends to be observed in the mantle during geomagnetically active times (Seki et al., 1998). At such times the convection is of the type of Figure 6(a) and field lines and plasma move equatorward in the tail lobe. The ionospheric ions could be carried quite significantly equatorward by this convection while they flow tailward along field lines to the distant tail. If energy of the oxygen beam is only 1.2 keV that corresponds to the field-aligned speed of 120 km s<sup>-1</sup>, even weak convection that is associated with electric field of only 0.1 mV m<sup>-1</sup> moves the ions equatorward by 10 R<sub>E</sub> or more before they reach the distant tail beyond 100 R<sub>E</sub> (Baker and Pulkkinen, 1998), so that these ions would not have been able to stay in the mantle down to the distant tail.

Figure 17 shows plots of perpendicular (top) and parallel (bottom) components of the plasma bulk velocity against distance  $X'$  along the tail. ( $X'$  is the same as used in Figure 4.) The data points for the oxygen beam events are plotted with red, while all the mantle data are plotted with blue. Mean, minimum and maximum velocities are given in each panel. The component  $V_{\perp}$  perpendicular to the magnetic field is the sum of the convection velocity and the velocity of the tail flapping which are the same for all species. The field-aligned velocity  $V_{\parallel}$  tends to be higher for observations at greater distances for the entire data including the oxygen beam data. It is also seen that while the perpendicular velocity  $|V_{\perp}|$  does not differ significantly between the entire mantle data and the oxygen beam events, there is a significant difference in the field-aligned velocity between them. For the oxygen beam events  $V_{\parallel}$  is always above the bottom area shaded by green, and the average of  $V_{\parallel}$  is significantly higher when the oxygen beam is observed as compared to when it is not. Hence it is not the weakening of the convection but high speeds of the field-aligned flow that make the oxygen beam stay in the mantle till far downstream (Seki et al., 1998). The ions upflowing from the dayside polar-cap ionosphere can indeed have energies of low tens of keV at the heights of a few R<sub>E</sub> (André and Yau, 1997). In the above analysis, selection criteria of the mantle points are  $N_i < 2.0 \text{ cm}^{-3}$ ,  $T_i < 400 \text{ eV}$ ,  $\beta_i < 0.5$ ,  $|B| > 5.0 \text{ nT}$ ,  $\theta_B < 30^\circ$  and duration  $> 5 \text{ min}$ . The mantle points accounted for about 9% of the data, and the cold oxygen beam was observed in about 10% of them. In such events, the O<sup>+</sup>/H<sup>+</sup> density ratio is about 1.2% on average.

The occurrence of the cold oxygen ion beams in the distant mantle is controlled also by the  $B_y$  component of the IMF. As illustrated in Figure 18(a'), these beams (COB) are observed preferentially in the 'loaded' sector of the tail lobe where the open field lines which are produced by reconnection on the dayside magnetopause are introduced and loaded. As illustrated in the figure the loaded sectors are on the north-dawn and south-dusk side when the IMF  $B_y$  is positive, and they are at mirror images of these when  $B_y$  is negative. This observation clearly demonstrates that

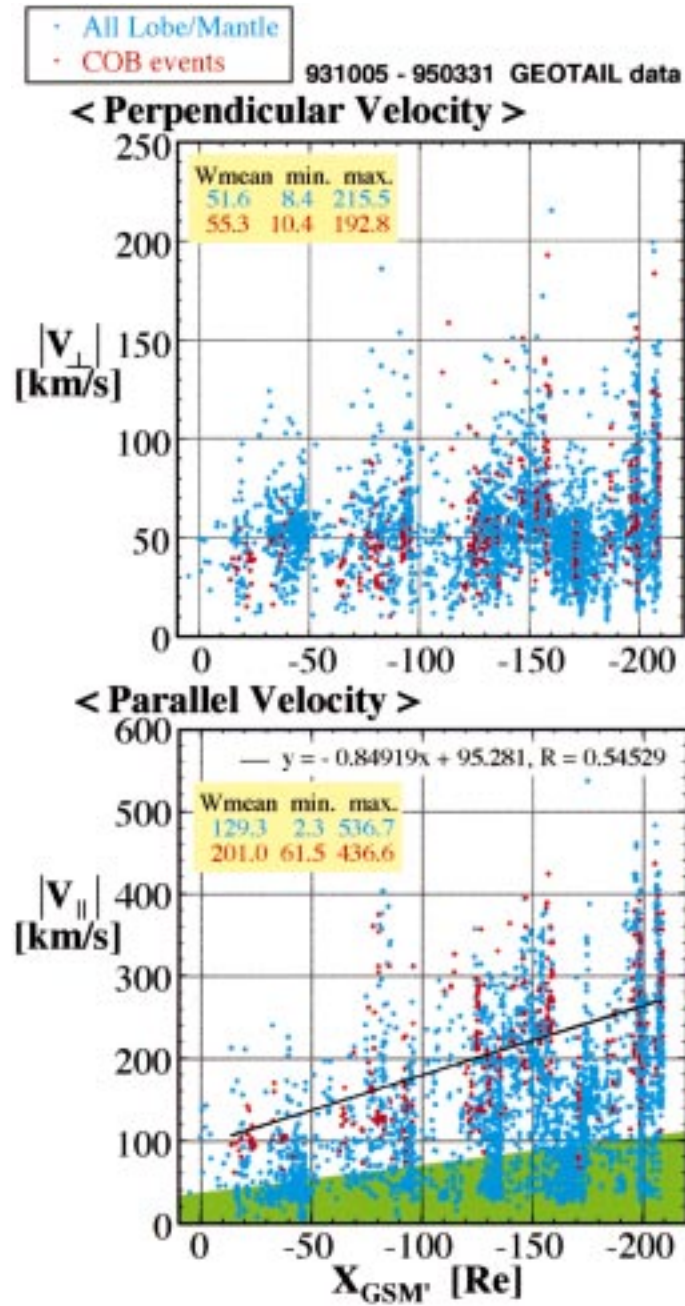


Figure 17. Dependence of the flow velocity on the  $X'$  coordinate which is in the sun-Earth direction corrected for the aberration. *Top*: component perpendicular to the magnetic field, and *bottom*: field-aligned component. Blue and red points correspond to the entire mantle data and the cold oxygen ion beam events, respectively (Seki et al., 1998).

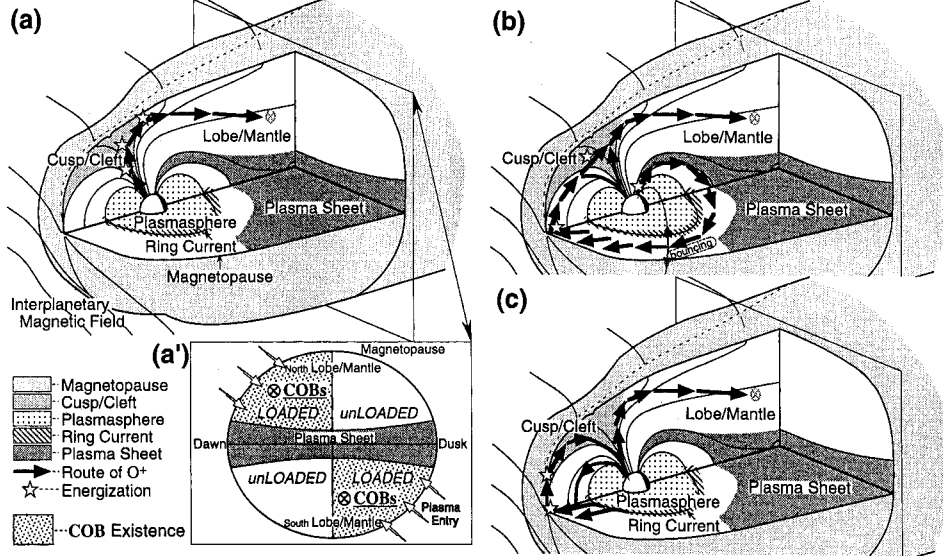
Possible Supply Routes of Cold  $O^+$  Beams (COBs) in Tail Lobe/Mantle

Figure 18. Observed positions of the cold oxygen ion beams in the tail and their possible supply routes. (a'): Cold oxygen ion beams (COB) are observed only in the loaded sectors where newly generated open field lines are transported from the dayside, and this suggests that they are brought to the magnetotail via one of the conceivable transport routes (a) through (c) (Seki et al., 1998).

acceleration and / or transport of the cold ions from the ionosphere is controlled by the IMF  $B_y$ -dependent interaction between the solar wind and the magnetosphere. Figure 18(a)–(c) illustrate possible supply routes of the cold oxygen ions to the mantle. In (a), the ions are supplied in the dayside cusp / cleft region into the newly generated open fluxes whose position depends on the sign of the IMF  $B_y$ . In (b), the upflowing ions on the nightside drift halfway around the Earth, and those which happen to be on the field lines that are reconnected with the IMF are transported to the mantle together with the newly generated open field lines. In (c) the ions of the ring current or the plasmasphere are convected toward the dayside magnetopause and loaded on the newly opened field lines when these closed field lines become reconnected with the IMF (Seki et al., 1998). From comparison of the phase space densities of the cold  $O^+$  ion beams with the precipitating  $O^+$  ions in the dayside polar region at low altitudes (1200–3400 km) observed by FAST it has been seen that  $O^+$  population in the dayside magnetosphere on closed flux tubes is quantitatively adequate to supply the  $O^+$  beams in the mantle (Seki et al., 1999).

## 3.3. LOW LATITUDE BOUNDARY LAYER

On the dawn / dusk flanks of the magnetosphere, there is a boundary region where plasma shows intermediate characteristics between the magnetosheath and the plasma sheet. This region, called 'Low Latitude Boundary Layer (LLBL),' consists of

two layers. One is characterized by lower density, higher temperature, and very slow flow speed, and the other by higher density, lower temperature, and speed comparable with that in the magnetosheath. Temperature and density in both layers of the LLBL are bracketed by the respective parameters in the magnetosheath and plasma sheet. The magnetic field is magnetosphere-like in both layers (Sckopke et al., 1981).

The higher-density layer is the outer layer and has been called 'boundary layer proper' (Sckopke et al., 1981), 'outer LLBL' (Traver et al., 1991), 'outer boundary layer' (Le et al., 1996) and 'MSBL' (Fuselier et al., 1995). The lower-density layer which Sckopke et al. (1981) designated as 'halo' is now considered to be the inner layer and called 'stagnation region' (Williams et al., 1985; Traver et al., 1991), 'inner boundary layer' (Le et al., 1996), and 'LLBL' (Fuselier et al., 1995). Hereafter we shall use the inner / outer LLBL designation.

While most earlier studies of the LLBL were made in the dayside and dawn / dusk terminator regions of the magnetopause, GEOTAIL has observed the extension of the LLBL downtail to distances of about  $40 R_E$  (Fujimoto et al., 1998a, b). Figures 19 to 21 represent an example of the LLBL observation on the duskside tail surface at  $x = -14 R_E$ . Figure 19 shows three components of the magnetic field (in nT), ion density ( $\text{cm}^{-3}$ ) and temperature (keV), and three components of the ion bulk flow speed ( $\text{km s}^{-1}$ ). The IMF is northward according to the simultaneous observation by the WIND satellite. The data can be divided into two intervals: those with the lower temperature and higher speed (the shaded intervals) and with the higher temperature and almost no flow. The former is the outer LLBL (or, magnetosheath) and the latter is the inner LLBL, and the magnetic field is northward in both regions. Top panel of Figure 20 is the  $E-t$  spectrogram of omnidirectional ions for an interval of the inner LLBL (06:30 to 08:30), and it shows that two ion populations coexist, of which one is at several keV and the other at  $<1$  keV. Figure 21(a) is the ion distribution function at 07:10:57 which is marked by a vertical arrow in Figure 20. Shown to the left is a slice of the three-dimensional distribution functions by a plane including the magnetic field ( $\mathbf{B}$  direction) and the ion bulk velocity ( $\mathbf{C}$  direction), and to the right is the cut of this distribution function along the dashed line in the left panel. The ion distribution function in Figure 21(a) consists of two components. The colder component that is located close to the origin is similar to the magnetosheath ions, and the warmer component above the transition energy of about 2.2 keV is like the plasma sheet ions. Note that flow speeds are low for both components; the slow speed of the bulk flow is not due to mixing of plasmas having opposite flow directions. The distribution function for electrons shown in Figure 21(b) is football shaped, which means that the electrons are characterized by bi-directional anisotropy where parallel-to-perpendicular ratio is  $\sim 10$  at 100–200 eV. The northward magnetic field, bi-directional electron anisotropy, and very low flow speed suggest that the inner LLBL is on the closed field lines. LLBL is observed on both dawn side and dusk side boundary regions of the tail, but the separation between the cold magnetosheath ions and the plasma

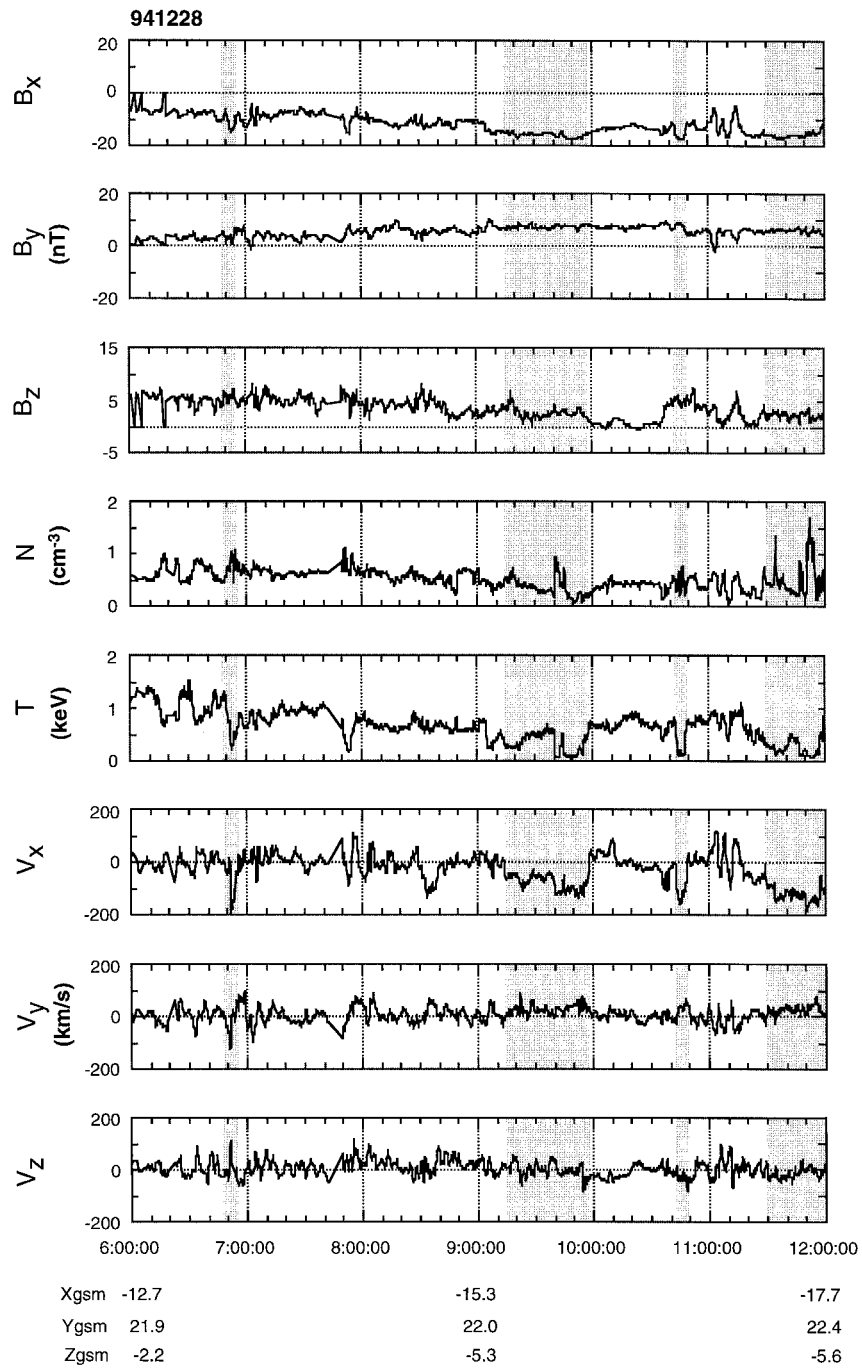


Figure 19. Overview of the field and particle data of the inner LLBL on the dusk side (Fujimoto et al., 1998a). The inner LLBL was observed except during the shaded intervals when the spacecraft was in the outer LLBL (or, magnetosheath).

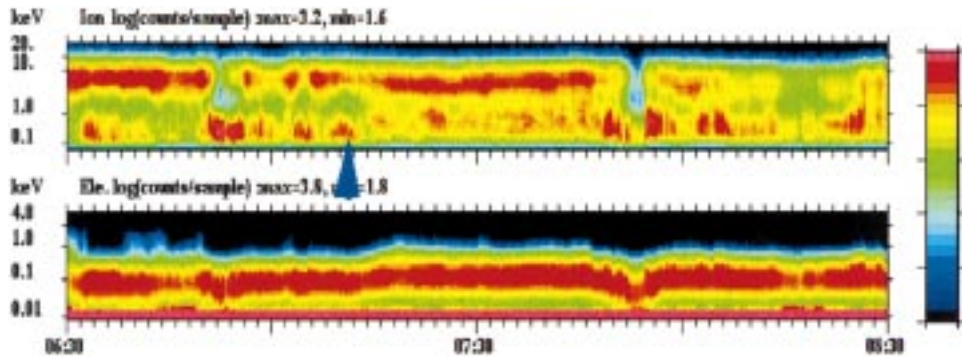


Figure 20. *E-t* spectrogram of omnidirectional (*top*) ion and (*bottom*) electron fluxes in the inner LLBL (Fujimoto et al., 1998a).

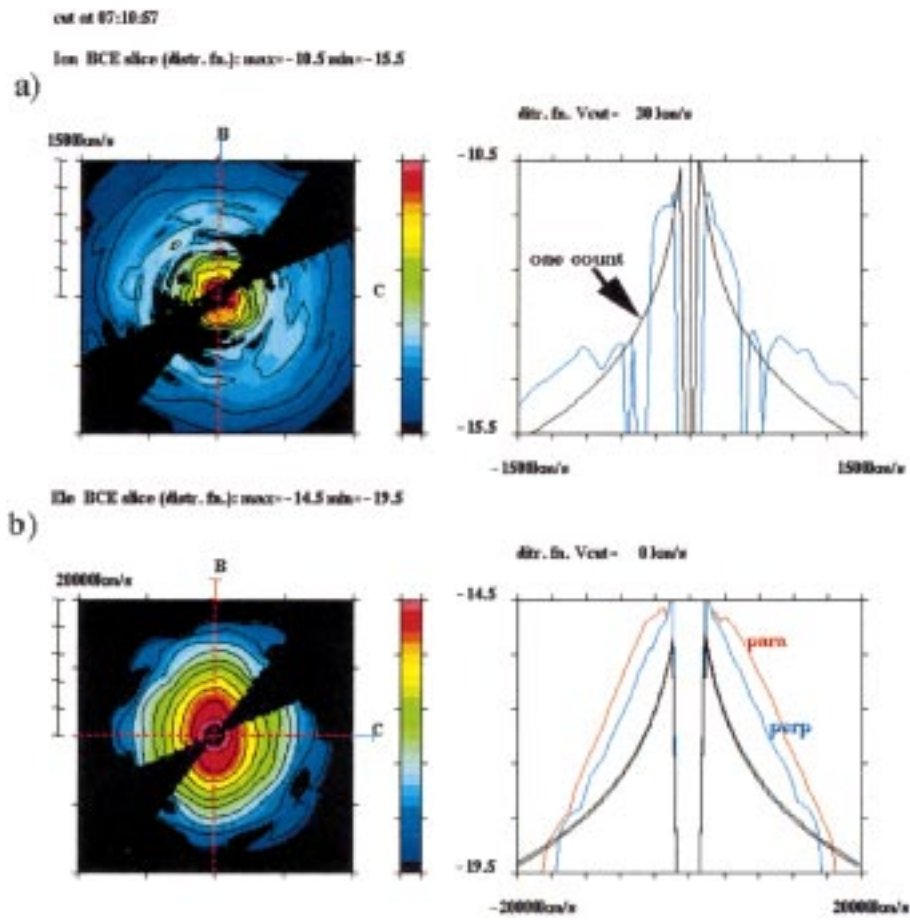


Figure 21. (a) Ion and (b) electron velocity distribution function in the inner LLBL. Two dimensional contours in a plane containing the magnetic field (**B**) and the bulk velocity (**C**) are on the left, and a cut along the dashed line(s) in the left panel is to the right (Fujimoto et al, 1998b).

sheet ions in energy spectrum is more evident in duskside cases. The observations suggest that the ions and electrons of the magnetosheath find access into the closed field lines in the boundary region, and in this process the magnetosheath electrons are heated in the parallel direction (Traver et al., 1991; Fujimoto et al., 1996a).

The inner LLBL which is characterized by cold dense ions and bidirectional electron anisotropy is not limited to a thin layer but can be seen over a thickness of several  $R_E$ ; The entrant magnetosheath plasma can be distributed over a significant volume (Fujimoto et al., 1998b). It has been suggested that the  $y$  dependence of temperature and density seen under the northward IMF, in which temperature is lower but density is higher at the dawn and dusk edges of the tail as compared with the central part, reflects the presence of the LLBL (Terasawa et al., 1997). The electron spectrometer on board INTERBALL-TAIL has also detected the characteristic features of the inner LLBL, that is, the coexistence of cold 100 eV electrons with bidirectional anisotropy and hot electrons with loss-cone distribution, up to  $5 R_E$  inside the dawnside magnetopause at  $x \sim -5 R_E$ . The detection of this feature was intermittent (Sauvaud et al., 1997).

The outer boundary layer in which the flow is tailward has been suggested to be on open field lines since it contains mainly the magnetosheath-like plasma and only a tenuous hot component. The bulk of the heated magnetosheath-like plasma in the outer boundary layer is often accelerated to a velocity well above that of the magnetosheath flow in the field-aligned direction, and this has been attributed to reconnection of the northward IMF with geomagnetic field lines on the high-latitude magnetopause (Le et al., 1996). When the IMF is northward the recently reconnected open field lines are carried by the solar wind along the tail flanks since they extend across the equatorial plane (Figure 1(c)) so that it is expected that they form a layer on the dawn / dusk flanks of the magnetotail.

It has been suggested that the inner boundary layer is formed on closed field lines which are produced by re-reconnection of open field lines. In Figure 6(b) which illustrates the configuration and convection of the open field lines when the IMF is northward, the field line labeled 2 is being reconnected and then it moves to 3. This field line, which is 'open' as it is connected to the ionosphere only on one (in this case, northern) end, may become 'closed' by reconnecting again with another open field line on the southern tail surface. Figure 22 illustrates this sequence where it is supposed that reconnection occurs first on the southern tail surface. Figure 22(a) indicates by a circle where geomagnetic field line (thin solid line) is to be reconnected with the northward IMF (thin dashed line), and Figure 22(b) shows a newly formed open field line (thick dashed line) and the point (circled) where this field line is to be reconnected again. In Figure 22(c) the second reconnection has transformed the open field line to a closed field line (thick solid line). The closed field lines that are formed in this manner can have plasmas of both magnetospheric and solar-wind origins; The magnetosheath plasma which has been accelerated in the course of the reconnection process streams into these field lines while they are open, and the magnetospheric plasma is provided from the closed

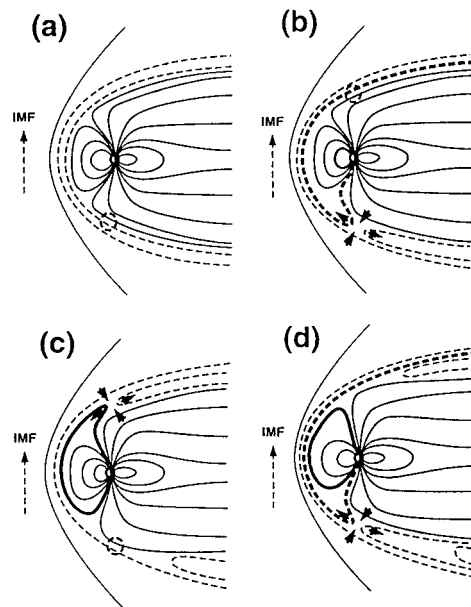


Figure 22. Sequence of reconnection to produce closed field lines that could have both magnetosheath and magnetospheric plasma populations. Reconnection (at b) followed by re-reconnection (at c) forms such closed field lines (solid curve at d) (Le et al., 1996).

field lines through gradient and curvature drifts (Le et al., 1996). The tailward motion of these field lines would be slow or stagnant since there is no longer any supply of momentum from the solar wind once the field lines become closed. It has also been suggested that re-reconnection of open field lines that would occur in random and patchy manner on the dayside magnetopause under the northward IMF produces closed field lines filled with the magnetosheath plasma (Nishida, 1989).

The presence of the magnetosheath plasma on the closed field lines could also be due to diffusion. Diffusion by resonant interaction with high-frequency plasma waves seems to be too weak (Treumann et al., 1995), but the ion mixing driven by the Kelvin-Helmholtz instability (Fujimoto and Terasawa, 1994) is another possibility that is to be explored. As an alternative interpretation of the inner LLBL, Fuselier et al. (1995) has suggested that it is on open field lines and the bidirectional electrons which characterize this layer represent the electrons which are energized at the magnetopause current layer and are reflected at mirror points in low altitudes.

#### 4. Acceleration and Heating in the Magnetotail

This section addresses acceleration and heating in the magnetotail. It should be no exaggeration to say that this is the most important role of the tail in magnetospheric physics. The magnetic energy stored in the magnetotail is converted to the kinetic

energy and produces hot and accelerated plasmas. The energy conversion is due to reconnection of the stretched field lines of the magnetotail. The site of energy conversion is not limited to vicinity of the X-type magnetic neutral line where reconnection takes place, however, and significant heating seems to occur over a broad range of the neural sheet as well as at the slow-mode shock that develops from the X-type neutral line.

The plasmas in the acceleration/heating regions are collisionless and are often characterized by high  $\beta$ . The behaviors of ions and electrons in these regions are kinetic, so that acceleration/heating produces non-Maxwellian and sometimes non-gyrotropic velocity distribution functions that reflect specific mechanisms of acceleration/heating. Extensive observations of the ion and electron properties in phase space and their interpretation with reference to computer simulations have significantly advanced understanding of these mechanisms.

Reconnection in the magnetotail is associated with magnetospheric substorms. There is mounting evidence that onset of reconnection at the radial distance of 22 and 30  $R_E$  precedes the substorm onset and thus is consistent with being the driving mechanism of the latter, but another view is also held that the process is initiated by filamentary disruption of the cross-tail current at much closer distances of the near-Earth plasma sheet.

#### 4.1. TAILWARD EJECTION OF PLASMOIDS

The most evident manifestation of the dynamic nature of the magnetotail would be tailward ejection of the plasmoids. The plasmoids are clouds of hot plasma in which magnetic loops are imbedded, and they are ejected tailward with high speeds which often exceed  $1000 \text{ km s}^{-1}$ . The magnetic loops are produced by magnetic reconnection which starts in the region of the closed magnetic field lines in the near-Earth magnetotail. The formation of plasmoids is intimately related to magnetospheric substorms, more specifically, to their expansion phase (e.g., Hones, 1979; Nishida et al., 1981; Richardson et al., 1987; Baker et al., 1987).

Figure 23 is an example of plasmoid observation that is made when the spacecraft is in the tail lobe (at  $x = -128 R_E$ ) before arrival of the plasmoid. Record of  $B_x$  (second panel) shows that the spacecraft enters the plasma sheet from the northern lobe around 21:20 and returns there around 21:38. The  $B_z$  component of the magnetic field (fourth panel) has a typical northward-then-southward bipolar signature that characterizes the plasmoid. Inside the plasmoid, ion temperature  $T$  (seventh panel) is a few keV and the plasma flow velocity (eighth panel) is tailward with speeds of several hundred  $\text{km s}^{-1}$ . Figure 24 is the corresponding  $E-t$  spectrogram. The encounter with the plasmoid is most clearly seen in the count rates of the ions flowing in the anti-sunward direction (second panel from the bottom). Before 21:20 the spacecraft is in the lobe and observes tailward streaming of the cold ions which is almost field-aligned. Just before the entry into the plasmoid energy of these ions rises sharply, and at the same time much hotter ions begin to be seen

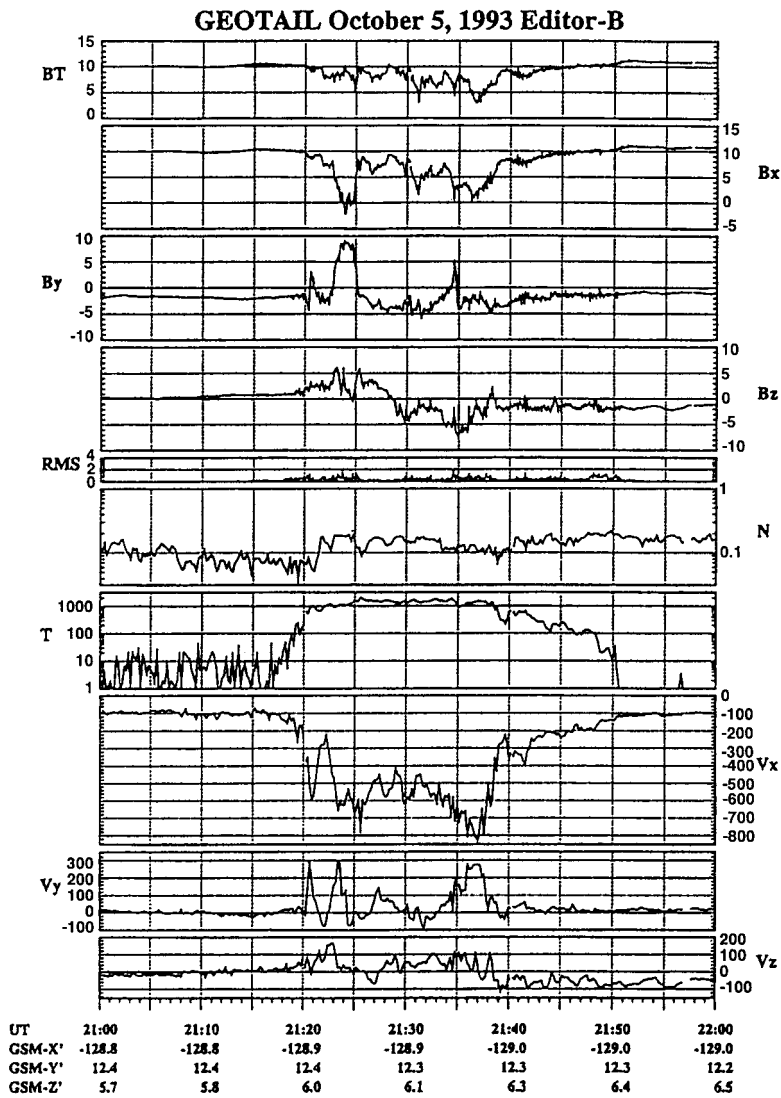


Figure 23. Field and particle data of a plasmoid observed by GEOTAIL at  $(-128, 21, 6) R_E$  (Mukai et al., 1998a). The first five panels show magnetic field data: BT (total force),  $B_x$ ,  $B_y$ ,  $B_z$ , and RMS (root mean square of BT sampled at  $\frac{1}{16}$  s over successive 3 s intervals). The other five panels show plasma moments:  $N$  (density),  $T$  (ion temperature),  $V_x$ ,  $V_y$  and  $V_z$ .

too. These hotter component also flows tailward along magnetic field lines and their energy decreases as the plasmoid approaches. Nearly symmetric structure can be seen at the exit from the plasmoid for a few minutes until  $\sim 21:40$ , but thereafter the hot component is observed for an extended interval until  $\sim 21:50$ . (Note that the speed of the hot component has been underestimated by the moment calculation because the ion energy exceeds the upper limit of the energy range of the LEP-

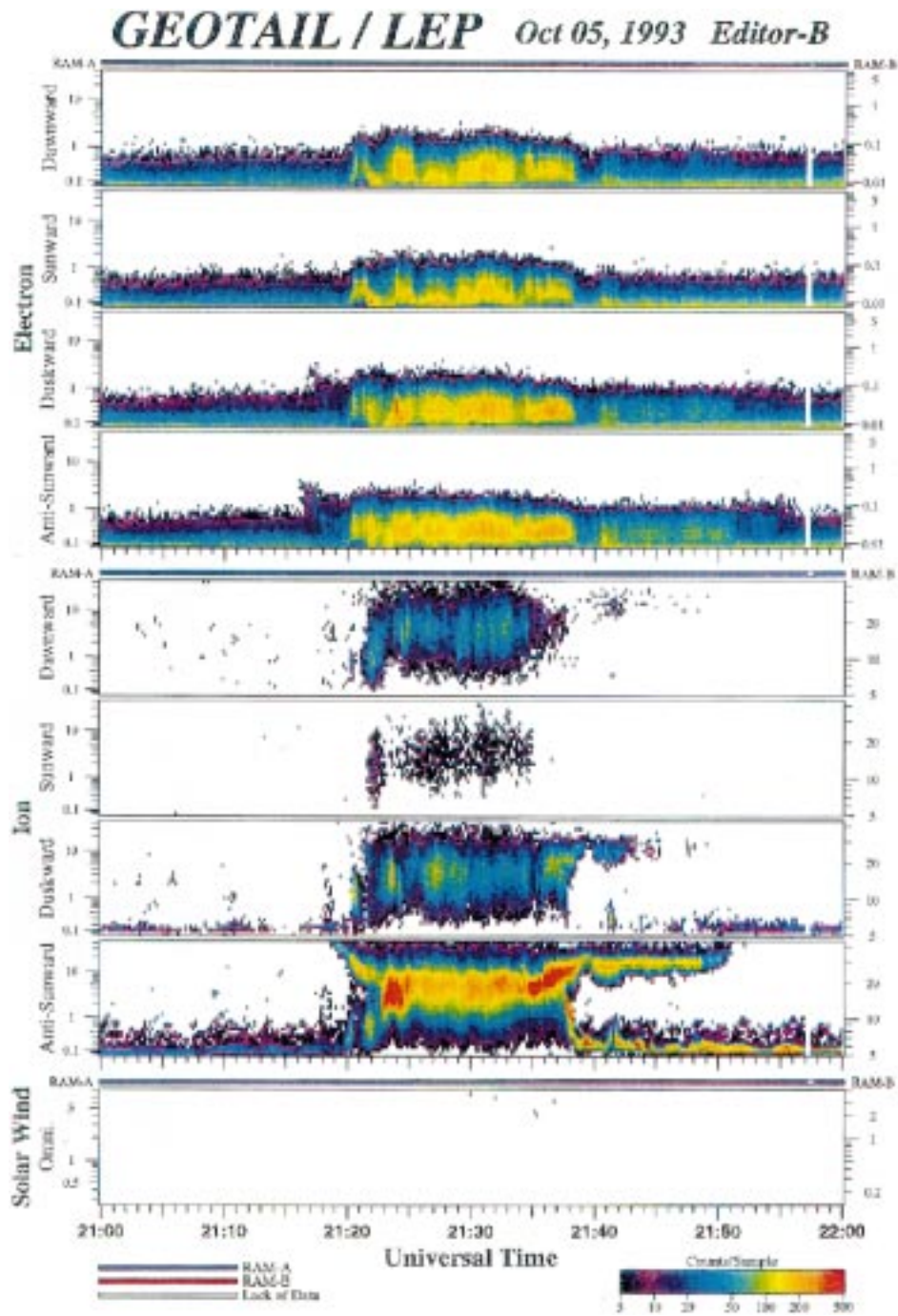


Figure 24. For the interval involving the plasmoid observation of Figure 23, electron (top four panels) and ion (next four panels) energy-time spectrograms are shown for four flow directions (downward, sunward, duskward and anti-sunward). The ordinate scale is energy ( $\text{keV e}^{-1}$ ) and refers to the left-hand scale here (Mukai et al., 1998a).

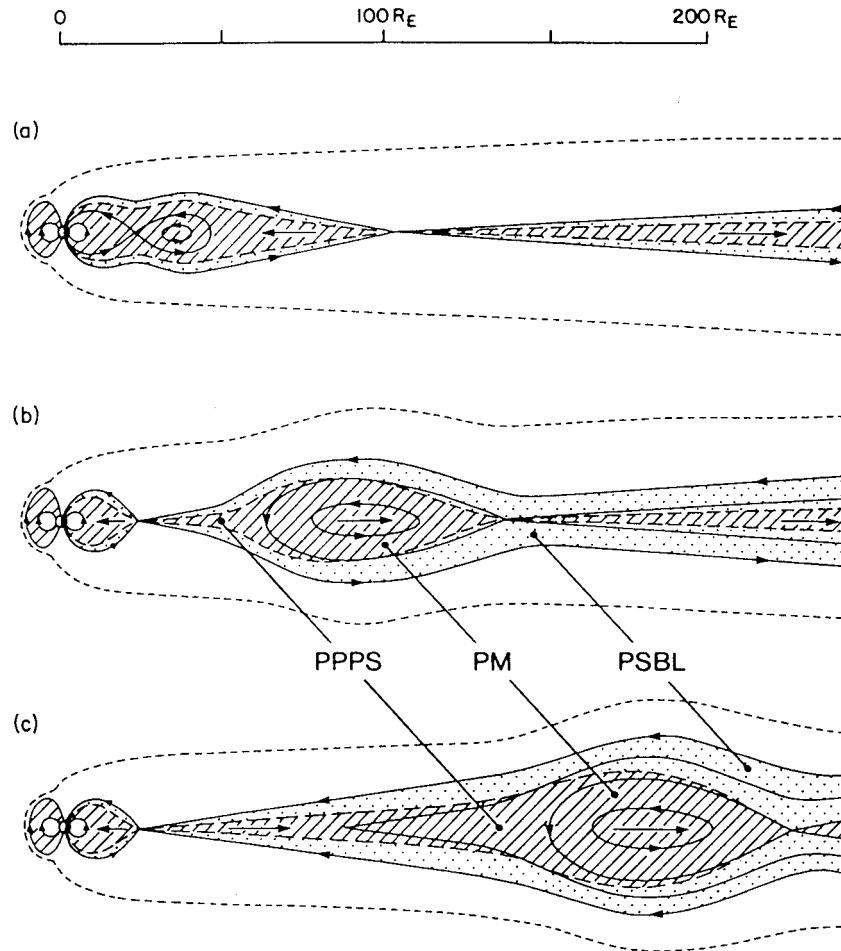


Figure 25. Development of the plasmoid (PM) and the postplasmoid plasma sheet (PPPS) following reconnection at the near-Earth neutral line (Richardson et al., 1987). PSBL means the plasma sheet boundary layer. Horizontal arrows in the plasma sheet represent the flow directions.

EA.) Correspondingly in Figure 23, the  $B_x$  component of the magnetic field does not completely recover to the previous level in the lobe and  $B_z$  remains slightly negative. Thus the plasma sheet remains energized for some time after the passage of the plasmoid. The flow velocity  $V_z$  in the  $z$  direction (bottom panel) is away from the neutral sheet and thus suggests expansion of the plasmoid before  $\sim 21:37$ , but it is directed thereafter toward the neutral sheet suggesting that reconnection is still operative on the wake of the plasmoid (Mukai et al., 1998a).

The observations such as the above can be interpreted in terms of a model of the development of plasmoids and postplasmoid plasma sheet illustrated in Figure 25. The hatched area bounded by dashed lines indicates high  $\beta$  plasma sheet and the dotted area between the dashed line and the solid line, which represents the field-

line separatrices mapping to the neutral line, is the PSBL (Plasma Sheet Boundary Layer). In Figure 25(a) the near-Earth neutral line and the magnetic loop have been formed in the closed field line region of the plasma sheet but the distant neutral line is still at the normal position. In Figure 25(b) reconnection at the near-Earth neutral line now operates on the open field lines, the plasmoid (PM) has been formed, and the postplasmoid plasma sheet (PPPS) is developing in its wake. The distant neutral line is being pushed away. In Figure 25(c), which is the continuation of (b), the field line loop of the plasmoid is surrounded by an expanding layer of draped IMF-type field lines produced from reconnection of the open field lines at the near-Earth neutral line (Richardson et al., 1987).

On the tailward side of the near-Earth neutral line, the bulk of the plasmas that are accelerated by the near-Earth reconnection constitutes the high  $\beta$  region of the plasmoid and the postplasmoid plasma sheet, but particles that are accelerated well above the thermal energy escape along the field lines and constitute the PSBL illustrated in Figure 25(b) and 25(c). The layer is stratified according to particle speeds such that the faster (slower) particles form the outer (inner) layer, because particles with faster speed can stay closer to the separatrix field lines that pass the X-type neutral line while slower particles are carried by the convection further away from the separatrix. The magnetic field and thermal plasma in this layer, however, should be that of the tail lobe origin (Richardson and Cowley, 1985; Richardson et al., 1987). The hot ions that are seen in Figure 24 before entry into and after exit from the plasmoid can be identified with such suprathermal particles in the PSBL, and the electron component of the layer is seen to have arrived a few minutes earlier at about 21:16 (fourth panel from the top) (Mukai et al., 1998a). Bursts of very energetic electrons in the 0.2 to 2 MeV range have also been observed in the PSBL of the distant tail in association with substorm activity (Richardson et al., 1996). From GEOTAIL observations in the distant tail it has been seen that other ion species ( $\text{He}^{++}$  and  $\text{O}^+$ ) are also stratified according to their speeds in the plasma sheet boundary layer (Sarafopoulos et al., 1997). Stratification of particles by their speeds in the direction perpendicular to the magnetic field due to combination of convection and field-aligned streaming has been called the velocity filter effect.

As illustrated in Figure 25 the X-type neutral line formed in the near-Earth tail is a dividing line of the flow directions since reconnection accelerates plasma tailward on its tailward side and earthward on its earthward side. Using this as the key signature, the position where the near-Earth neutral line is formed has been surveyed by Nagai et al. (1998) and Nagai and Machida (1998). Data of the ion moments are examined during the periods from  $-10$  to  $+10$  min relative to the substorm onset time as determined by the Pi 2 pulsations in the night sector on the ground. Tailward or earthward flows are considered to have occurred when the maximum flow velocity during this 20-min period exceeds  $300 \text{ km s}^{-1}$ , either tailward or earthward. Such flows tend to be observed when the spacecraft is located in the midnight to premidnight sector. Southward  $B_z$  occurs during tailward flow events. In Figure 26 where the observing sites of such flows are shown, the data points

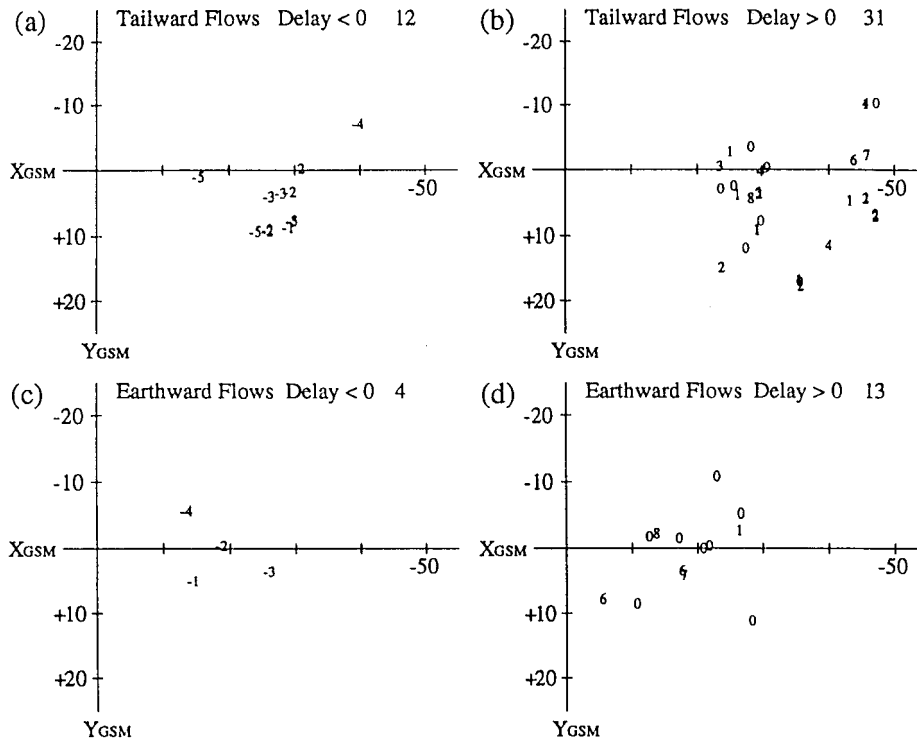


Figure 26. Start times of tailward flows ((a) and (b)) and earthward flows ((c) and (d)) relative to substorm onset shown in the aberrated GSM  $xy$  plane. The flows start prior to the substorm onset in (a) and (c), while the flows start after the onset in the cases in (b) and (d) (Nagai et al., 1998).

are divided by the flow direction and by the sign of the delay time where negative (positive) delay time means that the flow begins earlier (later) than the ground Pi 2 onset. Figure 26(a) shows the sites where the tailward flow starts before the substorm onset; most of the points are on the premidnight side and between  $x$  of  $-22$  and  $-30 R_E$ . Figure 26(b) shows that the tailward flow tends to lag behind the substorm onset at larger distances. Figure 26(c) and 26(d) show that the earthward flow starts before or nearly simultaneously with the substorm onset in the region earthward of about  $30 R_E$  around midnight. The observations in Figure 26 suggest that the near-Earth neutral line is typically formed between  $x$  of  $-22$  and  $-30 R_E$  a few min before the substorm onset on the ground.

Sergeev et al. (1995) have reported a case that suggests that the near-Earth neutral line is formed initially on the earthward side of the ISEE 1 and 2 (at  $x \sim -17$  and  $-16 R_E$ , respectively, and near midnight) 2–3 min before ground signatures of substorm onset and moves past the spacecraft with an apparent speed of about  $30 \text{ km s}^{-1}$ , the minimum thickness of the plasma sheet being less than  $0.2 R_E$ .

Development of plasmoids and their propagation downtail are summarized in Figure 27 based on extensive observations by GEOTAIL down to  $210 R_E$ . Since

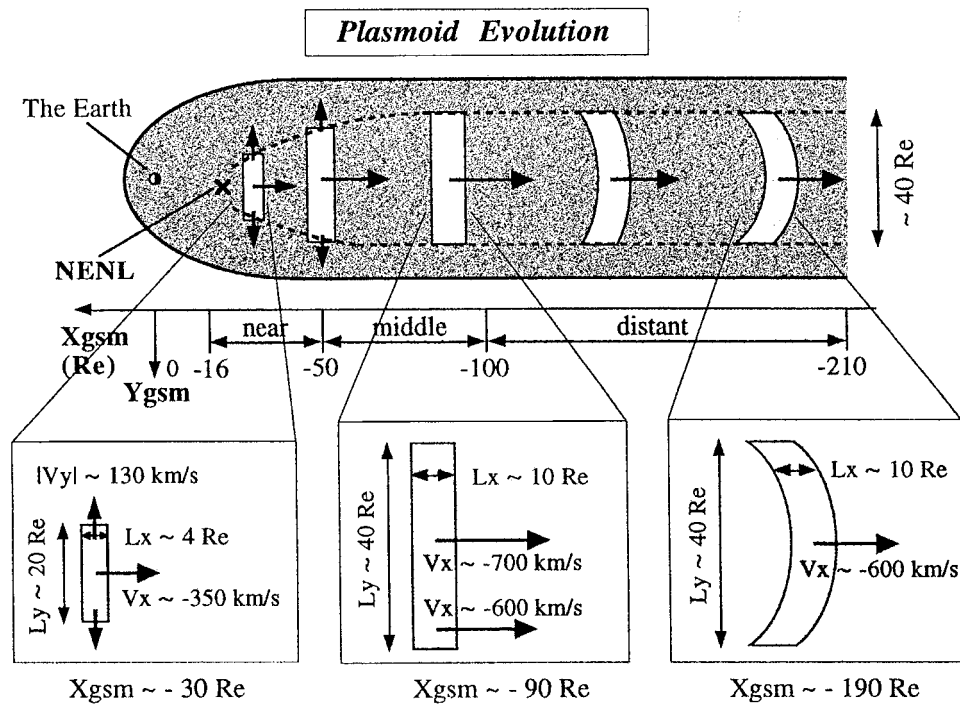


Figure 27. Schematic summary of the plasmoid evolution from the near to the distant tail. Typical velocities, dimensions, and shapes in the near, middle, and distant tail are displayed in each of the expanded panels (Ieda et al., 1998).

the near-Earth reconnection tends to occur initially in the premidnight sector, the plasmoids tend to be observed in the premidnight sector ( $|y' - 3| = 10 R_E$ ) in the near tail ( $x \geq -50 R_E$ ), but at larger distances they are observed widely in the  $|y'| \leq 20 R_E$  range, where  $y'$  refers to the coordinates where the  $x'$  axis is taken in the direction of the aberrated solar wind flow. In the near tail the plasmoids expand in  $\pm y'$  directions with typical velocities of  $\pm 130 \text{ km s}^{-1}$ . The average speeds of plasmoids increase downtail from about  $400 \text{ km s}^{-1}$  to about  $700 \text{ km s}^{-1}$  with propagation from the near to the middle tail. Typical plasmoid dimensions are estimated to be  $10 R_E$  (length)  $\times 40 R_E$  (width)  $\times 10 R_E$  (thickness) in the middle and distant tail, when the plasmoid is defined rather stringently (that is, narrowly) to be the region where the total pressure is enhanced by more than 10%. The average energy carried by each of these stringently defined plasmoids is  $2 \times 10^{14} \text{ J}$  in the middle tail, and the energy released tailward in the course of a substorm is estimated to be about  $10^{15} \text{ J}$  on average including contributions from such accompanying structures as the PPPS (Ieda et al., 1998).

When spacecraft is not engulfed and stays in the lobe while a plasmoid bulge propagates tailward in the plasma sheet, it observes an impulsive compression of the magnetic field in the lobe. Such compressions have been called 'Traveling

Compression Regions (TCR). At distances earthward of about  $150 R_E$  the TCRs propagate in parallel with the plasmoid, but at larger distances the TCRs tend to trail behind plasmoids since the local fast mode speed tends to be reduced in the distant tail by filling of the lobe with the mantle plasma (Slavin, 1998). Temporal expansions in diameter of the distant tail caused by passage of plasmoids have been observed in the distant tail at  $205 R_E$  (Sauvaud et al., 1996).

There are times when the near-Earth reconnection occurs while reconnection is still active at the distant neutral line so that the plasmoid cannot propagate rapidly tailward (Nishida et al., 1986). This corresponds to the configuration illustrated in Figure 25(a). When spacecraft enters such 'quasi-stagnant' plasmoids from the lobe side the earthward beam is observed first and then the tailward beam (Kawano et al., 1996; Hoshino et al., 1996b). Observations of energetic particles (such as 67 keV protons and  $>38$  keV electrons) confirm that in the very early stage of the near-Earth reconnection a tailward moving plasmoid can still be surrounded by flux tubes which are recently closed at the distant neutral line (Slavin et al., 1998).

Since the magnetic field in the tail has a  $B_y$  component that is due primarily to partial penetration of the IMF  $B_y$ , the magnetic structure that is produced by reconnection at the near-Earth neutral line is not exactly two-dimensional magnetic loops but helical field lines having a core component in the direction across the tail (Moldwin and Hughes, 1992). The term flux ropes is used for plasmoids when this three-dimensionality of the field structure is emphasized, and the field component along the axis of the flux rope is called the core field component. The presence of a  $B_y$  component means that the field lines in plasmoids are connected to the ionosphere when they are formed, and in order that the plasmoids can propagate tailward freely this connection has to be cut. Hughes and Sibeck (1987) have suggested that the helical field lines can become separated from the ionosphere by reconnection with open field lines, while Hesse et al. (1996) have suggested that the helical field lines become connected to the field lines of the magnetosheath when they reach the tail surface.

Sometimes enhancements of energetic oxygen ions in the 140–4000 keV channel are also observed in association with plasmoids. In two such events found by Zong et al. (1998) in the middle tail (at  $x \sim -65 R_E$ ), their enhancement lasted for about 30 min, and they showed tailward-directed anisotropy throughout. The energetic ( $\sim 10$  keV to 3 MeV) oxygen ions are not always observed in plasmoids, however (Lui et al., 1998).

It has been seen that the ejection of plasmoids and the dipolarization (see Section 4.4), which we take as signatures of the near-Earth reconnection, are preceded by an enhancement in the total (that is, thermal plus magnetic) pressure (Nagai et al., 1997) and an intensification of the cross-tail current density (derived directly from the velocity difference between ions and electrons) accompanied by a gradual increase in the tailward flow velocity (Mukai et al., 1998b). These features mean that energy stored in the magnetotail is enhanced prior to the substorm onset. It has also been noted from dual satellite observations that a very thin current sheet

( $\sim 0.2 R_E$ ) is imbedded in a thick (a few  $R_E$ ) plasma sheet during the substorm growth phase (McComas et al., 1986; Sergeev et al., 1993; Sanny et al., 1994). Simultaneous observations by GEOTAIL, INTERBALL-TAIL and GOES satellites have shown that a thin current sheet extends from the midtail to the quasi-dipolar region during the growth phase, and that processes within this extended thin current sheet lead to the expansion-phase onset (Pulkkinen et al., 1998a). However, the existence of the thin current sheet may be a necessary but not a sufficient condition for the expansion phase onset (Pulkkinen et al., 1998b); for the near-Earth reconnection to develop into a global feature it seems necessary that not only the local instability condition is reached but also the macroscopic tail structure is ripe for allowing the global development. We should also note in this connection that there are other ideas on the substorm initiation which involve external triggering by the IMF northward turning (Lyons, 1995) or ionosphere-magnetosphere coupling (Kan, 1993). Axford (1999) has emphasized a viewpoint in this concern that it is not so much the need to break the frozen-in theorem but rather that the evolution of a magnetic field configuration, controlled by external influences, should lead to the formation of a neutral point somewhere where magnetic field reconnection can take place rapidly in a manner which is controlled internally.

#### 4.2. ACCELERATION BY RECONNECTION; KINETIC ASPECT

For charged particles to be accelerated it is necessary in the first place that there is electric field and in the second place that particles are able to move in the direction of the electric force over a substantial distance. Both conditions are fulfilled at and near the neutral line where magnetic field lines are reconnected. There is electric field that carries magnetic field lines toward the neutral line, and this electric field tends to be enhanced inductively when reconnection is developing rapidly. The magnetic field is weak in the vicinity of the X-line so that particles can move in the direction of the electric force across the magnetic field. In collisionless plasmas non-Maxwellian velocity distributions tend to be produced by accelerations for two reasons; the first is that the acceleration of the collisionless plasma produces such distributions, and the second is that particles with different histories mix and are observed together. Complexity of the ion velocity distributions in the distant tail has been revealed by observations by the Galileo spacecraft and interpreted in terms of the particle dynamics in the neutral sheet (Frank et al., 1994). Kinetic aspect of the acceleration has been studied extensively with GEOTAIL observations using three dimensional, high sensitivity observations of both ions and electrons over a wide range of distances.

In order to study the acceleration that occurs in the neutral sheet we examine an example of plasmoid observations that was made when spacecraft was continuously in the plasma sheet. The example shown in Figures 28–31 was obtained when the spacecraft was at  $x = -96 R_E$ . The top four panels of Figure 28 are the magnetic field data. From 12:52 indicated by a vertical line,  $B_z$  (fourth panel)

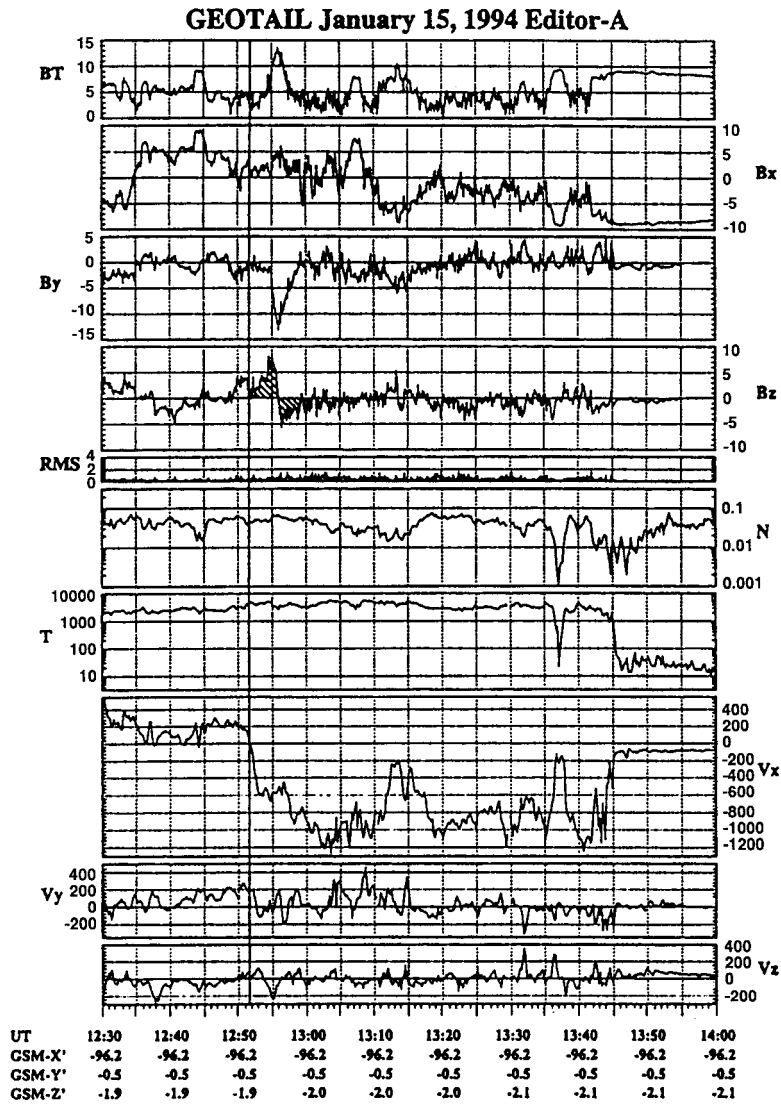


Figure 28. Observation of a plasmoid and the postplasmoid plasma sheet that was made when the spacecraft was in the plasma sheet from the outset (Mukai et al., 1996). The format is the same as in Figure 23.

shows a bipolar signature of the plasmoid while  $B_y$  (third panel) shows the presence of a large core field of the flux rope. The next panels are the ion data. Density  $N$  is rather low and ion temperature  $T$  is high in the plasma sheet, and these do not change very much at the arrival of the plasmoid. The velocity  $V_x$  changes significantly at the above time, however, and is kept above  $800 \text{ km s}^{-1}$  most of the time until the spacecraft exits to the lobe about 1 hour later.

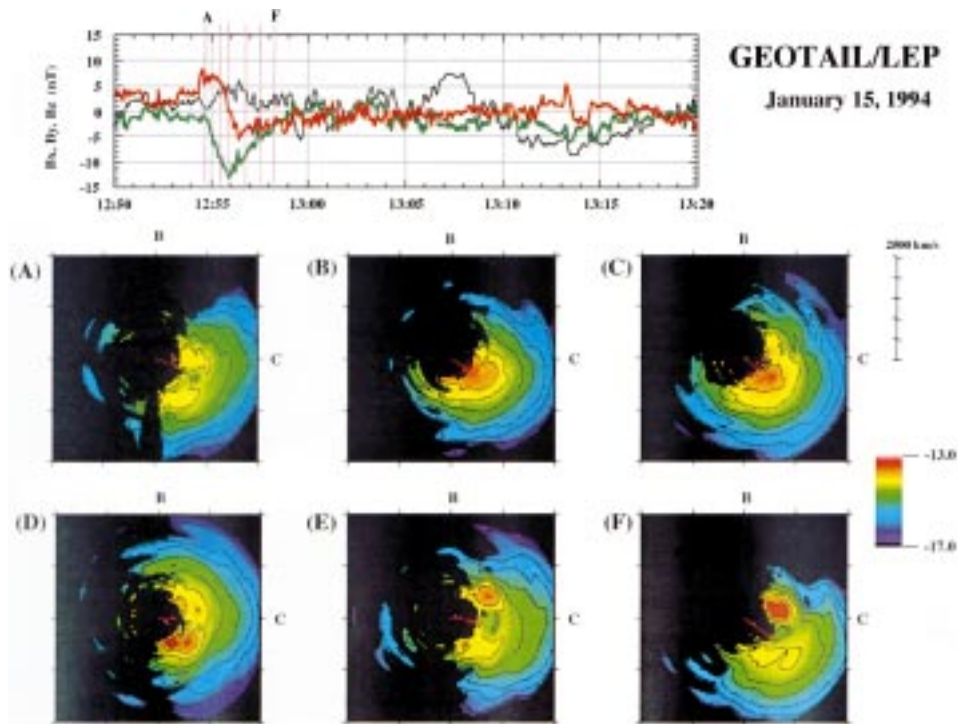


Figure 29. Ion velocity distribution functions at six epochs (A through F) during passage of a plasmoid. The distribution functions are shown as contours in the **B** (magnetic field) – **C** (convection velocity) plane (Mukai et al., 1998). The magnetic field data are reproduced on the top where  $B_x$  (black),  $B_y$  (green) and  $B_z$  (red) components are shown.

Figure 29 is velocity distribution functions of ions observed in this plasmoid in the **B**–**C** coordinates (see Section 3.3). In the top panel the magnetic field records are reproduced and the times when the distribution functions are sampled are indicated by vertical solid lines. In each of Figure 29(A)–(F) the bulk velocity is indicated by a red arrow. At (A) shortly after the northward  $B_z$  increase the ion distribution function suggests the presence of two components (yellow blobs) counterstreaming along the magnetic field relative to the convection velocity (red arrow). The velocity difference between the two beams is  $\sim 1000 \text{ km s}^{-1}$  while the bulk speed is  $\sim 700 \text{ km s}^{-1}$ . At (B) and (C) when  $B_z$  is still positive the ion distribution function consists of a single hot component with anisotropy  $T_{\perp} > T_{\parallel}$ . The  $B_y$  component peaks at the time C. At (D)–(F) after the southward turning of  $B_z$  the ions distribution functions consist clearly of two components that are counterstreaming along magnetic field lines. In each case the velocity difference between the two beams is 1.5–2 times the bulk flow velocity. Figure 30 is the velocity distribution functions of the electrons at the same epochs (A)–(F). Phase space densities are shown as contours in the **B**–**C** plane (left side of each set) and the cuts in the directions parallel (red) and perpendicular (green) to the magnetic

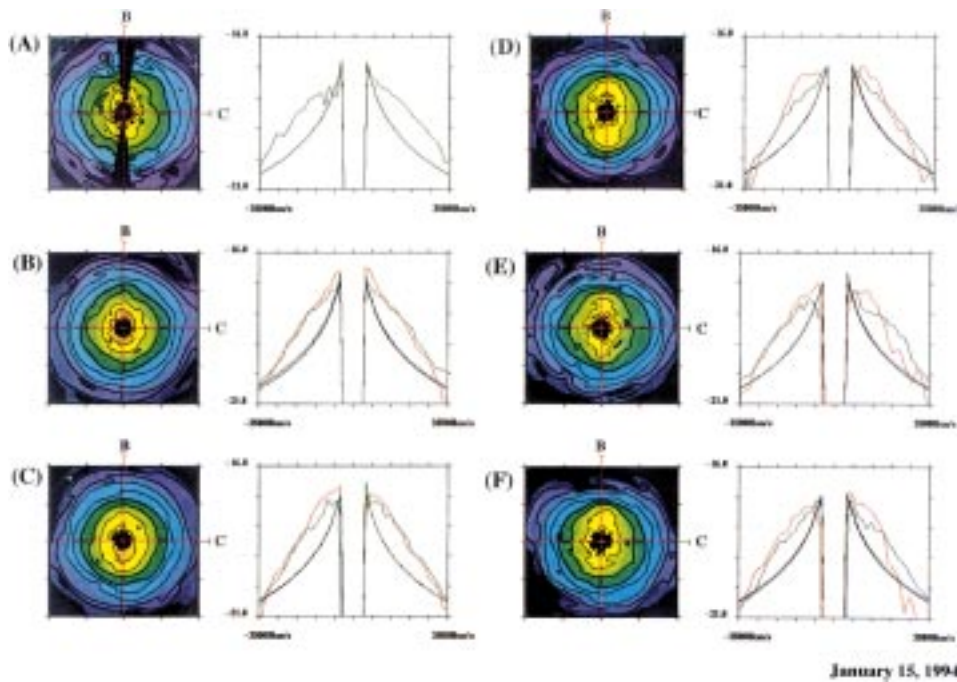


Figure 30. Electron velocity distribution functions corresponding to Figure 29. Contours in the B–C plane are to the left, and the velocity-space distributions in directions parallel (red) and perpendicular (green) to the magnetic field are to the right (Mukai et al., 1996).

field (right side). The electron distribution functions consist of two components: low-energy electrons bi-streaming along the magnetic field lines and high-energy electrons which are isotropic. Phase space densities at low energies tend to be higher in the parallel direction than in the perpendicular and they are flat-topped (Mukai et al., 1996 and 1998a).

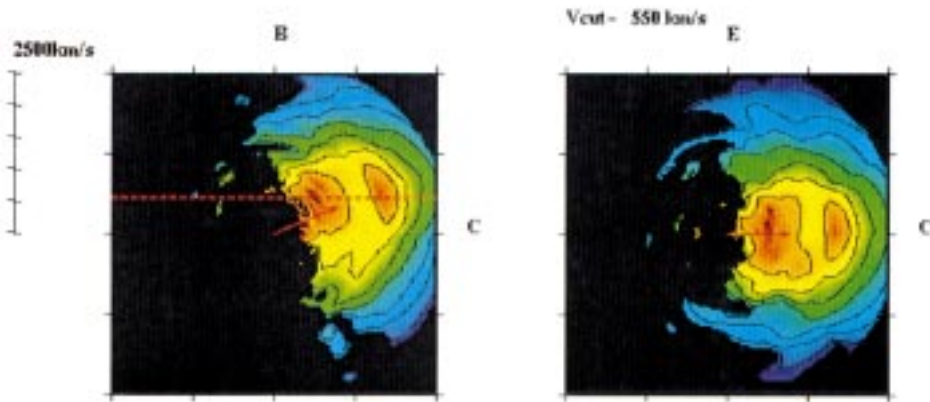
The observed ion distribution functions can be not merely anisotropic but non-gyrotropic. Figure 31 is examples of the non-gyrotropic distribution functions that are observed in the postplasmoid plasma sheet at 13:18 and 13:19. In each case the left panel is a cut by the B–C plane containing the magnetic field ( $\mathbf{B}$ ) and the convection velocity ( $\mathbf{V}_\perp$ ) while the right panel is a cut by the E–C plane containing the electric field ( $\mathbf{E}$ ) and  $\mathbf{V}_\perp$  at a level of  $V_B$  indicated in the left panel by a red dashed line. If the distributions were gyrotropic their contours in the E–C plane should have been circular around the tip of the convection velocity that is indicated by a red arrow, but clearly they are bunched around two gyro-phases (Mukai et al., 1998a).

Numerical simulations have been performed to understand the nature of the velocity distribution functions observed during reconnection events and thereby to extract information on the temporal / spatial development of the reconnection process (Fujimoto et al., 1996b; Hoshino, 1998a and b; Hoshino et al., 1998; Naka-

## GEOTAIL/LEP Ion Distribution functions    January 15, 1994

cut at 13:18:40

Ion BCE slice (distr. fn.): max = -13.0 min = -17.0



cut at 13:19:04

Ion BCE slice (distr. fn.): max = -13.0 min = -17.0

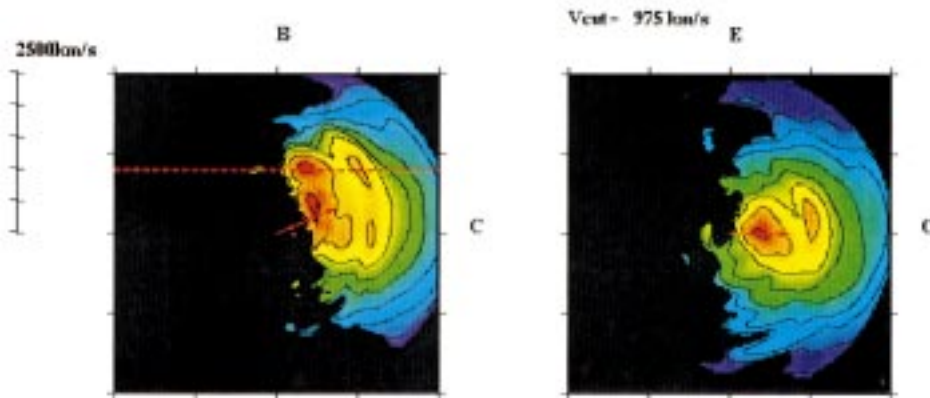


*Figure 31.* Non-gyrotropic velocity distribution functions of ions observed in the postplasmoid plasma sheet (Mukai et al., 1998). Non-gyrotropy is seen in the  $\mathbf{E}$  (electric field direction) -  $\mathbf{C}$  (convection velocity direction) plane which is perpendicular to the magnetic field.

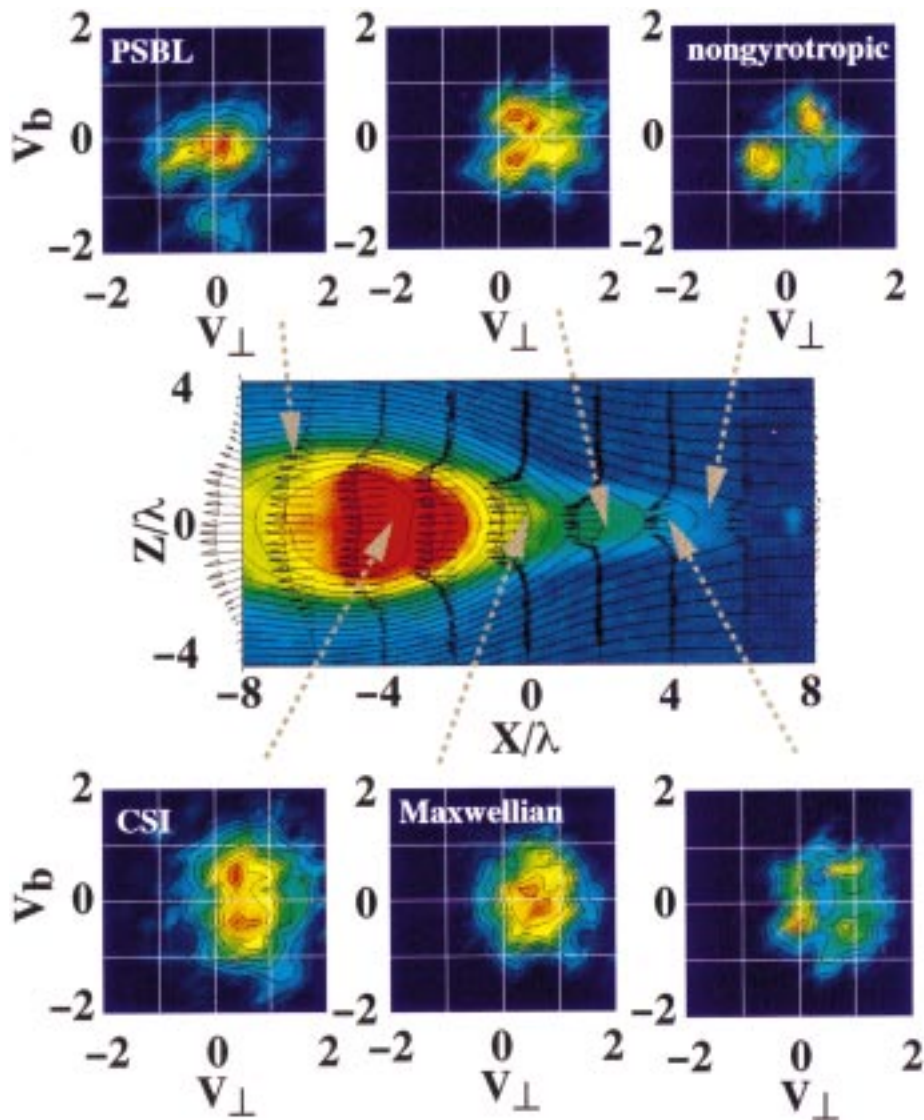


Figure 32. *Central panel:* Plasma density and flow velocity obtained by a numerical simulation at the normalized time of 53.7. The whole system of the simulation is much larger. *Upper and lower panels:* Ion velocity distribution functions at the positions indicated by arrows (Hoshino et al., 1998a, edited).  $V_b$  and  $V_{\perp}$  are in the directions of the magnetic field and the convection velocity, respectively.

mura et al., 1998; Lottermoser et al., 1998). The examples shown in Figures 32 and 33 are simulations of the collisionless reconnection where both ions and electrons are treated as particles (Hoshino, 1998a, b; Hoshino et al., 1998). The middle panel of Figure 32 shows the calculated magnetic field lines on the contours of density. Distance is scaled by  $\lambda$  which is the initial thickness of the plasma sheet, time by

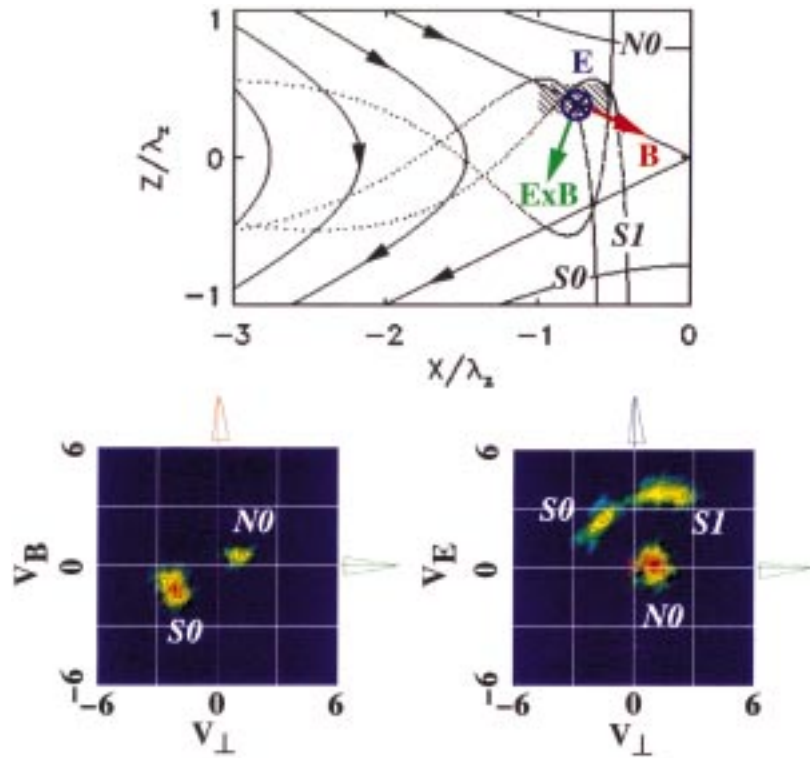


Figure 33. Upper panel: representative ion trajectories (labeled N0, S0 and S1) in the vicinity of the X-type neutral line, and lower panel: their signatures in the velocity distribution function (Hoshino et al., 1998a, edited).  $V_E$  is the component in the direction of the electric field.

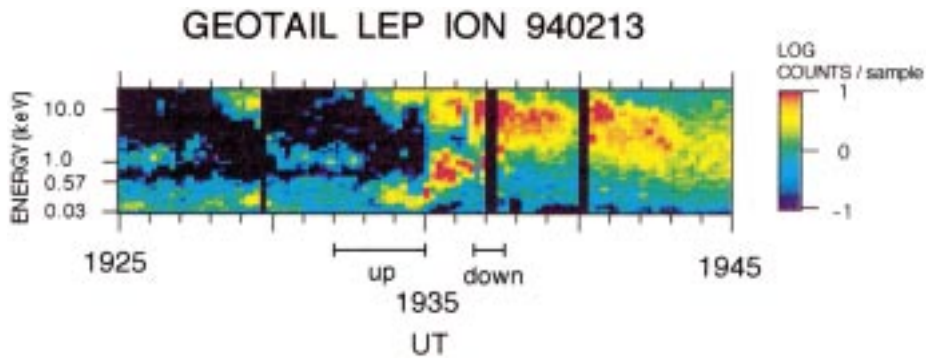


Figure 34.  $E-t$  spectrogram for the omnidirectional ion counts for an interval involving crossing of the slow-mode shock (Saito et al., 1996). 'Up' and 'Down' indicate representative upstream and downstream intervals.

the Alfvén transit time  $\lambda/V_A$ , where  $V_A$  is calculated by using the field strength in the lobe and the plasma density in the plasma sheet, and the velocity by  $V_A$ . The initial ratio of densities between the center of the plasma sheet and the lobe is assigned to be 3. Ion inertial length  $V_A/\Omega_i$  is  $0.56\lambda$  and the ion Larmor radius for the hot plasma sheet ions under the magnetic field of the lobe is  $0.5\lambda$ . Thus the plasma sheet is assumed to be thin. It can be seen that the lobe plasmas are convected toward the plasma sheet and accelerated in the  $-x$  direction up to the Alfvén velocity  $V_A$ . A region of the weak magnetic field extends from the X-type neutral line which is at  $x/\lambda \approx 8$ . The magnetic field is relatively enhanced around  $x/\lambda \sim 0$  where reconnected field lines pile up.

Smaller panels in top and the bottom rows of Figure 32 are velocity distribution functions in the B–C (that is,  $\mathbf{V}_b - \mathbf{V}_\perp$ ) coordinates. Central panel in the top row and three panels in the bottom row are velocity distribution functions at four locations along the neutral sheet ( $-\frac{1}{16} < z/\lambda < \frac{1}{16}$ ). The panel at bottom right is for  $x/\lambda \sim 4$  where the motion is influenced by the presence of the weak  $B_z$ , and there are four bunches of cold ions. The ions comprising two of the peaks which are almost on the  $V_b$  axis have just arrived from the lobe, while other peaks which are nearly centered at  $V_\perp = 1$  represent the ions which have traversed the neutral sheet and accelerated once or multiple times. The parameter  $\kappa = (R_{\min}/\rho_{\max})^{1/2}$  that characterizes the particle motion, where  $R_{\min}$  is the minimum radius of the field-line curvature and  $\rho_{\max}$  is Larmor radius in the neutral sheet (Büchner and Zelenyi, 1989), is about 0.5 so that the motion is a combination of the faster bounce motion along the magnetic field and the slower half gyration under the weak magnetic field  $B_z$  in the neutral sheet (Speiser, 1965). Particles gain energy as the half gyration carry them in the  $y$  direction. (In the magnetic field of 0.5 nT, the Larmor radius of a proton is  $0.6 R_E$  at 200 eV and  $2.0 R_E$  at 2 keV.)

The upper-middle panel is for  $x/\lambda \sim 2$  which is at the edge of the region where  $B_z$  in the neutral sheet is weak enough to allow ions to move substantially in the  $y$  direction. The distribution function has the dumbbell-like structure which consists of two cold ion components which are aligned along the magnetic field. The nature of this distribution is similar to the four bunches seen earlier; ions at the peaks of the dumbbell are the relatively low  $V_\perp$  population that has just arrived from the lobe, while the extensions to higher  $V_\perp$  represent the ions that have been accelerated near the X-line region by moving in the direction of  $\mathbf{E}$  along the neutral sheet. The dumbbell structure develops gradually in the edge region from the four-bunched structure since more ions escape from the neutral sheet without traversing it multiple times as the distance from the X-line increases. The structure thus obtained is very similar to the counterstreaming ion beams that have been observed in plasmoids by Mukai et al. (1996, 1998a). The ions that escape from this edge region flow into the PSBL along magnetic field lines.

The lower-center panel is for  $x/\lambda \sim 0$ . At this point the distribution is nearly Maxwellian. Acceleration through the meandering (Speiser-type half gyration) be-

comes less pronounced as  $B_z$  in the neutral sheet becomes stronger and the Larmor radius becomes smaller.

The lower-left panel is for  $x/\lambda \sim -4$  which is near the O-type neutral line. The distribution is dumbbell-shaped. These bouncing ions originate from the cold lobe ions which have been convected into the plasma sheet in the initial stage of evolution of the reconnection. Although they have meandered and accelerated in the neutral sheet before reaching here they still retain the memory of the cold ions injected from the lobe. The  $\kappa$  value is much greater than 1 and the motion is locally adiabatic.

The distribution function in the upper-left panel is for the PSBL (Plasma Sheet boundary Layer) at  $(x/\lambda \sim -6, z/\lambda \sim 2)$ . It consists of a high speed beam flowing tailward along the magnetic field and much slower ions near the origin. The beam component represents tailward streaming of the ions which have escaped from the acceleration region of the neutral sheet that extends from the X-type neutral line. The slow component represents the ions that are being convected from the lobe. It has an anisotropic temperature because these ions are compressed mainly in the direction perpendicular to the magnetic field when they enter the plasmoid that propagates tailward with high speed.

The upper-right panel shows the non-gyrotropic distribution at  $(x/\lambda \sim 5, z/\lambda \sim 3/8)$  near the X-type neutral line. The nature of the non-gyrotropy is explained in Figure 33. The upper panel illustrates magnetic field lines and typical trajectories of the ions which cross the shaded region where the above distribution function is sampled. The electric field  $\mathbf{E}$  is perpendicular to the sheet and the direction of the  $\mathbf{E} \times \mathbf{B}$  drift, namely  $\mathbf{V}_\perp$ , is given in the figure. The curves N0 and S0 are the trajectories of the ions which are convected toward the neutral sheet from the northern and southern lobes, respectively. The S1 trajectory has been reflected once in the region of the higher  $B_x$  before entering the shaded region. The lower-left panel shows the positions of these particles in the  $\mathbf{V}_\perp$ - $\mathbf{V}_B$  plane of the phase space. The N0 ions which are directed southward have positive  $\mathbf{V}_\perp$  and, due to inclination of the magnetic field relative to the neutral sheet, have a slightly positive  $\mathbf{V}_B$ . The S0 ions move opposite to the  $\mathbf{E} \times \mathbf{B}$  direction toward their mirror point and have larger velocities than N0 ions since they have already traversed the neutral sheet and been accelerated there. In the  $\mathbf{V}_\perp$ - $\mathbf{V}_E$  plane (right panel) which is perpendicular to the magnetic field, the N0 particles are merely convecting toward the neutral sheet so that their  $\mathbf{V}_E$  is zero on average, but S0 and S1 have been accelerated in the  $\mathbf{E}$  direction and are gyrating around  $\mathbf{B}$  as separate bunches. Thus non-gyrotropic velocity distribution is formed in the region where the plasma sheet thickness is comparable to the ion gyroradius.

The velocity difference between the two ion components N0 and S0 can be estimated in terms of the meandering. Since the ions gain energy by traveling in the  $y$  direction in the neutral sheet where they exert a half gyration with respect to  $B_x$ ,

$$\frac{1}{2}m_i v^2 \approx e E d_i, \quad (5)$$

where the distance  $d_i$  which the ions travel in the  $y$  direction is assumed to be almost equal to the meandering width  $(v\lambda_d/\Omega_i)^{1/2}$  where  $\lambda_d$  is the characteristic scale length of  $B_x$ . Hence the velocity difference of non-gyrotropic ions  $\Delta v$  is given by

$$\begin{aligned} \Delta v \approx 2^{2/3} \left( \frac{e E_y^2 c \lambda_d}{m_i B_x} \right)^{1/3} &\approx 870 \text{ km s}^{-1} \left( \frac{E}{4 \text{ mV m}^{-1}} \right)^{2/3} \left( \frac{\lambda_d}{0.1 R_E} \right)^{1/3} \times \\ &\times \left( \frac{12 \text{ nT}}{B_x} \right)^{1/3} \end{aligned} \quad (6)$$

The electric field could become 1–4 mV during reconnection. If  $\lambda_d$  is assumed to be as thin as  $d_i$ , we obtain  $\lambda_d = c E_y / B_x \Omega_i \approx 3 \times 10^2 \text{ km}$ . The observed velocity difference between the two ion components is consistent with this estimate (Hoshino, 1998a, b).

As for the electrons that enter the plasma sheet from the lobe near the X-type neutral line where  $k \ll 1$  they are accelerated by taking the Speiser orbit, and the resulting hot population flows away along field lines. These electrons are mirrored at lower altitudes and travel back toward the distant tail, and, if the condition  $k \sim 1$  prevails in the distant neutral sheet except in the vicinity of the neutral line, their pitch angle is scattered when they cross the neutral sheet. Pitch angle scattering occurs only in the high-energy part of the distribution, and the resulting flux is enhanced in the parallel direction at low energies and in the perpendicular direction at high energies. It has been suggested that this explains the observation of the electron distribution functions in the plasmoid such as presented in Figure 30 (Smets et al., 1998).

If, on the other hand,  $\kappa < 1$  everywhere in the distant tail a simulation suggests that the ion to electron temperature ratio  $T_i/T_e$  becomes proportional to  $(m_i/m_e)^{1/3}$  and is about 5 which is in the range of the observed values (Schriver et al., 1998). For the  $\kappa < 1$  condition to prevail for the electrons, however, the current sheet would have to be quite thin everywhere and at all times since the electron Larmor radius is as small as  $0.16 R_E$  even for  $B_z$  of 0.1 nT and energy of 1 keV.

If the thickness of the current sheet in fact is larger than the ion Larmor radius, the condition  $\kappa > 1$  holds for electrons and their motion is adiabatic. In that case the electrons which are originally injected to the region of weak  $B_z$  near the X-type neutral line will conserve the first adiabatic invariant and gain energy as the field strength becomes larger (Taktakishvili et al., 1998). Thus all possible  $\kappa$  conditions have been discussed for the electrons.

Around the X-type neutral line where the field lines are reconnected, the frozen-in condition between the particles and the magnetic field breaks down and the magnetic field diffuses through the plasma. In this magnetic diffusion region the

motions of ions and electrons in the direction perpendicular to the magnetic field are different. The electrons that have smaller Larmor radius still move with field lines and are accelerated quickly beyond the Alfvén speed, and it takes some distance (about  $10 V_A/\Omega_i$ ) for them to slow down to the speeds comparable to the ion bulk speed which is the lobe Alfvén speed. This difference generates Hall current that is directed toward the X-type neutral line along the neutral sheet, and its closure produces current loops in each quadrant that include field-aligned current away from the diffusion region (Nakamura et al., 1998). The field-aligned flow of electrons in the 0.1–1 keV range that carries this current has been observed in the boundary region of the postplasmoid plasma sheet. Its direction is opposite to more energetic electrons that flow away from this region (Fujimoto et al., 1997; Nagai et al., 1998). The field-aligned current pulse that is detected at  $x = -32 R_E$  directly from the difference between the ion and electron motions at substorm onset (Frank et al., 1997) probably represents the Hall current as well. The Hall current causes bending of field lines downward before getting reconnected and duskward after having been reconnected (Nakamura and Fujimoto, 1998). Duskward bending of the reconnected field lines due to the Hall current has been used to interpret  $B_y$  observed in plasmoids (Winglee et al., 1998).

In the collisionless plasma, particles can in principle be traced to their source regions by following their orbits backward. The self-consistent fields obtained from global magnetohydrodynamic simulation can be used as the magnetic and electric fields that govern the particle motion. It has been shown by this scheme that the ions observed at a given point in the inner magnetotail comprise contributions from multitudes of sources, that is, ionosphere, mantle, and low latitude boundary layer, each of which occupies different portions of the velocity distribution function (Ashour-Abdalla et al., 1997).

Particle motions can be significantly affected by waves if they are intense enough. Cattell and Mozer (1986) have suggested that large amplitude waves of the electric field exists in the neutral sheet and could play an important role in the formation of the neutral line by producing anomalous resistivity. In plasmoids GEOTAIL has observed the electromagnetic waves which can be interpreted to be produced by the lower hybrid drift instability, but the anomalous resistivity arising from these waves is estimated to be two orders of magnitude lower than required for the resistive tearing mode instability (Shinohara et al., 1998).

#### 4.3. SLOW-MODE SHOCK

Convection of magnetic field lines in the lobe brings the oppositely directed field lines of the northern and the southern lobes toward the neutral sheet. These field lines reconnect at the magnetic X-type neutral line where the frozen-in relation of magnetohydrodynamics breaks down. In this process the flow toward the neutral sheet is deflected and directed away from the X-type neutral line. It has been suggested that this deflection occurs at a pair of shock waves of the magneto-

drodynamic slow mode that develop from the X-type neutral line (Petschek, 1964) and mark the boundary between the lobe and the plasma sheet (Axford et al., 1965). The slow-mode shocks have been identified in the magnetotail by ISEE 3 (Feldman et al., 1984, 1987), but the Rankine-Hugoniot relation could not be fully tested because of absence of the ion measurement.

Figures 34 to 36 shows an example of a slow-mode shock observed by GEOTAIL (Saito et al., 1995, 1996). Figure 34 is the  $E-t$  spectrogram of omnidirectional ion counts. The slow-mode shock is located between the intervals which are indicated as upstream (up) and downstream (down) sides. It has been confirmed that this shock satisfies the basic requirements of the slow-mode shock, namely, the Rankine-Hugoniot relation, coplanarity condition, energy conservation, and slow-mode supersonic condition. The characteristic signatures of the slow-mode shock for electrons, that are, the heat flux that flows away from the shock into upstream and the flat-top velocity distribution in the downstream region, have also been observed but not shown here.

Figure 34 shows that the ion energy changes from cold to hot at the crossing of the shock. In addition, a high energy branch exists which extends upstream from the shock and whose energy increases with increasing distance from the shock front. These hot ions are backstreaming away from the shock. Figure 35 plots basic parameters for an interval encompassing this shock crossing including the foreshock region which is between the dashed lines. The velocity refers to the de-Hoffman Teller frame. It can be seen that the magnetic field strength drops at the shock (Figure 35(a)). The temperature of the cold ions increases slightly toward the shock and jumps at the shock crossing (Figure 35(b)). They are heated in the foreshock region by about 10% of the total ion heating in the shock. Flow velocity of the cold ions drops at the shock (Figure 35(c)). The density of the hot backstreaming ions increases appreciably in the foreshock region (Figure 35(d)) where magnetic fluctuations are enhanced (Figure 35(e)). The temperature of the backstreaming ions (not shown) is a few times higher in the direction perpendicular to  $\mathbf{B}$  than parallel to it, and they are above and below, respectively, the downstream ion temperature. The difference between the flow speeds of the cold and the hot ions (Figure 35(f)) is about twice the Alfvén speed.

Figure 36 shows how the velocity distribution in the de-Hoffman Teller frame changes across the shock. In this frame the plasma flows along the magnetic field on both upstream and downstream sides of the shock so that the electric field vanishes. On the right-hand side of each Panel horizontal and vertical axes correspond to ion velocities perpendicular and parallel to the magnetic field, respectively. On the left-hand side the horizontal axis is velocity and the vertical axis is the off-plane angle, which is the angle between the ion velocity vector and the plane in which both upstream and downstream magnetic fields and the ion bulk flow velocity are contained. In the upstream region (Figure 36(a)), only the cold ions are observed. These ions are flowing into the shock along the magnetic field with the velocity of about  $1500 \text{ km s}^{-1}$  in the above frame. Since the cold ions are streaming along the

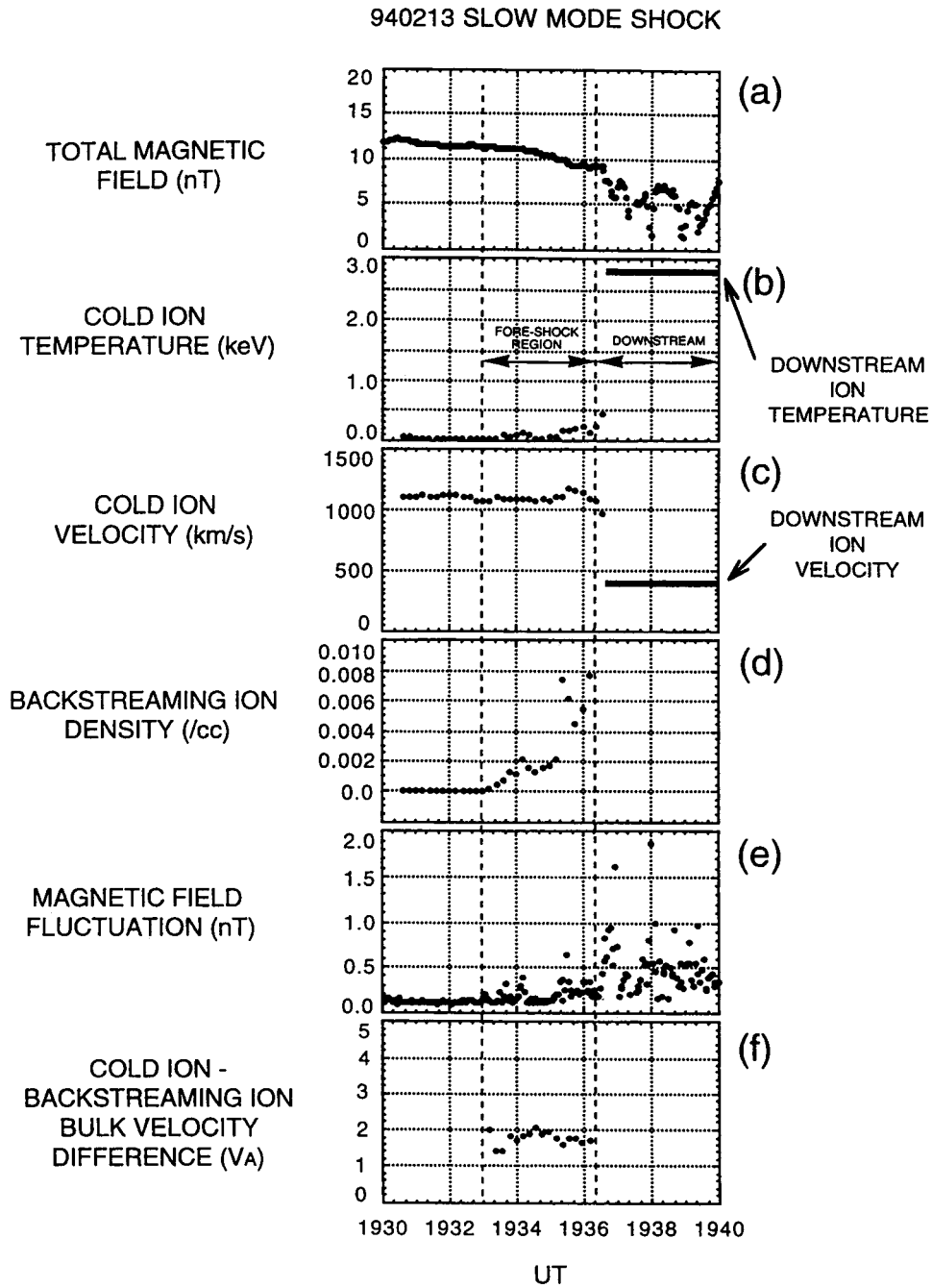


Figure 35. Basic parameters observed during an interval including a slow-mode shock and its foreshock region (Saito et al., 1996).

ION DISTRIBUTION 940213  
de Hoffmann Teller Frame

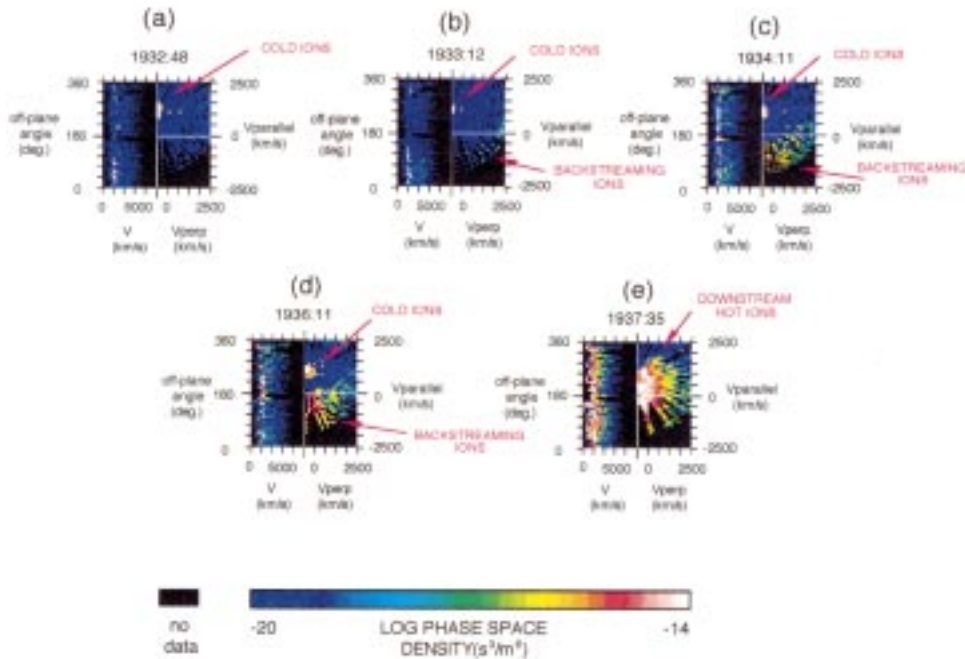


Figure 36. Variations of the ion distribution which are observed as spacecraft moves from upstream to downstream sides of the slow-mode shock. Principal ion components are indicated for the right side of each Panel where the horizontal and the vertical axes are velocity components perpendicular and parallel to the magnetic field, respectively (Saito et al, 1996).

magnetic field, the off-plane angle of the velocity of individual ions is distributed between  $0^\circ$  and  $360^\circ$ . As the spacecraft approaches the shock, ions with negative parallel velocity begin to be observed (Figure 36(b)). These are the backstreaming ions. As the spacecraft comes closer to the shock, the density of the backstreaming ions increases and the cold ions begin to be heated (Figure 36(c)). In Figure 36(d) these features become more pronounced and some of the backstreaming ions are reflected toward the shock. In the downstream region (Figure 36(e)), only the one-component ions that flow away from the shock are observed. Comparison of Figures 36(d) and 36(e) suggests that the backstreaming ions are leaking from the downstream side of the shock.

For the ten cases studied by Saito et al. (1996), the cold ions are heated to 3–20% in the foreshock region, and the backstreaming ion density is about 1 to 15% of the downstream ion density. The angle between the upstream shock normal and the magnetic field is nearly  $90^\circ$ , so that the shocks are nearly perpendicular. The ratio between densities of the backstreaming ions and the downstream ions tends to increase with a decrease in the above angle as would be expected from leakage of

ions. It has been suggested that energy is transferred from the backstreaming ions to the cold ions in the foreshock region through the action of the waves which are excited due to large difference in flow velocities between these ions. The waves are excited by the ion-ion resonant mode interaction when the relative speed between the two ion populations is above  $\sim 2 V_A$  (Gary et al., 1986; Tsurutani et al., 1985; Kawano et al., 1994).

The mechanism of energy dissipation in the slow-mode shock itself need be clarified. Although the structure of the foreshock region has been examined and a reasonable interpretation has been made about the mechanism by which the cold ions arriving from the upstream side are partially heated there, energy dissipation in the shock proper remains to be understood. A two-fluid theory of slow-mode shocks has predicted that left-hand polarized wave trains of magnetic fields should be found in the region extending from the leading edge of the shock layer into the downstream region (Coroniti et al., 1971), but the existence of such rotational structure of magnetic fields has not been confirmed by observations (Seon et al., 1996). The thickness of the shock layer as determined from ion observations is several tens of times of the ion inertial length  $c/\omega_{pi}$  in the upstream region for a few cases identified by Seon et al. (1996). This estimate of the thickness probably includes the foreshock region. The electron temperature rises in much a thinner layer of a few  $c/\omega_{pi}$  thick.

The number of the cases which can be clearly identified as slow-mode shocks is rather small. It is about 10% in the analysis by Saito et al. (1995) and even less according to Seon et al. (1996) who used more stringent criteria and emphasized importance of incorporating pressure anisotropy of the downstream plasma for the slow-mode shock identification. The primary reason for the low identification rate would be that the actual situation is seldom represented by a steady one-dimensional shock as theories assume. There are cases where the coplanarity does not hold but the slow shock layer is followed by an adjoining rotational discontinuity layer on the postshock side (Whang et al., 1997). It should also be noted that high variability of the magnetic field and plasma parameters often makes it difficult to define the downstream state unambiguously.

However, the paucity of the slow-mode shock identification could be due to a more fundamental reason. While the slow-mode shock should make the density higher on the downstream side (that is, in the plasma sheet) than on the upstream side (that is, in the lobe), observations show that the opposite is quite often the case (Saito et al., 1995; Seon et al., 1996). Note that the statistically obtained density-versus-flow speed diagram of Figure 11 demonstrates that the plasma sheet has lower densities than the lobe most of the time (Maezawa and Hori, 1998); the cases where the density is higher downstream in agreement with the standard slow-mode shock model may have to be considered rather exceptional. On the other hand, continuous supply of plasma from the lobe to the plasma sheet is suggested by the smooth transition in the ion  $E-t$  spectrogram from the colder lobe to the warmer plasma sheet. The continuity of lobe and plasma-sheet data points in Figure 11

itself also demonstrates that the lobe plasma is supplied into the plasma sheet. Hence it is not likely that the lobe and the plasma sheet are separated normally by the tangential discontinuity. This view is supported by the observation that the magnetic structure in the plasma sheet can often be represented by a double-peaked current sheet which probably corresponds to the slow-mode shock (Hoshino et al., 1996a).

There seems to be an important feature in observations that is not considered in the Rankine–Hugoniot relation. In the downstream region of the slow-mode shock there often is an additional component of high speed flow which seems to come from the direction of the X-type neutral line (Nagai et al., 1998). The downstream plasma is not only supplied locally from the lobe but also from the X-type neutral line region where significant heating and acceleration take place. Such a structure is entirely out of the scope of the Rankine–Hugoniot relation where the flow is assumed to originate from a single upstream region and to be directed to a single downstream region. Probably the shock relation has to be reformulated taking account of dual plasma sources that are actually observed in the magnetotail away from the X-type neutral line.

In fact an alternative model of the collisionless reconnection has been proposed which does not involve the slow-mode shock. Hill (1975) has discussed the problem of reconnection in a plasma of non-interacting particles, explicitly avoiding the magnetohydrodynamic approximation. The self-consistency requirement is imposed that the motion of charged particles in the field reversal region must balance the magnetic stress, or equivalently, must provide the electric current of the magnetic field reversal. In this model the acceleration of plasma occurs only in the field reversal region, but the bulk flow pattern which results from summation of the individual particle motions is found to be similar to that of the magnetohydrodynamic fluid model of Petschek (1964). Result of a hybrid simulation has supported this conjecture; it has been shown that the slow-mode shock is produced only beyond a few hundred ion inertial length downstream from the X-type neutral line where the cross-tail current has become patchy and ions have been isotropized (Lottermoser et al., 1998). This suggests that the acceleration in the current sheet could produce a slow-shock like configuration in the field and flow.

#### 4.4. DIPOLARIZATION IN THE NEAR-EARTH TAIL

Since the near-Earth reconnection reduces the magnetic tension that is applied on the stretched field lines, the reconnected field lines on the earthward side of the X-type neutral line shrink toward more dipolar configurations while those on the tailward side are ejected (Fairfield and Ness, 1970; McPherron et al., 1973a). These two kinds of field lines have been observed simultaneously at  $12 R_E$  (by INTERBALL-TAIL) and at  $28 R_E$  (by GEOTAIL) approximately 1 min before initial brightening of the aurora signifying the substorm onset (Petrukovich et al., 1998). Reduction in the cross-tail electric current that is associated with the dipolarization is observed at the same time.

larization has often been called ‘current disruption’ although it is not necessarily the case that the current is fully disrupted even locally. Channeling of the cross-tail current to the ionosphere via field-aligned currents has been called ‘current wedge’ (McPherron et al., 1973b).

The dipolarization is accomplished by sharp enhancements in the earthward convection of field lines that have time scales of the order of 1 min. These sharp enhancements, called ‘Flow Bursts (FB),’ are embedded in 10-min scale enhanced flow events called ‘Bursty Bulk Flows (BBF),’ which are operationally defined to be segments of continuous flow magnitude above  $100 \text{ km s}^{-1}$  in the plasma sheet during which the speed exceeds  $400 \text{ km s}^{-1}$  for at least one sample period (Angelopoulos et al., 1992). The enhancements can in general be earthward or tailward, but the earthward BBF’s are more frequent up to a distance of  $\sim 19 R_E$ . Although BBF’s occupy only 10–15% of the observation time in the inner plasma sheet, they are responsible for 60–100% of the earthward transport of mass, energy and magnetic flux past the satellite in the regions of maximum occurrence rate (Angelopoulos et al., 1994).

Figure 37 is an example of the dipolarization and BBF event observed by GEOTAIL on 03:50 to 04:30 August 14, 1996, during which two onsets of the substorm expansion phase are observed on the ground at 04:05 and 04:20 (Nagai et al., 1999). GEOTAIL was located at a radial distance of  $10.2 R_E$  and local time of 23.2 hour at 04:00. The top five panels are three components, total magnitude and latitude angle of the magnetic field, and the sixth and the seventh panels are  $x$  and  $y$  components of the flow velocity  $\mathbf{V}$  (thin curves) or the convection velocity  $\mathbf{V}_\perp$  (solid curves). The bottom five panels are  $E$ - $t$  spectrograms.

The earthward flow velocity increases at 04:02:42, and it is followed immediately by a step-like increase in  $B_z$ , namely, the dipolarization, at 04:03:15. Except around a sharp peak at 04:05:08 the flow is convective, that is, essentially perpendicular to the magnetic field. For about 15 min that follows  $B_z$  fluctuates with large amplitudes while  $V_x$  as well as  $V_{\perp,x}$  slowly oscillates around zero. Around 04:20  $B_z$  becomes enhanced further and the latitude angle becomes almost  $90^\circ$ . For this later interval the flow velocity cannot be reliably estimated since plasma observations are contaminated by penetrating energetic particles. (This contamination has been suppressed in the  $E$ - $t$  spectrogram of Figure 37.)

Statistical analysis of 24 events observed by GEOTAIL at  $-10 R_E > x > -20 R_E$  has confirmed that a step-like increase in  $B_z$  is usually seen at substorm onsets. The increase is preceded by the flow activity of the BBF type, and in the onset sector the earthward flowing ions with speeds higher than  $500 \text{ km s}^{-1}$  appear even near  $10 R_E$  in association with energization of ions and electrons. These ions usually have the dawnward component of velocity on the morning side and the duskward component on the evening side, which suggest that the earthward flow region expands longitudinally both westward and eastward. After the increase in  $B_z$  the magnetic field becomes almost due northward and highly variable in and near the equatorial plane. Sometimes slow tailward flows are observed but they

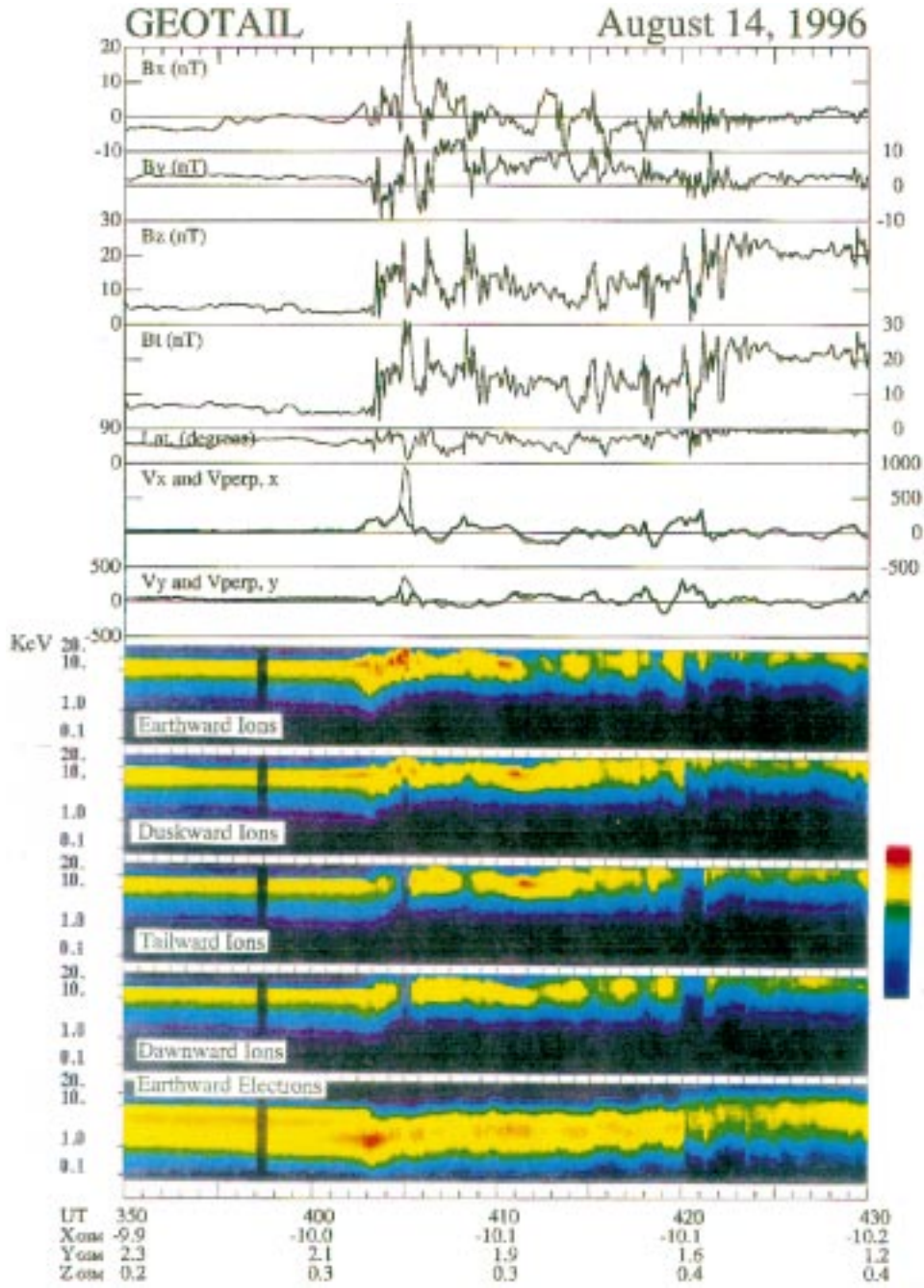


Figure 37. Dipolarization and bursty bulk flow observed in the near tail region (Nagai et al., 1999).

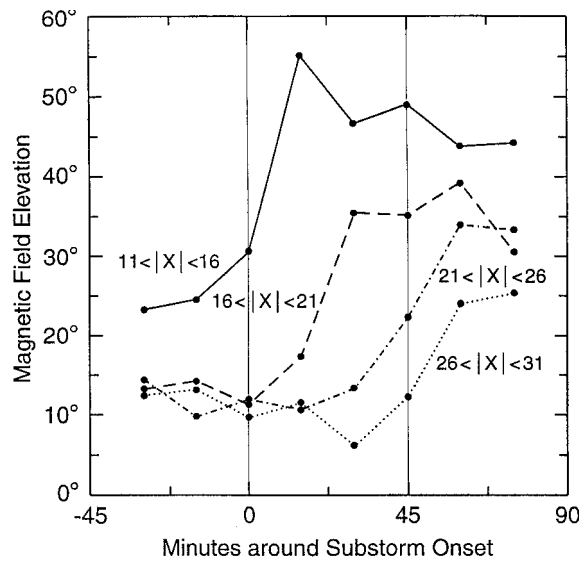


Figure 38. Average temporal evolution of the magnetic field inclination in the plasma sheet at different distance ranges around the substorm onset (Baumjohann et al., 1999).

seem to represent vortical flows that are generated outside the onset sector since these flows are associated with the northward  $B_z$  (Nagai et al., 1999). Study of an event observed at  $13 R_E$  has shown that the earthward convection speed can be as fast as  $2000 \text{ km s}^{-1}$  for a few min as estimated from the electric field of  $50 \text{ mV m}^{-1}$  (Fairfield et al., 1998).

The progression of the earthward flow is studied by superposed-epoch analysis in Figure 38 where time variations of the inclination of the magnetic field at four distance ranges are shown for an interval of  $-45 \text{ min}$  to  $90 \text{ min}$  relative to the substorm onset time. Averages have been calculated for 66 cases of substorms. It is seen that the dipolarization starts inside  $16 R_E$  at substorm onset (with a resolution of  $\pm 7.5 \text{ min}$ ) and moves tailward with an apparent speed of  $0.5 R_E \text{ min}^{-1}$  (Baumjohann et al., 1999). Tailward progression has also been deduced from the sequence of changes in  $B_z$  and  $B_x$  observed at dipolarization events at  $x \sim -15 R_E$  (Ohtani et al., 1992). This progression, however, does not necessarily mean that the current disruption actually occurs at successively further distances from the Earth. As the plasma is convected toward the Earth, its convection velocity which is inversely proportional to the magnetic field strength should decrease, and indeed the occurrence rate of high-speed earthward flows faster than  $400 \text{ km s}^{-1}$  drops sharply between  $19$  and  $12 R_E$  (Shiokawa et al., 1997). This decrease in the convection velocity would produce pile up of the field lines, and hence the dipolarization. The region of the dipolarization would move tailward as the sharp gradient in the field strength is formed at further distances with the progress of the pile up. Thus the tailward motion of the dipolarization is not inconsistent with the generation of

the earthward flow by reconnection which occurs tailward of dipolarization region (Hesse and Birn, 1991; Birn and Hesse, 1996).

It has been suggested that high-speed flows are braked by the tailward gradient of the pressure. The inertial current associated with the braking process is directed from dusk to dawn which is opposite to the direction of the cross-tail current, and this has been suggested to be the cause of the current disruption (Shiokawa et al., 1998). The braking process could also produce vortical and bouncing motions that involve tailward flows.

Although the earthward flow enhancements of the BBF type are the major carrier of energy and magnetic flux during substorms, significant quantitative discrepancy has been noted. The median values of earthward BBF particle, energy and magnetic flux transport are  $0.65 \times 10^{27} / R_E^2$ ,  $1.5 \times 10^{19} \text{ erg} / R_E^2$ , and  $2.5 \times 10^6 \text{ Wb} / R_E$ , respectively, whereas the median duration is 550 s. These median values are only 10% of the estimated values of the energy dissipated at the ionospheric heights during substorms, if cross sectional area is  $3 \times 3 R_E^2$  (Angelopoulos et al., 1994). Although the cross sectional area cannot be determined except in fortuitous cases when there is a dense network of satellites, they would not significantly exceed the above median values. On the other hand, the median rate of the BBF power transport of  $2.7 \times 10^{17} \text{ erg s}^{-1}$  is comparable to the dissipation rate  $4.0 \times 10^{17} \text{ erg s}^{-1}$  in substorms where energy is not injected into the ring current (Angelopoulos et al., 1994), and this suggests that the discrepancy stems mainly from difference in durations between BBF and substorm. Thus the issue seems to relate to the nature of the recovery phase of substorms which last several tens of minutes.

It should be noted that proper care must be used in deriving the moments from the plasma observations in the near-Earth tail. In active times it often happens that ion energies extend beyond the upper limit of the energy range of instruments, which is usually a few tens of keV. Moreover, penetration of energetic particles could sometimes produces spurious counts. At such times the moments derived straightforwardly from the data would not provide correct estimates of the fluxes.

As seen in Figure 37 the magnetic field becomes highly variable after  $B_z$  has started to increase, that is, after the dipolarization has set in. Large-amplitude fluctuations in the magnetic field are commonly associated with dipolarizations observed in the neutral sheet around midnight (Lui et al., 1992; Sergeev et al., 1993). The fluctuations reflect local and temporal variability in the current disruption. Case studies of these magnetic fluctuations using dual satellite observations at about  $8 R_E$  have shown that they have time scales of several times proton gyroperiod and there is noticeable delay between the onsets of magnetic fluctuations at two spacecraft which are separated by less than 10 proton gyroradii, which is too long to be due to the fast-mode propagation. Hence the disruption seems to represent a system of chaotic electric current filaments (Ohtani et al., 1998). Noting also that the particle pressure increases and density of the cross-tail current intensifies toward the onset of the dipolarization in the above distance range, it has been suggested that the chaotic current disruption is due to cross-field current instability

(Lui et al., 1992) and that it plays a key role in the substorm initiation by causing the diversion of the tail current to the ionosphere, that is, by generating the substorm current wedge (Lui, 1991). Lui (1996) has summarized the proposed scenario as follows. During the substorm growth phase the plasma sheet starts to thin and the cross-tail current density increases. When the relative drift between ions and electrons becomes sufficiently high to exceed the onset threshold of the cross-field current instability, broadband electromagnetic waves are excited. The turbulence after this instability onset impedes the particle motion and reduces the current density locally. Substorm expansion phase onset will occur when the global constraint is favorable for establishing the substorm current wedge. The onset of this instability causes near-Earth current disruption which offsets the global equilibrium, resulting in earthward particle injection and collapse of stretched magnetic field lines. The near-Earth activity launches a rarefaction wave down the tail, modifying the midtail plasma sheet to allow the onset of magnetic reconnection there. Thus in this scenario magnetic reconnection occurs after the current disruption in the current sheet nearer to the Earth rather than initiating the sequence of disturbances.

It remains to be seen how the cross-field current instability, which is intrinsically a local process having scale lengths comparable to the thermal ion gyroradius and time scales comparable to or shorter than the ion gyroperiod, can generate global disturbance that is observed during substorms. Vasyliunas (1998) has pointed out that the current disruption is expected to cause tailward, instead of earthward, motion of plasma and field lines since outward pressure gradient is no longer balanced with the  $\mathbf{j} \times \mathbf{B}$  force when the current is disrupted. Although Wiechen et al. (1996) have claimed that their simulation shows that earthward flow can occur even tailward of the reconnection region, inspection of their figure reveals that what is taking place is not reconnection but reverse reconnection in which the flow through the X-type neutral line region is away from the equator. Moreover, their earthward flow represents the  $\mathbf{E} \times \mathbf{B}$  drift where  $\mathbf{E}$  is generated artificially as the resistivity is introduced in the region where current in the dawn-to-dusk direction has existed.

Although most of the BBF events take place under geomagnetically active conditions, it has been noted that some events take place during quiet intervals (Angelopoulos et al., 1994). In fact the earthward injection of plasma from the tail is observed even in intervals when the geomagnetic activity as measured by  $Kp$  is extremely low. Figure 39 shows the ion temperature and density (in the top panel), magnetic field (second panel), convection velocity (third panel), and  $E-t$  spectrogram (fourth panel) that are observed during a tail traversal along the inner edge of the plasma sheet in an extremely quiet geomagnetic condition (where  $Kp$  was less than 1-). The perigee of the spacecraft orbit was around 17 UT when the distance was  $10 R_E$  and the local time was midnight, and the orbit was almost symmetric with respect to it. In the ion and electron spectrograms (second and third data from the bottom) there are several enhancements which are indicated by wedge marks below the ion spectrogram. Since these enhancements occur simultaneously over

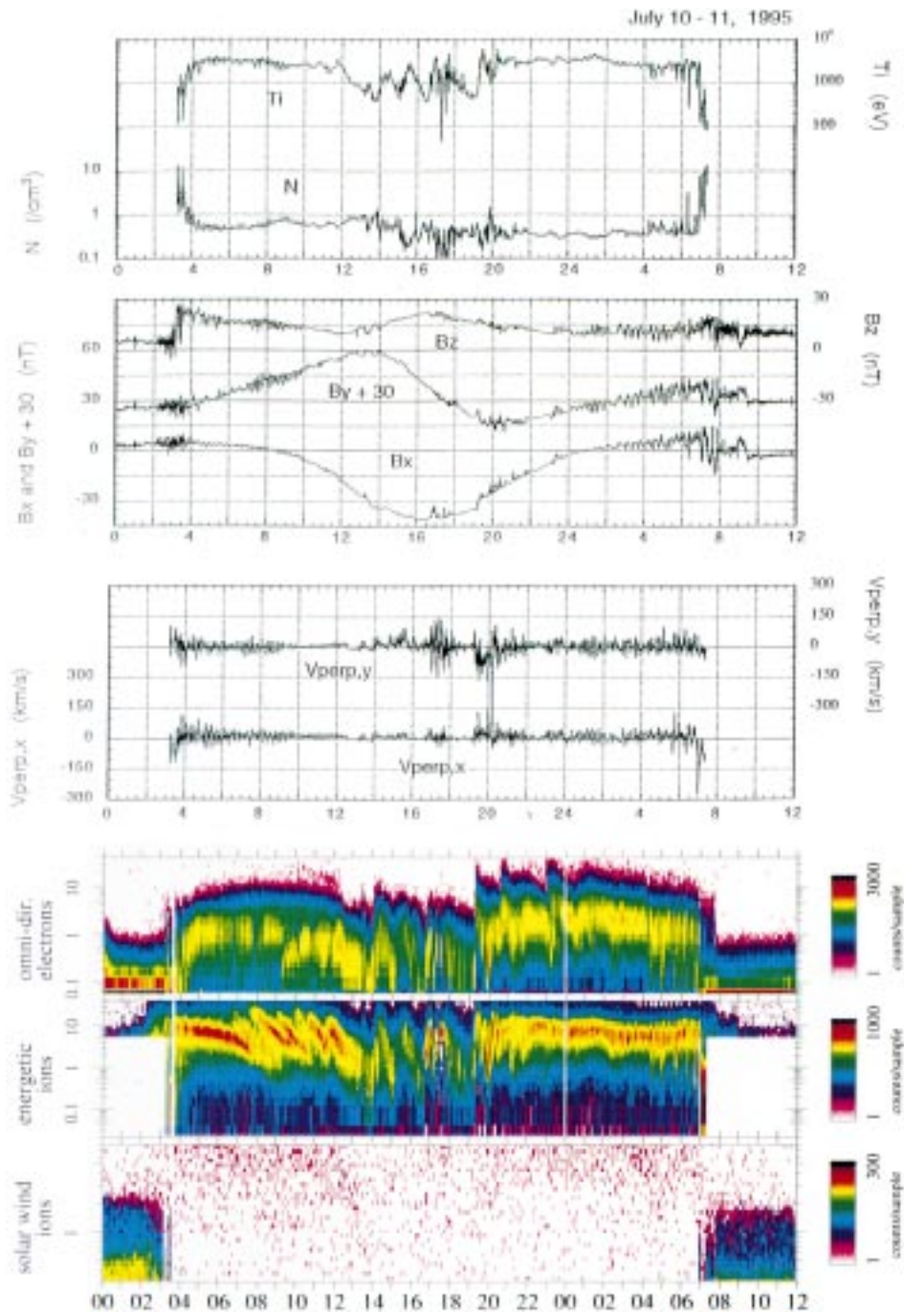


Figure 39. Earthward plasma injection observed at 10  $R_E$  during an extremely quiet geomagnetic condition. The injection events are marked by wedges below the second panel (showing the magnetic field data), inside the third panel (showing the convection velocity) and below the second data from the bottom (showing the ion  $E-t$  spectrogram) (Nishida et al., 1997).

a wide energy range of 1 to 10 keV, these can be interpreted to be injections with the  $\mathbf{E} \times \mathbf{B}$  drift velocity, while the dispersive (that is, energy dependent) structures of ions that are seen in the dusk sector before 12 UT represent the azimuthal drift of the ion patches after the injection. The injection events are seen during several hours' interval around the midnight crossing and are accompanied by increases in the ion temperature  $T_i$ , decrease in  $B_x$ , and increase in  $V_{\perp,x}$ . (Weakness or absence of  $B_z$  enhancements for the first three events is due to large separation of the spacecraft from the neutral sheet as demonstrated by large  $|B_x|$ .) Thus the mechanism that drives the tail plasma earthward and has been ascribed to magnetic reconnection operates during extremely quiet conditions as well (Nishida et al., 1997). Lyons et al. (1998) have suggested that the earthward flows during quiet times are associated with 'separatrix disturbances' in aurora which initiate near the boundary between open and closed field lines and move equatorward at speeds of  $\sim 500 \text{ km s}^{-1}$ . The auroral disturbances of this kind occur during all levels of geomagnetic activity and seem to reflect bursty enhancements in the reconnection rate at the distant neutral line.

The  $\kappa$  parameter for the ions is greater than 1 in the inner magnetosphere so that the ion motions are adiabatic, while it tends to be less than 1 in the distant tail. In the intermediate distance range in the near-Earth tail where  $\kappa$  is about unity the ion motion is stochastic due to deterministic chaos. Because times scales of the bounce motion along field lines and of the half gyration in the neutral sheet are comparable, ions undergo complicated motions. The perturbation to the ion motion can be interpreted to be due to an impulsive centrifugal force that operates when ions traverse the neutral sheet, and pitch angle is scattered and prominent bunching occurs in gyrophase at relatively small pitch angles (Delcourt and Belmont, 1998).

The plasma sheet boundary layer (PSBL) in the near-Earth magnetotail has been illustrated in Figure 25. Earthward moving beams of energetic ions ( $>24 \text{ keV}$ ) are observed at the plasma sheet boundary at distances of 16 to 22  $R_E$  and they are sometimes accompanied on its equatorward side by the tailward beam which is interpreted as representing reflections from the mirror point near the Earth (Williams, 1981). Layered structure of the earthward beam and the counterstreaming ion beam on the equatorward side has been observed also for the bulk of the ions having kinetic energies of 1 to 29 keV at distances of  $x = -7$  and  $-13 R_E$  near local midnight (Takahashi and Hones, 1988). We note that the PSBL beams originating from the near-Earth and distant neutral lines are not clearly distinguished in these works.

## 5. Problems for Future Studies

While much has been learned about physics of the Earth's magnetotail by decades of intense studies, several important questions remain. These are listed below.

(1) Ion acceleration: respective roles of slow-mode shock and neutral sheet. The mechanism by which cold ions of the tail lobe are heated and fill the plasma sheet is not yet fully understood. The classical model of Axford et al. (1965) where the plasma is heated at a pair of slow shocks that bound the plasma sheet is often taken as a norm, but both theory and observations have clearly demonstrated that heating occurs also in the neutral sheet. We should understand how the heating mechanisms operating at the slow shock and in the neutral sheet combine to produce the plasma sheet as observed. Each of these two mechanisms has its own character: Ion acceleration in the neutral sheet requires  $k$  parameter of about 1 or less, that is, thin plasma sheet and/or weak magnetic field across the neutral sheet, while the slow-mode shock is formed when the slow-mode Mach number exceeds 1. Relative contributions of respective mechanisms in the plasma sheet formation are likely to vary from time to time.

(2) Electron acceleration. The mechanism of the electron heating and acceleration is even less well understood than that of ions. We still have little idea about why the temperature ratio between ions and electrons tends to take a relatively constant value. This is all the more puzzling because the dominant acceleration mechanism probably differs between ions and electrons; frequent appearance of electron dumbbell-type pitch angle distribution suggests that acceleration by field-aligned electric field plays an important role in the electron case, while the condition for acceleration in the neutral sheet is much more difficult to satisfy for electrons than for ions. It also remains to explain how bursts of energetic electrons with relativistic energies are generated in the magnetotail in association with substorm onsets. The electron temperature in the slow-mode expansion fan does not vary as expected from a simple model, either. The clarification of the electron dynamics should be one of the principal targets of the magnetotail research in future.

(3) Low-latitude boundary layer. Origin of the LLBL, specifically the inner LLBL, is still a problem. In this layer two plasma components from different origins are mixed in real space but well separated in velocity space. The formation of the LLBL could be more than a boundary-layer issue since mixture of cold sheath-type ions with hot tail-type ions is sometimes observed over a thickness of several  $R_E$  and at distances quite far from the magnetopause. The flow speed is low and variable for both components, so that it is not obvious what trajectories they have taken before reaching there. In the framework of the open magnetosphere model where reconnection plays a pivotal role, the mixing could occur when field lines which have been loaded with one of the components reconnect again with field lines that have another component. Alternatively the mixing may be due to diffusion that occurs in some specific region, but so far we have not seen unambiguous evidence of diffusive transport itself nor of presence of waves that are strong enough for significant diffusion to take place.

(4) Beginning and end of reconnection. Sequence of processes that lead to onset of the near-Earth reconnection and its relation to substorm onset remain to be pursued. It is also important to understand what makes the near-Earth recon-

nection stop operating. Kinetic/inertia effects play crucial role in the proximity of the X-type neutral line, while the progress of reconnection should be controlled by global conditions. Hence to answer the question raised here is to understand how the microscopic dynamics matches the requirements from the macroscopic dynamics. Understanding this coupling is important not only for understanding the reconnection process but the magnetospheric physics in general. The same can be said for turbulences which are often seen in the magnetotail. The global condition for development of turbulences as well as the effects of turbulences on global dynamics through plasma mixing, heating and modulation of electric currents need be better understood.

(5) Coupling between the tail dynamics and the auroral processes. Part of energy that is released in the magnetotail is deposited to the polar ionosphere and produces auroral phenomena. Conversely the disturbances that result in the ionosphere are projected back to the magnetotail. Thus dynamics of the magnetotail and the aurora are closely coupled and need be understood as a unified entity. Moreover, spacecraft observations of the global aurora have a distinct advantage in presenting a synoptic picture of the global disturbance while the tail observations are available only at one point, or a few points at best. Naturally it is important to promote comparative studies of the tail dynamics and the auroral features. Such studies have already been conducted, but attention has tended to be focused on the magnetospheric substorm and, more specifically, on its onset. Although this is obviously a vital subject which deserves intense research efforts, I would emphasize that substorm is not the only category of the auroral activity. The auroral morphology includes a large variety of features such as arcs, surges, bands and recently proposed separatrix disturbances, which are considered to reflect such basic processes as the convection of open flux tubes, instability in the plasma sheet, reconnection at the distant neutral line, and ionosphere-magnetosphere coupling. Clarification of the relation of these features with the tail dynamics should also be an important and rewarding area for future research. A wealth of new signatures of the tail dynamics probably remains to be identified in the GEOTAIL data.

### **Acknowledgements**

I thank the GEOTAIL team members for successfully conducting the mission. Very useful comments by M. Fujimoto, M. Hoshino, H. Kawano, K. Maezawa, T. Mukai, T. Nagai, and T. Terasawa are gratefully acknowledged. For some of the diagrams new versions are produced by M. Hoshino and K. Seki.

## References

- Anderson, K. A., Harris, H. K. and Paoli, R. J.: 1965, 'Energetic Electron Fluxes in and Beyond the Earth's Outer Magnetosphere', *J. Geophys. Res.* **70**: 1039–1050.
- André, M. and Yau, A.: 1997, 'Theories and Observations of Ion Energization and Outflow in the High Latitude Magnetosphere', *Space Sci. Rev.* **80**: 27–48.
- Angelopoulos, V., Baumjohann, W., Kennel, C. F., Coroniti, F. V., Kivelson, M. G., Pellat, R., Walker, R. J., Lühr, H. and Paschmann, G.: 1992, 'Bursty Bulk Flows in the Inner Central Plasma Sheet', *J. Geophys. Res.* **97**: 4027–4039.
- Angelopoulos, V., Kennel, C. F., Coroniti, F. V., Pellat, R., Kivelson, M. G., Walker, R. J., Russell, C. T., Baumjohann, W., Feldman, W. C. and Gosling, J. T.: 1994, 'Statistical Characteristics of Bursty Bulk Flow Events', *J. Geophys. Res.* **99**: 21257–21280.
- Ashour-Abdalla, M., El-Alaoui, M., Perroomian, V., Raeder, J., Walker, R. J., Richard, R. L., Zelenyi, L. M., Frank, L. A., Paterson, W. R., Bosqued, J. M., Lepping, R. P., Ogilvie, K., Kokubun, S. and Yamamoto, T.: 1997, 'Ion Sources and Acceleration Mechanisms Inferred from Local Distribution Functions', *Geophys. Res. Lett.* **24**: 955–958.
- Ashour-Abdalla, M., Raeder, J., El-Alaoui, M. and Perroomian, V.: 1998, in A. Nishida, D. N. Baker and S. W. H. Cowley (eds.), 'Magnetotail Structure and Its Internal Dynamics During Northward IMF', *New Perspectives on the Earth's Magnetotail*, Geophys. Mono., Vol. 105, Amer. Geophys. Union, Washington D. C., pp. 77–95.
- Axford, W. I., Petschek, H. E. and Siscoe, G. L.: 1965, 'Tail of the Magnetosphere', *J. Geophys. Res.* **70**: 1231–1236.
- Axford, W. I.: 1999, 'Reconnection, Substorms, and Solar Flares', *Phys. Chem. Earth* **24**: 147–151.
- Baker, D. N., Bame, S. J., Feldman, W. C., Gosling, J. T., Zwickl, R. D., Slavin, J. A. and Smith, E. J.: 1986, 'Strong Electron Bidirectional Anisotropies in the Distant Tail; ISEE 3 Observations of Polar Rain', *J. Geophys. Res.* **91**: 5637–5662.
- Baker, D. N., Anderson, R. C., Zwickl, R. D. and Slavin, J. A.: 1987, 'Average Plasma and Magnetic Field Variations in the Distant Magnetotail Associated with Near-Earth Substorm Effects', *J. Geophys. Res.* **92**: 71–81.
- Baker, D. N. and Pulkkinen, T. I.: 1998, in A. Nishida, D. N. Baker and S. W. H. Cowley, 'Large-Scale Structure of the Magnetosphere', *New Perspectives on the Earth's Magnetotail*, Geophys. Mono., Vol. 105, pp. 21–31, Amer. Geophys. Union, Washington D. C.
- Baumjohann, W., Paschmann, G. and Cattell, C. A.: 1989, 'Average Plasma Properties in the Central Plasma Sheet', *J. Geophys. Res.* **94**: 6597–6606.
- Baumjohann, W.: 1998, in A. Nishida, D. N. Baker and S. W. H. Cowley (eds), 'Ion and Electron Heating in the Near-Earth Tail', *New Perspectives on the Earth's Magnetotail*, Geophys. Mono., Vol. 105, pp. 97–102, Amer. Geophys. Union, Washington D. C.
- Baumjohann, W., Hesse, M., Kokubun, S., Mukai, T., Nagai, T. and Petrukovich, A.: 1999, 'Substorm Dipolarization and Recovery', *J. Geophys. Res.* **104**: 24995–25000.
- Birn, J. and Hesse, M.: 1996, 'Details of Current Disruption and Diversion in Simulations of Magnetotail Dynamics', *J. Geophys. Res.* **101**: 15345–15358.
- Büchner, J. and Zelenyi, L. M.: 1989, 'Regular and Chaotic Charged Particle Motion in Magnetotail-like Field Reversals, 1, Basic Theory of Trapped Motion', *J. Geophys. Res.* **94**: 11821–11842.
- Candidi, M., Orsini, S. and Formisano, V.: 1982, 'The Properties of Ionospheric O<sup>+</sup> Ions as Observed in the Magnetotail Boundary Layer and Northern Plasma Lobe', *J. Geophys. Res.* **87**: 9097–9106.
- Cattell, C. A. and Mozer, F. S.: 1986, 'Experimental Determination of the Dominant Wave Mode in the Active Near-Earth Magnetotail', *Geophys. Res. Lett.* **13**: 221–224.
- Chappell, D. R., Moore, T. E. and Waite, J. H. Jr.: 1987, 'The Ionosphere as a Fully Adequate Source of Plasma for the Earth's Magnetosphere', *J. Geophys. Res.* **92**: 5896–59107.

- Christon, S. P., Eastman, T. E., Doke, T., Frank, L. A., Gloeckler, G., Kojima, H., Kokubun, S., Lui, A. T. Y., Matsumoto, H., McEntire, R. M., Mukai, T., Nylund, S. R., Paterson, W. R., Roelof, E. C., Saito, Y., Sotirelis, T., Tsuruda, K., Williams, D. J. and Yamamoto, T.: 1998, 'Magnetospheric Plasma Regimes Identified Using Geotail Measurements 2. Statistics, Spatial Distribution, and Geomagnetic Dependence', *J. Geophys. Res.* **103**: 23521–23542.
- Coroniti, F. V.: 1971, 'Laminar Wave-Train Structure of Collisionless Magnetic Slow Shocks', *Nucl. Fusion* **11**: 261–283.
- Cowley, S. W. H.: 1981, 'Magnetospheric Asymmetries Associated with the Y-Component of the IMF', *Planet. Space Sci.* **29**: 79–96.
- Delcourt, D. C. and Belmont, G.: 1998, in A. Nishida, D. N. Baker and S. W. H. Cowley (eds.), 'Particle Dynamics in the Near-Earth Magnetotail and Macroscopic Consequences', *New Perspectives on the Earth's Magnetotail*, Geophys. Mono., Vol. 105, pp. 193–210, Amer. Geophys. Union, Washington D. C.
- Dungey, J. W.: 1965, 'The Length of the Magnetospheric Tail', *J. Geophys. Res.* **70**: 1753.
- Eastman, T. E., Christon, S. P., Doke, T., Frank, L. A., Gloeckler, G., Kojima, H., Kokubun, S., Lui, A. T. Y., Matsumoto, H., McEntire, R. M., Mukai, T., Paterson, W. R., Roelof, E. C., Saito, Y., Tsuruda, K., Williams, D. J. and Yamamoto, T.: 1998, 'Magnetospheric Plasma Regimes Identified Using Geotail Measurements 1. Regime Identification and Distant Tail Variability', *J. Geophys. Res.* **103**: 23503–23520.
- Fairfield, D. H.: 1992, 'On the Structure of the Distant Tail: ISEE 3', *J. Geophys. Res.* **97**: 1403–1410.
- Fairfield, D. H. and Ness, N. F.: 1970, 'Configuration of the Geomagnetic Tail During Substorms', *J. Geophys. Res.* **75**: 7032–7047.
- Fairfield, D. H. and Jones, J.: 1996, 'Variability of the Tail Lobe Field Strength', *J. Geophys. Res.* **101**: 7785–7791.
- Fairfield, D. H., Mukai, T., Lui, A. T. Y., Cattell, C. A., Reeves, G. D., Nagai, T., Rostoker, G., Singer, H. J., Kaiser, M. L., Kokubun, S., Lazarus, A. J., Lepping, R. P., Nakamura, M., Steinberg, J. T., Tsuruda, K., Williams, D. J. and Yamamoto, T.: 1998, 'Geotail Observations of Substorm Onset in the Inner Magnetotail', *J. Geophys. Res.* **103**: 103–117.
- Fedder, J. A. and Lyon, J. G.: 1995, 'The Earth's Magnetosphere is 165  $R_E$  Long: Self-Consistent Currents, Convection, Magnetic Structure, and Processes for Northward Interplanetary Magnetic Field', *J. Geophys. Res.* **100**: 3623–3635.
- Feldman, W. C., Schwartz, S. J., Bame, S. J., Baker, D. N., Birn, J., Gosling, J. T., Hones, E. W. Jr., McComas, D. J., Slavin, J. A., Smith, E. J. and Zwickl, R. D.: 1984, 'Evidence for Slow-Mode Shocks in the Deep Geomagnetic Tail', *Geophys. Res. Lett.* **11**: 599–602.
- Feldman, W. C., Tokar, R. L., Birn, J., Hones, E. W. Jr., Bame, S. J. and Russell, C. T.: 1987, 'Structure of a Slow Mode Shock Observed in the Plasma Sheet Boundary Layer', *J. Geophys. Res.* **92**: 83–94.
- Frank, L. A., Ackerson, K. L. and Yeager, D. M.: 1977, 'Observations of Atomic Oxygen ( $O^+$ ) in the Earth's Magnetotail', *J. Geophys. Res.* **82**: 129–134.
- Frank, L. A., Paterson, W. R. and Kivelson, M. G.: 1994, 'Observations of Nonadiabatic Acceleration of Ions in Earth's Magnetotail', *J. Geophys. Res.* **99**: 14877–14890.
- Frank, L. A., Paterson, W. R., Kokubun, S., Yamamoto, T., Lepping, R. P. and Ogilvie, K. W.: 1997, 'Observations of a Current Pulse in the Near-Earth Plasma Sheet Associated with a Substorm Onset', *Geophys. Res. Lett.* **24**: 967–970.
- Fujimoto, M. and Terasawa, T.: 1994, 'Anomalous Ion Mixing Within an MHD Scale K-H Vortex', *J. Geophys. Res.* **99**: 8601–8613.
- Fujimoto, M., Nishida, A., Mukai, T., Saito, Y., Yamamoto, T. and Kokubun, S.: 1996a, 'Plasma Entry from the Flanks of the Near-Earth Magnetotail: Geotail Observations in the Dawnside LLBL and the Plasma Sheet', *J. Geomag. Geoelectr.* **48**: 711–727.

- Fujimoto, M., Nakamura, M. S., Nagai, T., Mukai, T., Yamamoto, T. and Kokubun, S.: 1996b, 'New Kinetic Evidence for the Near-Earth Reconnection', *Geophys. Res. Lett.* **23**: 2533–2536.
- Fujimoto, M., Nakamura, M. S., Shinohara, I., Nagai, T., Mukai, T., Saito, Y., Yamamoto, T. and Kokubun, S.: 1997, 'Observations of Earthward Streaming Electrons at the Trailing Boundary of a Plasmoid', *Geophys. Res. Lett.* **24**: 2893–2896.
- Fujimoto, M., Terasawa, T., Mukai, T., Saito, Y., Yamamoto, T. and Kokubun, S.: 1998a, 'Plasma Entry from the Flanks of the Near-Earth Magnetotail: Geotail Observations', *J. Geophys. Res.* **103**: 4391–4408.
- Fujimoto, M., Terasawa, T. and Mukai, T.: 1998b, in A. Nishida, D. N. Baker and S. W. H. Cowley (eds), 'The Low-Latitude Boundary Layer in the Tail-Flanks', *New Perspectives on the Earth's Magnetotail*, Geophys. Mono., Vol. 105, pp. 33–44, Amer. Geophys. Union, Washington D. C.
- Fuselier, S. A., Anderson, B. J. and Onsager, T. G.: 1995, 'Particle Signature of Magnetic Topology at the Magnetopause: AMPTE/CCE Observations', *J. Geophys. Res.* **100**: 11805–11821.
- Gary, S. P., Madland, C. D., Schriver, D. and Winske, D.: 1986, 'Computer Simulations of Electromagnetic Cool Ion Beam Instabilities', *J. Geophys. Res.* **91**: 4188–4200.
- Gosling, J. T., Baker, D. N., Bame, S. J., Feldman, W. C., Zwickl, R. and Smith, E. J.: 1985, 'North-South and Dawn-Dusk Asymmetries in the Distant Tail Lobes: ISEE 3', *J. Geophys. Res.* **90**: 6354–6360.
- Gosling, J. T., Thomsen, M. F., Bame, S. J., Elphic, R. C. and Russell, C. T.: 1991, 'Observations of Reconnection of Interplanetary and Lobe Magnetic Field Lines at the High-Latitude Magnetopause', *J. Geophys. Res.* **96**: 14097–14106.
- Gosling, J. T., Thomsen, M. F., Le, G. and Russell, C. T.: 1996, 'Observations of Magnetic Reconnection at the Lobe Magnetopause', *J. Geophys. Res.* **101**: 24765–24773.
- Heikkila, W. J.: 1988, 'Current-Sheet Crossings in the Distant Magnetotail', *Geophys. Res. Lett.* **15**: 299–302.
- Hess, M. and Birn, J.: 1991, 'On Dipolarization and its Relation to the Substorm Current Wedge', *J. Geophys. Res.* **96**: 19417–19426.
- Hesse, M., Birn, J., Kuznetsova, M. M. and Dreher, J.: 1996, 'A Simple Model of Core Field Generation During Plasmoid Evolution', *J. Geophys. Res.* **101**: 10797–10804.
- Hill, T. W.: 1975, 'Magnetic Merging in a Collisionless Plasma', *J. Geophys. Res.* **80**: 4689–4699.
- Hirahara, M., Terasawa, T., Mukai, T., Hoshino, M., Saito, Y., Machida, S., Yamamoto, T. and Kokubun, S.: 1997, 'Cold Ion Streams Consisting of Double Proton Populations and Singly Charged Oxygen Observed at the Distant Magnetopause by Geotail: A Case Study', *J. Geophys. Res.* **102**: 2359–2372.
- Hirahara, M., Seki, K. and Mukai, T.: 1998, in A. Nishida, D. N. Baker and S. W. H. Cowley (eds), 'Cold Dense Ion Flows in the Distant Magnetotail: The Geotail Results', *New Perspectives on the Earth's Magnetotail*, Geophys. Mono. Vol. 105, pp. 45–60, Amer. Geophys. Union, Washington D. C.
- Hones, E. W., Jr.: 1979, 'Transient Phenomena in the Magnetotail and their Relation to Substorms', *Space Sci. Rev.* **23**: 393–410.
- Hoshino, M., Nishida, A., Mukai, T., Saito, Y., Yamamoto, T. and Kokubun, S.: 1996a, 'Structure of Plasma Sheet in Magnetotail: Double-Peaked Electric Current', *J. Geophys. Res.* **101**: 24775–24786.
- Hoshino, M., Mukai, T., Nishida, A., Saito, Y., Yamamoto, T. and Kokubun, S.: 1996b, 'Evidence of Two Active Reconnection Sites in the Distant Magnetotail', *J. Geomag. Geoelectr.* **48**: 515–523.
- Hoshino, M.: 1998a, in A. Nishida, D. N. Baker and S. W. H. Cowley (eds), 'Kinetic Ion Behavior in Magnetic Reconnection Region', *New Perspectives on the Earth's Magnetotail*, Geophys. Mono., Vol. 105, pp. 153–166, Amer. Geophys. Union, Washington D. C.
- Hoshino, M.: 1998b, in S. Kokubun and Y. Kamide (eds), 'Magnetic Reconnection Beyond Ion Inertial Scale', *Substorms-4*, pp. 473–478, Kluwer Academic Publishers, The Netherlands.

- Hoshino, M., Mukai, T., Yamamoto, T. and Kokubun, S.: 1998, 'Ion Dynamics in Magnetic Reconnection: Comparison between Numerical Simulation and Geotail Observations', *J. Geophys. Res.* **103**: 4509–4530.
- Hughes, W. J. and Sibeck, D. G.: 1987, 'On the 3-Dimensional Structure of Plasmoids', *Geophys. Res. Lett.* **14**: 636–639.
- Ieda, A., Machida, S., Mukai, T., Saito, Y., Yamamoto, T., Nishida, A., Terasawa, T. and Kokubun, S.: 1998, 'Statistical Analysis of the Plasmoid Evolution with Geotail Observations', *J. Geophys. Res.* **103**: 4453–4465.
- Kawano, H., Fujimoto, M., Mukai, T., Yamamoto, T., Terasawa, T., Saito, Y., Machida, S., Kokubun, S. and Nishida, A.: 1994, 'Right-Handed Ion/Ion Resonant Instability in the Plasma Sheet Boundary Layer: Geotail Observation in the Distant Tail', *Geophys. Res. Lett.* **21**: 2887–2890.
- Kawano, H., Nishida, A., Fujimoto, M., Mukai, T., Kokubun, S., Yamamoto, T., Terasawa, T., Hirahara, M., Saito, Y., Machida, S., Yumoto, K., Matsumoto, H. and Murata, T.: 1996, 'A Quasi-Stagnant Plasmoid Observed with Geotail on October 15, 1993', *J. Geomag. Geoelectr.* **48**: 526–539.
- Kan, J. R.: 1993, 'A Global Magnetosphere-Ionosphere Coupling Model of Substorms', *J. Geophys. Res.* **98**: 17263–17275.
- Kokubun, S., Frank, L. A., Hayashi, K., Kamide, Y., Lepping, R. P., Mukai, T., Nakamura, R., Paterson, W. R., Yamamoto, T. and Yumoto, K.: 1996, 'Large Field Events in the Distant Magnetotail During Magnetic Storms', *J. Geomag. Geoelectr.* **48**: 561–575.
- Le, G., Russell, C. T., Gosling, J. T. and Thomsen, M. F.: 1996, 'ISEE Observations of Low-Latitude Boundary Layer for Northward Interplanetary Magnetic Field: Implications for Cusp Reconnection', *J. Geophys. Res.* **101**: 27239–27249.
- Lennartsson, W.: 1992, 'A Scenario for Solar Wind Penetration of Earth's Magnetic Tail Based on Ion Composition Data from the ISEE 1 Spacecraft', *J. Geophys. Res.* **97**: 19221–19238.
- Levy, R. H., Petschek, H. E. and Siscoe, G. L.: 1964, 'Aerodynamic Aspects of the Magnetosphere Flow', *AIAA J.* **2**: 2065–2076.
- Lottermoser, R.-F., Scholer, M. and Matthews, A. P.: 1998, 'Ion Kinetic Effects in Magnetic Reconnection: Hybrid Simulations', *J. Geophys. Res.* **103**, 4547–4559.
- Lui, A. T. Y.: 1991, 'A Synthesis of Magnetospheric Substorm Models', *J. Geophys. Res.* **96**: 1849–1856.
- Lui, A. T. Y., Lopez, R. E., Anderson, B. J., Takahashi, K., Zanetti, L. J., McEntire, R. E., Potemra, T. A., Klumpp, D. M., Greene, E. M. and Strangeway, R.: 1992, 'Current Disruptions in the Near-Earth Neutral Sheet Region', *J. Geophys. Res.* **97**: 1461–1480.
- Lui, A. T. Y.: 1996, 'Current Disruption in the Earth's Magnetosphere: Observations and Models', *J. Geophys. Res.* **100**: 13067–13088.
- Lui, A. T. Y., Williams, D. J., McEntire, R. W., Christon, S. P., Eastman, T. E., Yamamoto, T. and Kokubun, S.: 1998, 'Ion Composition and Charge State of Energetic Particles in Flux Ropes/Plasmoids', *J. Geophys. Res.* **103**: 4467–4475.
- Lyons, L. R.: 1995, 'A New Theory for Magnetospheric Substorms', *J. Geophys. Res.* **100**: 19069–19081.
- Lyons, L. R., Blanchard, G. T., Samson, J. C., Rouhoniemi, J. M., Greewald, R. A., Reeves, D. and Scudder, J. D.: 1998, in A. Nishida, D. N. Baker and S. W. H. Cowley (eds), 'Near Earth Plasma Sheet Penetration and Geomagnetic Disturbances', *New Perspectives on the Earth's Magnetotail*, Geophys. Mono., Vol. 105, pp. 241–257, Amer. Geophys. Union, Washington D. C.
- McComas, D. J., Russell, C. T., Elphic, R. C. and Bame, S. J.: 1986, 'The Near-Earth Cross-Tail Current Sheet: Detailed ISEE 1 and 2 Case Studies', *J. Geophys. Res.* **91**: 4287–4301.
- Macwan, S. E.: 1992, 'A Determination of Twisting of the Earth's Magnetotail at Distances 115–220  $R_E$ : ISEE 3', *J. Geophys. Res.* **97**: 19239–19249.

- Maezawa, K.: 1976, 'Magnetic Convection Induced by the Positive and Negative  $z$  Components of the Interplanetary Magnetic Field: Quantitative Analysis Using Polar Cap Magnetic Records', *J. Geophys. Res.* **81**: 2289–2303.
- Maezawa, K. and Hori, T.: 1998, in A. Nishida, D. N. Baker and S. W. H. Cowley (eds), 'The Distant Magnetotail: Its Structure, IMF Dependence and Thermal Properties', *New Perspectives on the Earth's Magnetotail*, Geophys. Mono., Vol. 105, pp. 1–19, Amer. Geophys. Union, Washington D.C.
- Maezawa, K., Hori, T., Mukai, T., Saito, Y., Yamamoto, T., Kokubun, S. and Nishida, A.: 1997, 'Structure of the Distant Magnetotail and its Dependence on the IMF By Component: Geotail Observations', *Adv. Space Res.* **20**: 949–959.
- Matsumoto, H., Kojima, H., Omura, Y. and Nagano, I.: 1998, in A. Nishida, D. N. Baker and S. W. H. Cowley (eds), 'Plasma Waves in Geospace: Geotail Observations', *New Perspectives on the Earth's Magnetotail*, Geophys. Mono., Vol. 105, pp. 259–319, Amer. Geophys. Union, Washington D. C.
- McPherron, R. L., Aubry, M. P., Russell, C. T. and Coleman, P. J. Jr.: 1973a, 'Satellite Studies of Magnetospheric Substorms on August 15, 1968, 4. Ogo 4 Magnetic Field Observations', *J. Geophys. Res.* **78**: 3068–3078.
- McPherron, R. L., Russell, C. T. and Aubry, M. P.: 1973b, 'Satellite Studies of Magnetospheric Substorms on August 15, 1968, 9. Phenomenological Model for Substorms', *J. Geophys. Res.* **78**: 3131–3149.
- Moldwin, M. B. and Hughes, W. J.: 1992, 'On the Formation and Evolution of Plasmoids: A Survey of ISEE 3 Geotail Data', *J. Geophys. Res.* **97**: 19259–19282.
- Mozer, F. S., Hayakawa, H., Kokubun, S., Nakamura, M., Okada, T., Yamamoto, T. and Tsuruda, K.: 1994, 'The Morning Side Low-Latitude Boundary Layer as Determined from Electric and Magnetic Field Measurements on Geotail', *Geophys. Res. Lett.* **21**: 2983–2986.
- Mukai, T., Hirahara, M., Machida, S., Saito, Y., Terasawa, T. and Nishida, A.: 1994, 'Geotail Observation of Cold Ion Streams in the Medium Distance Magnetotail Lobe in the Course of a Substorm', *Geophys. Res. Lett.* **21**: 1023–1026.
- Mukai, T., Fujimoto, M., Hoshino, M., Kokubun, S., Machida, S., Maezawa, K., Nishida, A., Saito, Y., Terasawa, T. and Yamamoto, T.: 1996, 'Structure and Kinetic Properties of Plasmoids and Their Boundary Regions', *J. Geomag. Geoelectr.* **48**: 541–560.
- Mukai, T., Yamamoto, T. and Machida, S.: 1998a, in A. Nishida, D. N. Baker and S. W. H. Cowley (eds), 'Dynamic and Kinetic Properties of Plasmoids and Flux Ropes: Geotail Observations', *New Perspectives on the Earth's Magnetotail*, Geophys. Mono., Vol. 105, pp. 117–137, Amer. Geophys. Union, Washington D. C.
- Mukai, T., Hoshino, M., Saito, Y., Shinohara, I., Yamamoto, T., Nagai, T. and Kokubun, S.: 1998b, in S. Kokubun and Y. Kamide (eds), 'Pre-Onset and Onset Signatures for Substorms in the Near-Tail Plasma Sheet: Geotail Observations', *Substorms-4*, pp. 131–136, Kluwer Academic Publishers, The Netherlands.
- Nagai, T., Mukai, T., Yamamoto, T., Nishida, A., Kokubun, S. and Lepping, R. P.: 1997, 'Plasma Sheet Pressure Changes During the Substorm Growth Phase', *Geophys. Res. Lett.* **24**: 963–966.
- Nagai, T., Fujimoto, M., Saito, Y., Machida, S., Terasawa, T., Nakamura, R., Yamamoto, T., Mukai, T., Nishida, A. and Kokubun, S.: 1998, 'Structure and Dynamics of Magnetic Reconnection for Substorm Onsets with Geotail Observations', *J. Geophys. Res.* **103**: 4419–4440.
- Nagai, T. and Machida, S.: 1998, in A. Nishida, D. N. Baker and S. W. H. Cowley (eds), 'Magnetic Reconnection in the Near-Earth Magnetotail', *New Perspectives on the Earth's Magnetotail*, Geophys. Mono., Vol. 105, pp. 211–224, Amer. Geophys. Union, Washington D. C.
- Nagai, T., Singer, H. J., Mukai, T., Yamamoto, T. and Kokubun, S.: 1999, 'Development of Substorms in the Near-Earth Tail', *Adv. Space Res.*, in press.

- Nakai, H., Kamide, Y. and Russell, C. T.: 1991, 'Influences of Solar Wind Parameters and Geomagnetic Activity on the Tail Lobe Magnetic Field: A Statistical Study', *J. Geophys. Res.* **96**: 5511–5523.
- Nakamura, M. S. and Fujimoto, M.: 1998, 'A Three-Dimensional Hybrid Simulation of Magnetic Reconnection', *Geophys. Res. Lett.* **25**: 2917–2920.
- Nakamura, R., Kokubun, S., Mukai, T. and Yamamoto, T.: 1997, 'Changes in the Distant Tail Configuration During Magnetic Storms', *J. Geophys. Res.* **102**: 9587–9601.
- Nakamura, M. S., Fujimoto, M. and Maezawa, K.: 1998, 'Ion Dynamics and Resultant Velocity Space Distributions in the Course of Magnetotail Reconnection', *J. Geophys. Res.* **103**: 4531–4546.
- Ness, N. F.: 1969, 'The Geomagnetic Tail', *Rev. Geophys.* **7**: 97–127.
- Newell, P. T., Xu, D., Meng, C.-I. and Kivelson, M.: 1997, 'Dynamic Polar Cap: A Unifying Approach', *J. Geophys. Res.* **102**: 127–139.
- Nishida, A.: 1989, 'Can Random Reconnection on the Magnetopause Produce the Low Latitude Boundary Layer?' *Geophys. Res. Lett.* **16**: 227–230.
- Nishida, A., Hayakawa, H. and Hones, E. W. Jr.: 1981, 'Observed Signatures of Reconnection in the Magnetotail', *J. Geophys. Res.* **86**: 1422–1436.
- Nishida, A., Scholer, M., Terasawa, T., Bame, S. J., Gloeckler, G., Smith, E. J. and Zwickl, R. D.: 1986, 'Quasi-Stagnant Plasmoid in the Middle Tail: A New Preexpansion Phase Phenomenon', *J. Geophys. Res.* **91**: 4245–4255.
- Nishida, A., Mukai, T., Yamamoto, T. and Saito, Y.: 1995, 'Geotail Observation of Magnetospheric Convection in the Distant Tail at 200 R<sub>E</sub> in Quiet Times', *J. Geophys. Res.* **100**: 23663–23675.
- Nishida, A., Mukai, T., Yamamoto, T., Saito, Y. and Kokubun, S.: 1996, 'Magnetotail Convection in Geomagnetically Active Times, 1. Distance to Neutral Lines', *J. Geomag. Geoelectr.* **48**: 489–501.
- Nishida, A., Mukai, T., Yamamoto, T., Saito, Y., Kokubun, S. and Lepping, R. P.: 1997, 'Traversal of the Nightside Magnetosphere at 10 to 15 Re During Northward IMF', *Geophys. Res. Lett.* **24**: 939–942.
- Nishida, A., Mukai, T., Yamamoto, T., Kokubun, S. and Maezawa, K.: 1998, 'A Unified Model of the Magnetotail Convection in Geomagnetically Quiet and Active Times', *J. Geophys. Res.* **103**: 4409–4418.
- Nishida, A. and Ogino, T.: 1998, in A. Nishida, D. N. Baker and S. W. H. Cowley (eds), 'Convection and Reconnection in the Earth's Magnetotail', *New Perspectives on the Earth's Magnetotail*, Geophys. Mono., Vol. 105, pp. 61–75, Amer. Geophys. Union, Washington D. C.
- Ogino, T., Walker, R. J. and Ashour-Abdalla, M.: 1992, 'A Global Magnetohydrodynamic Simulation of the Magnetosheath and Magnetosphere when the Interplanetary Magnetic Field is Northward', *IEEE Trans. Plasma Sci.* **20**(6): 817–828.
- Ohtani, S., Kokubun, S. and Russell, C. T.: 1992, 'Radial Expansion of the Tail Current Disruption During Substorms: A New Approach to the Substorm Onset Region', *J. Geophys. Res.* **97**: 3129–3136.
- Ohtani, S., Takahashi, K., Higuchi, T., Lui, A. T. Y., Spence, H. E. and Fennell, J. F.: 1998, 'AMPTE/CCE-SCATHA Simultaneous Observations of Substorm-Associated Magnetic Fluctuations', *J. Geophys. Res.* **103**: 4671–4682.
- Owen, C. J., Slavin, J. A., Richardson, I. G., Murphy, N. and Hynds, R. J.: 1995, 'Average Motion, Structure and Orientation of Distant Magnetotail Determined from Remote Sensing of the Edge of the Plasma Sheet Boundary Layer with  $E > 35$  keV Ions', *J. Geophys. Res.* **100**: 185–204.
- Paterson, W. R. and Frank, L. A.: 1994, 'Survey of Plasma Parameters in the Earth's Distant Magnetotail With the Geotail Spacecraft', *Geophys. Res. Lett.* **21**: 2971–2974.
- Petrinec, S. M. and Russell, C. T.: 1996, 'Near-Earth Magnetotail Shape and Size as Determined from the Magnetopause Flaring Angle', *J. Geophys. Res.* **101**: 137–152.

- Petrukovich, A. A., Sergeev, V. A., Zelenyi, L. M., Mukai, T., Yamamoto, T., Kokubun, S., Shiokawa, K., Deehr, C. S., Budnick, E. Y., Büchner, J., Fedorov, A. O., Grigorieva, V. P., Hughes, T. J., Pissarenko, N. F., Romanov, S. A. and Sandahl, I.: 1998, 'Two Spacecraft Observations of a Reconnection Pulse During an Auroral Breakup', *J. Geophys. Res.* **103**: 47–59.
- Petschek, H. E.: 1964, in W. N. Hess (ed.), 'Magnetic Field Annihilation', *Proc. AAS-NASA Symp. Phys. Solar Flares, NASA SP-50*, pp. 425–439.
- Pulkkinen, T. I., Baker, D. N., Cogger, L. L., Mukai, T. and Singer, H. J.: 1998a, in S. Kokubun and Y. Kamide (eds), 'Coupling of Inner Tail and Midtail Processes', *Substorms-4*, pp. 749–754, Kluwer Academic Publishers, The Netherlands.
- Pulkkinen, T. I., Baker, D. N., Frank, L. A., Sigwarth, J. B., Opgenoorth, H. J., Greenwald, R., Friis-Christensen, E., Mukai, T., Nakamura, R., Singer, H., Reeves, G. D. and Lester, M.: 1998b, 'Two Substorm Intensifications Compared: Onset, Expansion, and Global Consequences', *J. Geophys. Res.* **103**: 15–27.
- Reiff, P. H. and Burch, J. L.: 1985, 'IMF By-Dependent Plasma Flow and Birkeland Currents in the Dayside Magnetosphere, 2. A Global Model for Northward and Southward IMF', *J. Geophys. Res.* **90**: 1595–1609.
- Richardson, I. G. and Cowley, S. W. H.: 1985, 'Plasmoid-Associated Ion Bursts in the Deep Geomagnetic Tail: Properties of the Boundary Layer', *J. Geophys. Res.* **90**: 12133–12158.
- Richardson, I. G., Cowley, S. W. H., Hones, E. W. Jr. and Bame, S. J.: 1987, 'Plasmoid-Associated Energetic Ion Bursts in the Deep Geomagnetic Tail: Properties of Plasmoids and the Postplasmoid Plasma Sheet', *J. Geophys. Res.* **92**: 9997–10013.
- Richardson, I. G., Owen, C. J. and Slavin, J. A.: 1996, 'Energetic ( $> 0.2$  MeV) Electron Bursts in the Deep Geomagnetic Tail Observed by ISEE 3: Association with Substorms and Magnetic Structures', *J. Geomag. Geoelectr.* **48**: 657–673.
- Saito, Y., Mukai, T., Terasawa, T., Nishida, A., Machida, S., Hirahara, M., Maezawa, K., Kokubun, S. and Yamamoto, T.: 1995, 'Slow-Mode Shocks in the Magnetotail', *J. Geophys. Res.* **100**: 23567–23581.
- Saito, Y., Mukai, T., Terasawa, T., Nishida, A., Machida, S., Kokubun, S. and Yamamoto, T.: 1996, 'Foresock Structure of the Slow-Mode Shocks in the Earth's Magnetotail', *J. Geophys. Res.* **101**: 13267–13274.
- Sanny, J., McPherron, R. L., Russell, C. T., Baker, D. N., Pulkkinen, T. I. and Nishida, A.: 1994, 'Growth Phase Thinning of the Near-Earth Current Sheet During the CDAW-6 Substorm', *J. Geophys. Res.* **99**: 5805–5816.
- Sarafopoulos, D. V., Sarris, E. T., Angelopoulos, V., Yamamoto, T. and Kokubun, S.: 1997, 'Spatial Structure of the Plasma Sheet Boundary Layer at Distances Greater than  $180 R_E$  as Derived from Energetic Particle Measurements on Geotail', *Ann. Geophysicae* **15**: 1246–1256.
- Sauvaud, J.-A., Jacquey, C., Beutier, T., Owen, C., Lepping, R. P., Russell, C. T. and Belian, R. J.: 1996, 'Large Scale Dynamics of the Magnetospheric Tail Induced by Substorms: A Multisatellite Study', *J. Geomag. Geoelectr.* **48**: 675–686.
- Sauvaud, J.-A., Koperski, P., Beutier, T., Barthe, H., Aoustin, C., Thocaven, J. J., Rouzaud, J., Penou, E., Vaisberg, O. and Borodkova, N.: 1997, 'The INTERBALL-TAIL Electron Experiment: Initial Results on the Low-Latitude Boundary Layer of the Dawn Magnetosphere', *Ann. Geophysicae* **15**: 587–595.
- Schriver, D., Ashour-Abdalla, M. and Richard, R. L.: 1998, 'On the Origin of the Ion-Electron Temperature Difference in the Plasma Sheet', *J. Geophys. Res.* **103**: 14879–14895.
- Sckopke, N., Paschmann, G., Haerendel, G., Sonnerup, B. U. Ö., Bame, S. J., Forbes, T. G., Hones, E. W. Jr. and Russell, C. T.: 1981, 'Structure of the Low-Latitude Boundary Layer', *J. Geophys. Res.* **86**: 2099–2110.
- Seki, K., Hirahara, M., Terasawa, T., Mukai, T., Saito, Y., Machida, S., Yamamoto, T. and Kokubun, S.: 1998, 'Statistical Properties and Possible Supply Mechanisms of Tailward Cold  $O^+$  Beams in the Lobe/Mantle Regions', *J. Geophys. Res.* **103**: 4477–4489.

- Seki, K., Elphic, R. C., Thomsen, M. F., Bonnell, J., Lund, E. J., Hirahara, M., Terasawa, T. and Mukai, T.: 1999, 'Cold flowing O<sup>+</sup> beams in the lobe/mantle at GEOTAIL: Does FAST observe the source?', *J. Geophys. Res.* **105**, in press.
- Seon, J., Frank, L. A., Paterson, W. R., Scudder, J. D., Coroniti, F. V., Kokubun, S. and Yamamoto, T.: 1996, 'Observations of Slow-Mode Shocks in the Earth's Distant Magnetotail with Geotail Spacecraft', *J. Geophys. Res.* **101**: 27383–27398.
- Sergeev, V. A., Mitchell, D. G., Russell, C. T. and Williams, D. J.: 1993, 'Structure of the Tail Plasma/Current Sheet at 11 Re and its Changes in the Course of a Substorm', *J. Geophys. Res.* **98**: 17345–17365.
- Sergeev, V. A., Angelopoulos, V., Mitchell, D. G. and Russell, C. T.: 1995, 'In Situ Observations of Magnetotail Reconnection Prior to the Onset of a Small Substorm', *J. Geophys. Res.* **100**: 19121–19133.
- Shiokawa, K., Baumjohann, W. and Haerendel, G.: 1997, 'Braking of High-Speed Flows in the Near-Earth Tail', *Geophys. Res. Lett.* **24**: 1179–1182.
- Shiokawa, K., Baumjohann, W., Haerendel, G., Paschmann, G., Fennel, J. F., Friis-Christensen, E., Lühr, H., Reeves, G. D., Russell, C. T., Sutcliffe, P. R. and Takahashi, K.: 1998, 'High-Speed Ion Flow, Substorm Current Wedge, and Multiple Pi 2 Pulsations', *J. Geophys. Res.* **103**: 4491–4507.
- Shinohara, I., Nagai, T., Fujimoto, M., Terasawa, T., Mukai, T., Tsuruda, K. and Yamamoto, T.: 1998, 'Low-Frequency Electromagnetic Turbulence Observed Near the Substorm Onset Site', *J. Geophys. Res.* **103**: 20365–20388.
- Shodhan, S., Siscoe, G. L., Frank, L. A., Ackerson, K. L., Paterson, W. R., Fairfield, D., Kokubun, S. and Yamamoto, T.: 1996, 'Mantle Crossing at Geotail: Comparison with MHD Model', *J. Geophys. Res.* **101**: 153–159.
- Shirai, H., Maezawa, K., Fujimoto, M., Mukai, T., Yamamoto, T., Saito, Y., Kokubun, S. and Kaya, N.: 1997, 'Drop-Off of the Polar Rain Flux Near the Plasma Sheet Boundary', *J. Geophys. Res.* **102**: 2271–2278.
- Shirai, H., Maezawa, K., Fujimoto, M., Mukai, T., Yamamoto, T., Saito, Y. and Kokubun, S.: 1998, 'Entry Processes of Low-Energy Electrons into the Magnetosphere Along Open Field Lines: Polar Rain Electrons as Field Line Tracers', *J. Geophys. Res.* **103**: 4379–4390.
- Sibeck, D. G., Siscoe, G. L., Slavin, J. A., Smith, E. J., Tsurutani, B. T. and Lepping, R. P.: 1985, 'The Distant Magnetotail's Response to a Strong Interplanetary Magnetic Field B<sub>y</sub>: Twisting, Flattening, and Field Lines Bending', *J. Geophys. Res.* **90**: 4011–4019.
- Siscoe, G. L. and Sanchez, E.: 1987, 'An MHD Model for the Complete Open Magnetotail Boundary', *J. Geophys. Res.* **92**: 7405–7412.
- Slavin, J. A., Smith, E. J., Sibeck, D. G., Baker, D. N., Zwickl, R. D. and Akasofu, S.-I.: 1985, 'An ISEE-3 Study of Average and Substorm Conditions in the Distant Magnetotail', *J. Geophys. Res.* **90**: 10875–10895.
- Slavin, J. A.: 1998, in A. Nishida, D. N. Baker and S. W. H. Cowley (eds), 'Traveling Compression Regions', *New Perspectives on the Earth's Magnetotail*, Geophys. Mono., Vol. 105, pp. 225–240, Amer. Geophys. Union, Washington D. C.
- Slavin, J. A., Fairfield, D. H., Kuznetsova, M. M., Owen, C. J., Lepping, R. P., Taguchi, S., Mukai, T., Saito, Y., Yamamoto, T., Kokubun, S., Lui, A. T. Y. and Reeves, G. D.: 1998, 'ISTP Observations of Plasmoid Ejection: IMP 8 and Geotail', *J. Geophys. Res.* **103**: 119–133.
- Smets, R., Delcourt, D. and Fontaine, D.: 1998, 'Ion and Electron Distribution Functions in the Distant Magnetotail: Modeling of Geotail Observations', *J. Geophys. Res.* **103**: 20407–20417.
- Speiser, T. W.: 1965, 'Particle Trajectories in Model Current Sheet, 1. Analytical Motion', *J. Geophys. Res.* **70**: 4219–4226.
- Taktakishvili, A. L., Zelenyi, L. M., Lutsenko, V. N. and Kudela, K.: 1998, 'On the Spectra of Energetic Particles in the Earth's Magnetotail', *Cosmic Res.* **36**: 265–273.

- Tanaka, T.: 1999, 'Configuration of the Magnetosphere-Ionosphere Convection System Under Northward IMF Conditions with Non-Zero IMF By', *J. Geophys. Res.* **104**: 14683–14690.
- Takahashi, K. and Hones, E. W. Jr.: 1988, 'ISEE 1 and 2 Observations of Ion Distributions at the Plasma Sheet-Tail Lobe Boundary', *J. Geophys. Res.* **93**: 8558–8582.
- Terasawa, T., Fujimoto, M., Mukai, T., Shinohara, I., Saito, Y., Yamamoto, T., Machida, S., Kokubun, S., Lazarus, A. J., Steinberg, J. T. and Lepping, R. P.: 1997, 'Solar Wind Control of Density and Temperature in the Near-Earth Plasma Sheet: WIND-Geotail Collaboration', *Geophys. Res. Lett.* **24**: 935–938.
- Traver, D. P., Mitchell, G., Williams, D. J., Frank, L. A. and Huang, C. Y.: 1991, 'Two Encounters with the Flank Low-Latitude Boundary Layer: Further Evidence for Closed Topology and Investigation of the Internal Structure', *J. Geophys. Res.* **96**: 21025–21035.
- Treumann, R. A., LaBelle, J., Bauer, N. T. M.: 1995, in P. Song, B. U. Ö. Sonnerup and M. F. Thomson (eds), 'Diffusion Processes: An Observational Perspective', *Physics of the Magnetopause*, Geophys. Mono., Vol. 90, pp. 331–341, Amer. Geophys. Union, Washington D. C.
- Tsurutani, B. T., Richardson, I. G., Thorne, R. M., Butler, W., Smith, E. J., Cowley, S. W. H., Gary, S. P., Akasofu, S.-I. and Zwickl, R. D.: 1985, 'Observations of the Right-Hand Resonant Ion Beam Instability in the Distant Plasma Sheet Boundary Layer', *J. Geophys. Res.* **90**: 12159–12172.
- Whang, Y. C., Fairfield, D., Smith, E. J., Lepping, R. P., Kokubun, S. and Saito, Y.: 1999, 'Observations of Double Discontinuity in the Magnetotail', *Geophys. Res. Lett.* **24**: 3153–3156.
- Wiechen, H., Büchner, J. and Otto, A.: 1986, 'Reconnection in the Near-Earth Plasma Sheet: A Three Dimensional Model', *J. Geophys. Res.* **101**: 24911–24918.
- Williams, D. J.: 1981, 'Energetic Ion Beams at the Edge of the Plasma Sheet: ISEE 1 Observations Plus a Simple Explanatory Model', *J. Geophys. Res.* **86**: 5507–5518.
- Williams, D. J., Mitchell, D. G., Eastman, T. E. and Frank, L. A.: 1985, 'Energetic Particle Observations in the Low-Latitude Boundary Layer', *J. Geophys. Res.* **90**: 5097–5116.
- Winglee, R. M., Kokubun, S., Lin, R. P. and Lepping, R. P.: 1998, 'Flux Rope Structure in the Magnetotail: Comparison Between Wind/Geotail Observations and Global Simulations', *J. Geophys. Res.* **103**: 135–150.
- Yamamoto, T., Shiokawa, K. and Kokubun, S.: 1994, 'Magnetic Field Structures of the Magnetotail as Observed by Geotail', *Geophys. Res. Lett.* **21**: 2875–2878.
- Vasyliunas, V. M.: 1998, in S. Kokubun and Y. Kamide (eds), 'Theoretical Considerations on where a Substorm Begins', *Substorms-4*, pp. 9–14, Kluwer Academic Publishers, The Netherlands.
- Zong, Q.-G., Wilken, B., Woch, J., Mukai, T., Yamamoto, T., Reeves, G. D., Doke, T., Maezawa, K., Williams, D. J., Kokubun, S. and Ulland, S.: 1998, 'Energetic Oxygen Ions Bursts in the Distant Magnetotail as a Product of Intense Substorms: Three Case Studies', *J. Geophys. Res.* **103**: 20339–20363.